



รายงานวิจัยฉบับสมบูรณ์

โครงการ การศึกษาเชิงทฤษฎีของรอยต่อโจเซฟสันหลายแบบ

โดย รองศาสตราจารย์ ดร. พวงรัตน์ ไพเราะ

กันยายน ๒๕๕๑

รายงานวิจัยฉบับสมบูรณ์

โครงการ การศึกษาเชิงทฤษฎีของรอยต่อโจเซฟสันหลายแบบ

ผู้วิจัย รองศาสตราจารย์ ดร. พวงรัตน์ ไพเราะ นางสาว เบญจมาศ ศรีสองเมือง

สังกัด มหาวิทยาลัยเทคโนโลยีสุรนารี มหาวิทยาลัยเทคโนโลยีสุรนารี

สนับสนุนโดยสำนักงานคณะกรรมการการอุดมศึกษา และสำนักงานกองทุนสนับสนุนการวิจัย

(ความเห็นในรายงานนี้เป็นของผู้วิจัย สกอ. และ สกว. ไม่จำเป็นต้องเห็นด้วยเสมอไป)

สารบัญ

	หน้า
บทคัดย่อภาษาอังกฤษ	2
บทคัดย่อภาษาไทย	3
Executive summary	4
เนื้อหางานวิจัย	6
Output จากโครงการ	8
ภาคผนวก	9

Abstract

Project Code: RMU4880012

Project Title: Theoretical study of various types of Josephson junctions

Investigator: Dr. Puangratana Pairor

E-mail Address: pairor@sut.ac.th

Project Period: 3 years

Erosion of nodal Fermi spheres in nonequilibrium d-wave superconductors, tunneling spectroscopy and spin transport of metal-Rashba system and superconductor-Rashba system, and Josephson tunneling between two YBCO grains were studied in this research project. It was found that when a d-wave superconductor that has been driven out of equilibrium by an optical pulse, in the high density limit for the photoinjected quasiparticles, the decay rate dn/dt is found to vary as $n^{5/2}$, which differs from the n^2 form commonly adopted in phenomenological models of the relaxation dynamics. In the low density limit, the decay is exponential.

For the junction of metal-Rashba system, the energy spacing between two distinct features in the conductance spectrum can be used to directly measure the Rashba energy. Also, the interfacial scattering greatly affects the spin polarization of the conductance in metal, but hardly affects that in the Rashba system.

The tunneling conductance spectrum of superconductor-Rashba system depends strongly on 1) the strength of Rashba spin-orbit coupling (RSOC), 2) the potential barrier and 3) the mismatch of electron effective masses. The influence of the RSOC, potential barrier and mismatch of electron effective mass are associated and also depends on the Fermi levels of the Rashba system. Andreev reflection amplitude at the superconducting gap energy is always increased with the RSOC strength, but is unaffected by the change in the potential barrier. The effect of the mismatch effective mass and the potential barrier are not always equivalent as it was believed.

Lastly, the free energies of both untwinned and twinned systems of orthorhombic symmetry are studied in order to derive the Josephson tunneling between two YBCO grains. A model based on the Ginzburg-Landau theory and the idea of twinning is introduced to describe the anomalous dependence of the critical current on an external magnetic field in a YBCO asymmetric grain boundary.

Keywords: tunneling spectroscopy; josephson junctions; superconductor; Rashba spin-orbit coupling;spin transport

2

บทคัดย่อ

รหัสโครงการ: RMU4880012

ชื่อโครงการ: การศึกษาเชิงทฤษฎีของรอยต่อโจเซฟสันหลายแบบ

ชื่อหักวิจัย: ดร. พวงรัตห์ ไพเราะ E-mail Address: pairor@sut.ac.th

ระยะเวลาโครงการ: 3 ปี

รายงานวิจัยฉบับนี้ประกอบด้วย ผลการศึกษา 1) สลายไปของทรงกลมเฟร์มีที่จุดบัพของตัวนำยิ่งยวด แบบดีเวฟในสภาวะไม่สมดุล 2) สเปกโตรสโคปีทะลุผ่านและการขนส่งสปินของรอยต่อโลหะกับระบบรัชบา 3) สเปกโตรสโคปีทะลุผ่านของรอยต่อระบบรัชบากับตัวนำยิ่งยวด และ 4) การทะลุผ่านโจเซฟสันระหว่าง YBCO/YBCO จากการศึกษา พบว่า ในลิมิตที่อนุภาคที่ได้รับการกระตุ้นจากแสงมีความหนาแน่นสูง เมื่อตัวนำ ยิ่งยวดแบบดีเวฟที่ถูกขับดันให้ออกจากสภาวะสมดุลด้วยพัลส์แสง อัตราการสลายตัว dn/ dt ของอนุภาคเหล่านี้มี ค่าแปรตาม $n^{5/2}$ ซึ่งต่างไปจาก n^2 ที่คิดมาจากแบบจำลองฟิโนมีโนโลจิคอล ในลิมิตที่มีความหนาแน่นต่ำ การ สลายตัวมีลักษณะเป็นเอกซ์โปเนนเชียลที่มีค่าลดลง

สำหรับรอยต่อโลหะกับระบบรัชบา จากการศึกษาพบว่า ระยะระหว่างตำแหน่งเชิงพลังงานของลักษณะ โดดเด่นที่เกิดขึ้นในสเปกตรัมความนำไฟฟ้า 2 ตำแหน่ง มีค่าเท่ากับพลังงานรัชบา นอกจากนี้ เรายังพบว่า การ กระเจิงที่รอยต่อมีผลต่อสปินโพลาไรเซชันของความนำไฟฟ้าในโลหะเป็นอย่างมาก แต่กลับมีผลต่อสปินโพลาไร เซชันของความนำไฟฟ้าในระบบรัชบาน้อยมาก

สเปกตรัมความนำไฟฟ้าของรอยต่อระบบรัชบากับตัวนำยิ่งยวดขึ้นอยู่เป็นอย่างมากกับ 1) ความแรงของ คู่ควบรัชบา 2) ศักย์กีดกั้นที่รอยต่อ และ 3) ความไม่เท่ากันของมวลยังผลของอิเล็กตรอนของตัวนำยิ่งยวดและ ของระบบรัชบา ผลของความแรงของคู่ควบรัชบา ศักย์กีดกั้น และความไม่เท่ากันของมวลยังผลของอิเล็กตรอนต่อ สเปกตรัมความนำไฟฟ้านั้นมีความสัมพันธ์กัน และสเปกตรัมความนำไฟฟ้ายังขึ้นกับระดับพลังงานเฟร์มีของ ระบบรัชบาอีกด้วย ค่าอัมปลิจูดของการสะท้อนอังเดรฟที่ค่าช่องว่างพลังงานของตัวนำยิ่งยวดมีค่าเพิ่มขึ้นตามค่า ความแรงของค่าคู่ควบรัชบาแต่มีค่าไม่ขึ้นกับค่าศักย์กีดกั้นที่รอยต่อ นอกจากนี้ เรายังพบว่าผลของความแตกต่าง ของมวลยังผลของอิเล็กตรอนและศักย์กีดกั้นมีลักษณะไม่เหมือนกันอย่างที่เคยเป็นที่เชื่อกัน

และท้ายที่สุด เราได้ทำการศึกษาค่าพลังงานอิสระของระบบที่มีสมมาตรออร์โธรอมบิก ทั้งแบบที่มีทวิน และไม่มีทวิน เพื่อหาค่าการทะลุผ่านโจเซฟสันระหว่าง YBCO สองชิ้น แบบจำลองที่ใช้คือทฤษฎีกินส์เบิร์ก-แลน เดา เมื่อเรารวมเอาผลของทวินเข้ามา เราสามารถอธิบายลักษณะที่กระแสวิกฤตโจเซฟสันขึ้นกับสนามแม่เหล็ก ภายนอกที่พบในรอยต่อไม่สมมาตรของ YBCO/YBCO ได้

คำหลัก: สเปกโตรสโคปีทะลุผ่าน; รอยต่อโจเซฟสัน; ตัวนำยิ่งยวด; คู่ควบรัชบา; การขนส่งสปิน

Executive Summary

1. ความสำคัญและที่มาของปัญหา

โครงการนี้ได้ทำการศึกษา 1) สลายไปของทรงกลมเฟร์มีที่จุดบัพของตัวนำยิ่งยวดแบบดีเวฟในสภาวะ ไม่สมดุล 2) สเปกโตรสโคปีทะลุผ่านและการขนส่งสปินของรอยต่อโลหะกับระบบรัชบา 3) สเปกโตรสโคปีทะลุผ่านของรอยต่อระบบรัชบากับตัวนำยิ่งยวด และ 4) การทะลุผ่านโจเซฟสันระหว่าง YBCO/YBCO ตัวนำยวดยิ่ง และสารที่มีคู่ควบรัชบามีศักยภาพเชิงเทคโนโลยีสูง การศึกษาสมบัติทะลุผ่านของกระแสไฟฟ้าของตัวนำยวดยิ่ง รวมไปถึงการเข้าใจการขนส่งสปินในรอยต่อที่มีคู่ควบรัชบาเป็นส่วนประกอบ เป็นส่วนหนึ่งของการนำไปสู่ความ เข้าใจการขนส่งทั้งประจุและสปิน และการออกแบบอุปกรณ์ทางอิเล็กทรอนิกส์และสปินทรอนิกส์อีกด้วย

2. วัตถุประสงค์

เพื่อศึกษาการขนส่งอนุภาค ประจุ และสปินของรอยต่อที่มีตัวนำยิ่งยวด และ/หรือ สารที่มีคู่ควบรัชบา เป็นส่วนประกอบ โดยการคำนวณด้วยวิธีการกระเจิงและทฤษฎีกินส์เบริ์ก-แลนเดา

3. ระเบียบวิธีการวิจัย

งานวิจัยนี้เป็นงานวิจัยทางด้านทฤษฎี ซึ่งมีระเบียบวิธีและขั้นตอนการวิจัยดังนี้

- 3.1 คันคว้าเอกสารที่เกี่ยวข้องกับหัวข้อของโครงการ (ขั้นตอนนี้เกิดขึ้นตลอดการดำเนินงาน)
- 3.2 ทำการคำนวณสลายไปของทรงกลมเฟร์มีที่จุดบัพของตัวนำยิ่งยวดแบบดีเวฟในสภาวะไม่สมดุลด้วยวิธีการ กระเจิง
- 3.3 ทำการคำนวณสเปกโตรสโคปีทะลุผ่านและการขนส่งสปินของรอยต่อโลหะกับระบบรัชบาด้วยวิธีการกระเจิง
- 3.4 ทำการคำนวณสเปกโตรสโคปีทะลุผ่านของรอยต่อระบบรัชบากับตัวนำยิ่งยวดด้วยวิธีการกระเจิง
- 3.5 ทำการคำนวณการทะลุผ่านโจเซฟสันระหว่าง YBCO/YBCO ด้วยทฤษฎีกินส์เบริ์ก-แลนเดา
- 3.6 เปรียบเทียบผลที่ได้กับผลงานทางการทดลองที่เกี่ยวข้อง
- 3.7 เตรียมต้นฉบับของผลงานที่ได้จากข้อ 3.2 ถึง 3.5 เพื่อส่งไปพิจารณาตีพิมพ์ในวารสารระดับนานาชาติ (สำหรับผลงานจากข้อ 3.2 ได้ตีพิมพ์แล้ว 1 เรื่อง ที่ Physical Review B ผลงานจากข้อ 3.3 ส่งไปพิจารณา การตีพิมพ์ 1 เรื่อง ในวารสาร Physical Review B สำหรับผลงานจากข้อ 3.4 จะส่งไปที่ Physical Review B เช่นกัน เป็นจำนวน 2 เรื่อง และ ผลงานจากข้อ 3.5 จะส่งไปที่ Physica C เป็นจำนวน 1 เรื่อง โปรดดูใน ภาคผนวก)

4. แผนการดำเนินงานวิจัยตลอดโครงการ

การดำเนินงานของโครงการนี้ ไม่ได้เป็นไปตามที่ได้วางแผนไว้ในข้อเสนอของโครงการ เนื่องจากใน ระหว่างการดำเนินงาน หัวหน้าโครงการได้พูดคุยและถกปัญหากับนักวิจัยต่างชาติเกี่ยวกับ 1) ตัวนำยิ่งยวดแบบ ดีเวฟในสถานะไม่สมดุล และ 2) สารที่มีคู่ควบรัชบา หัวหน้าโครงการเห็นว่า การศึกษาเกี่ยวกับสถานะไม่สมดุล ของตัวนำยิ่งยวดเป็นสิ่งจำเป็นเพื่อนำไปสู่ความเข้าใจ ปรากฏการณ์ที่เกิดในรอยต่อโจเซฟสันแบบดีเวฟที่ไม่อยู่ใน สภาวะสมดุลได้ และยังเห็นว่า สเปกตรัมความนำไฟฟ้าอาจเป็นเครื่องมือที่ช่วยในการวัดค่าความแรงของคู่ควบรัช บาได้ จึงทำการคำนวณเกี่ยวกับเรื่องเหล่านี้ ซึ่งไม่ได้รวมอยู่ในแผนการดำเนินงาน แต่เป็นการคำนวณที่ใกล้เคียง

กัน ซึ่งผลลัพธ์ที่ได้เป็นที่น่าพอใจมาก และเรื่องแรกได้ตีพิมพ์ในวารสาร Physical Review B และเรื่องที่สอง กำลัง อยู่ในระหว่างการพิจารณาโดย Reviewer ที่วารสาร Physical Review B เช่นกัน

ต่อมาหัวหน้าโครงการได้ทำการศึกษารอยต่อระหว่างสารที่มีคู่ควบรัชบากับตัวนำยิ่งยวด ทั้งที่เป็นแบบ เอสเวฟ และดีเวฟ และได้เตรียม Manuscript จำนวน 2 ฉบับ เพื่อส่งไป ที่วารสาร Physical Review B ต่อไป และในช่วงสุดท้ายของงานวิจัย หัวหน้าโครงการได้ทำการศึกษารอยต่อโจเซฟสันระหว่าง YBCO กับ YBCO เพื่อที่จะเข้าใจกราฟความสัมพันธ์ระหว่างกระแสโจเซฟสันวิกฤตกับสนามแม่เหล็กภายนอก ผลที่ได้นั้น ได้นำไป เขียนเป็น Manuscript 1 ฉบับ เพื่อส่งไป ที่วารสาร Physica C ต่อไป

โดยสรุปแล้ว การดำเนินงานของโครงการวิจัยนี้ตามที่เกิดขึ้นจริง เป็นไปตามตารางข้างล่างนี้

ปีที่ 1												
กิจกรรม	เดือนที่ 1	2	3	4	5	6	7	8	9	10	11	12
Literature search												
Calculation of erosion of nodal Fermi spheres												
in nonequilibrium d-wave superconductors												
Preparation of a manuscript for publication												
ปีที่ 2				•		ı	ı	ı	1	1		
กิจกรรม	เดือนที่ 1	2	3	4	5	6	7	8	9	10	11	12
Literature search												
Calculation of tunneling spectroscopy and												
spin transport of metal-Rashba system												
Calculation of tunneling spectroscopy of												
superconductor-Rashba system (for both s-												
wave and d-wave superconductors)												
ปีที่ 3												
กิจกรรม	เดือนที่ 1	2	3	4	5	6	7	8	9	10	11	12
Preparation of a manuscript for publication												
for metal-Rashba system												
Literature search and calculation of												

กิจกรรม	เดือนที่ 1	2	3	4	5	6	7	8	9	10	11	12
Preparation of a manuscript for publication												
for metal-Rashba system												
Literature search and calculation of												
Josephson tunneling between two YBCO												
grains												
Preparation of two manuscripts for												
publication for superconductor-Rashba												
system (both for s-wave and d-wave												
superconductors)												
Preparation of a manuscript for publication												
for Josephson tunneling between two YBCO												
grains												

เนื้อหางานวิจัย

บทน้ำ

งานวิจัยทางด้านตัวนำยิ่งยวดเป็นที่แพร่หลายมาเป็นเวลานาน โดยเฉพาะเมื่อมีการค้นพบตัวนำยวดยิ่ง ที่มีอุณหภูมิวิกฤตสูง ซึ่งเป็นพวกเซรามิกส์คอปเปอร์ออกไซด์ (Copper oxides) ในปี ค.ศ.1986 ตัวนำยิ่งยวดมี สมบัติพิเศษหลายอย่าง เช่น นำไฟฟ้าโดยไม่มีความต้านทาน ผลักสนามแม่เหล็กออกจากเนื้อได้อย่างสมบูรณ์ เป็นต้น มีการนำตัวนำยิ่งยวดไปประยุกต์เป็นอุปกรณ์ในการใช้งานต่าง ๆ เช่น SQUID (เป็นอุปกรณ์ที่ทำมาจาก รอยต่อโจเซฟสัน) ซึ่งสามารถใช้ตรวจวัดค่าสนามแม่เหล็กที่มีความเข้มน้อย ๆ ได้ เป็นตัน การศึกษาทางพื้นฐาน เกี่ยวกับตัวนำยิ่งยวดยังเป็นสิ่งจำเป็น โดยเฉพาะอย่างยิ่ง ความเข้าใจการขนส่งอนุภาคในรอยต่อที่มีตัวนำยิ่งยวด เป็นส่วนประกอบอาจนำไปสู่การสร้างอุปกรณ์ทางอิเล็กทรอนิกส์ใหม่ ๆ ได้ นอกจากนี้ ในปัจจุบัน ยังมีสารที่มีคู่ ควบรัชบาซึ่งกำลังได้รับความสนใจเป็นอย่างมาก เนื่องจากสารเหล่านี้มีสมบัติที่เกี่ยวกับสปินที่นำไปสู่ ปรากฏการณ์ทางฟิสิกส์ที่น่าสนใจ เช่น ปรากฏการณ์สปินฮอลล์ และการประยุกต์ทางสปินทรอนิกส์ อีกด้วย

โครงการวิจัยนี้ เป็นการศึกษาทางทฤษฎีเกี่ยวกับรอยต่อที่มีตัวนำยิ่งยวด และ/หรือ สารที่มีคู่ควบรัชบา เป็นส่วนประกอบ โดยผลงานที่ได้แบ่งออกเป็น 4 หัวข้อคือ 1) สลายไปของทรงกลมเฟร์มีที่จุดบัพของตัวนำ ยิ่งยวดแบบดีเวฟในสภาวะไม่สมดุล 2) สเปกโตรสโคปีทะลุผ่านและการขนส่งสปินของรอยต่อโลหะกับระบบรัชบา 3) สเปกโตรสโคปีทะลุผ่านของรอยต่อระบบรัชบากับตัวนำยิ่งยวด และ 4) การทะลุผ่านโจเซฟสันระหว่าง YBCO/YBCO

วิธีการศึกษา

ในงานวิจัยนี้ เราใช้วิธีการศึกษาหลัก ๆ 2 วิธี คือ วิธีการทางกลศาสตร์ควอนตัมที่เรียกว่า วิธีการกระเจิง (ซึ่งนิยมใช้ในการศึกษารอยต่อระหว่างโลหะกับตัวนำยิ่งยวด) และทฤษฎีกินส์เบิร์ก-แลนเดา ในที่นี้จะไม่ขอ กล่าวถึงรายละเอียดของวิธีการศึกษาทั้งสอง หากท่านผู้อ่านต้องการทราบรายละเอียด โปรดดูในภาคผนวกซึ่ง ประกอบด้วย Published paper และ Manuscripts ของผลงานที่ได้จากโครงการนี้

ผลการศึกษา

โดยสรุปแล้ว ผลการศึกษในแต่ละหัวข้อเป็นดังนี้

1) การศึกษาสลายไปของทรงกลมเฟร์มีที่จุดบัพของตัวนำยิ่งยวดแบบดีเวฟในสภาวะไม่สมดุล

พบว่า ในลิมิตที่อนุภาคที่ได้รับการกระตุ้นจากแสงมีความหนาแน่นสูง เมื่อตัวนำยิ่งยวดแบบดีเวฟที่ถูก ขับดันให้ออกจากสภาวะสมดุลด้วยพัลส์แสง อัตราการสลายตัว dn/dt ของอนุภาคเหล่านี้มีค่าแปรตาม $n^{5/2}$ ซึ่ง ต่างไปจาก n^2 ที่คิดมาจากแบบจำลอง Phenominological ในลิมิตที่มีความหนาแน่นต่ำ การสลายตัวมีลักษณะ เป็นเอกซ์โปเนนเชียลที่มีค่าลดลง

2) สเปกโตรสโคปีทะลุผ่านและการขนส่งสปินของรอยต่อโลหะกับระบบรัชบา

พบว่า เราสามารถใช้สเปกโตรสโคปีทะลุผ่านเป็นเครื่องมือในการวัดค่าความแรงของคู่ควบรัชบาได้ กล่าวคือ ระยะเชิงพลังงานระหว่างลักษณะโดดเด่น 2 ตำแหน่ง ที่เกิดขึ้นในสเปกตรัมความนำไฟฟ้ามีค่าเท่ากับ พลังงานรัชบาพอดี ในการศึกษาของเรา เราได้รวมเอาผลของการกระเจิงที่รอยต่อมาศึกษาด้วย โดยพบว่า การ กระเจิงที่รอยต่อไม่มีผลต่อตำแหน่งของลักษณะโดดเด่นทั้งสองที่เกิดขึ้นในสเปกตรัมความนำไฟฟ้า แต่มีผลต่อ สปินโพลาไรเซชันของความนำไฟฟ้า โดยที่ในโลหะมีผลกระทบเป็นอย่างมาก แต่ในระบบรัชบามีผลน้อยน้อยมาก

3) สเปกโตรสโคปีทะลุผ่านของรอยต่อระบบรัชบากับตัวนำยิ่งยวด

เราได้ศึกษาทั้งในกรณีที่ตัวนำยิ่งยวดเป็นแบบเอสเวฟ และดีเวฟ เราพบว่า สเปกตรัมความนำไฟฟ้าของ รอยต่อระบบรัชบากับตัวนำยิ่งยวดขึ้นอยู่เป็นอย่างมากกับ 1) ความแรงของคู่ควบรัชบา 2) ศักย์กีดกั้นที่รอยต่อ และ 3) ความไม่เท่ากันของมวลยังผลของอิเล็กตรอนของตัวนำยิ่งยวดและของระบบรัชบา ผลของความแรงของคู่ ควบรัชบา ศักย์กีดกั้น และความไม่เท่ากันของมวลยังผลของอิเล็กตรอนต่อสเปกตรัมความนำไฟฟ้านั้น มี ความสัมพันธ์กัน และสเปกตรัมความนำไฟฟ้ายังขึ้นกับระดับพลังงานเฟร์มีของระบบรัชบาอีกด้วย ค่าอัมปลิจูด ของการสะท้อนอังเดรฟที่ค่าช่องว่างพลังงานของตัวนำยิ่งยวดมีค่าเพิ่มขึ้นตามค่าความแรงของค่าคู่ควบรัชบาแต่มี ค่าไม่ขึ้นกับค่าศักย์กีดกั้นที่รอยต่อ นอกจากนี้ เรายังพบว่าผลของความแตกต่างของมวลยังผลของอิเล็กตรอนและ ศักย์กีดกั้นมีลักษณะไม่เหมือนกันอย่างที่เคยเป็นที่เชื่อกัน

4) การทะลุผ่านโจเซฟสันระหว่าง YBCO/YBCO

เราได้ทำการศึกษาค่าพลังงานอิสระของระบบที่มีสมมาตรออร์โธรอมบิก ทั้งแบบที่มีทวินและไม่มีทวิน เพื่อหาค่าการทะลุผ่านโจเซฟสันระหว่าง YBCO สองชิ้น เมื่อเรารวมเอาผลของทวินเข้ามา เราสามารถอธิบาย ลักษณะที่กระแสวิกฤตโจเซฟสันขึ้นกับสนามแม่เหล็กภายนอกที่พบในรอยต่อไม่สมมาตรของ YBCO/YBCO ได้

หนังสืออ้างอิง

- 1. J. G. Bednoz and K. A. Muller, Z. Phys. B 64,189 (1986).
- 2. I. Zutic, J. Fabian, and S. Das Sarma, Rev. Mod. Phys. 76, 323 (2004).
- 3. H. Engel, E. I. Rashba, and B. I. Halperin, *Handbook of Magnetism and Advanced Magnetic Materials* (Chichester: John Wiley and Sons Limited, 2007).
- G. E. Blonder, M. Tinkham, and T. M. Klapwijk, Phys. Rev. B 25, 4515 (1982)
 โปรดดูหนังสือเอกสารอ้างอิงอื่น ๆ ที่อยู่ใน paper, preprints ในภาคผนวกด้วย

ภาคผนวก

ภาคผนวกนี้ประกอบด้วย ผลงานตีพิมพ์แล้ว 1 เรื่อง

"Erosion of nodal Fermi spheres in nonequilibrium d-wave superconductors" วารสารที่ลงตีพิมพ์
 คือ Physical Review B ปี 2005 เล่มที่ 72 เลขที่ 212513

ผลงานที่กำลังอยู่ในระหว่างการพิจารณา 1 เรื่อง

● "Tunneling conductance of a two-dimensional electron gas with Rashba spin-orbit coupling" ส่งไปที่ Physical Review B

และผลงานที่กำลังจะนำส่งไปที่วารสารเพื่อพิจารณาการตีพิมพ์ 3 เรื่อง

- "Tunneling conductance in two-dimensional electron gas/s-wave superconductor junctions with Rashba spin-orbit coupling" (คาดว่าจะส่งไปที่ Physical Review B),
- "Tunneling conductance in two-dimensional electron gas/d-wave superconductor junctions with Rashba spin-orbit coupling" (คาดว่าจะส่งไปที่ Physical Review B) และ
- "Josephson Effect in two YBCO twinned Crystals"(คาดว่าจะส่งไปที่ Physica C)

Erosion of nodal Fermi spheres in nonequilibrium d-wave superconductors

M. F. Smith*

National Synchrotron Research Center, Nakhon Ratchasima, Thailand, 30000

P. Pairor

School of Physics, Institute of Science, Suranaree University of Technology, Nakhon Ratchasima, Thailand, 30000 (Received 3 October 2005; revised manuscript received 15 November 2005; published 29 December 2005)

The relaxation of a d-wave superconductor that has been driven out of equilibrium by an optical pulse is investigated. We consider a simple model for the low-energy nonequilibrium state, one in which the unpaired quasiparticles form Fermi spheres near the gap nodes, and calculate the decay rate of the quasiparticle population due to phonon-assisted recombination. In the high density limit for the photoinjected quasiparticles, the decay rate dn/dt is found to vary as $n^{5/2}$, which differs from the n^2 form commonly adopted in phenomenological models of the relaxation dynamics. In the low density limit, the decay is exponential. From numerical estimates, we determine that phonon-assisted recombination could play an important role over the picosecond time scales of current interest. We compare our results to pump-probe optical experiments on high T_C cuprates and find reasonable agreement for the decay rate in underdoped YBCO for low laser intensity.

DOI: 10.1103/PhysRevB.72.212513

Over the last several years, there have been numerous reports of femtosecond-resolved optical pump-probe measurements on high T_C cuprates in the superconducting state. The data have revealed intriguing properties of the picosecond dynamics, including unusual dependence on laser intensity, temperature and doping. For example, recent measurements on BSCCO (Ref. 8) uncovered a change in the qualitative behavior, of both the initial optical response and its subsequent decay, that occurs suddenly as a function of doping at a value close to that giving optimal T_C . Such data could have far-reaching implications for the study of the high T_C phase diagram. In order to interpret them, some understanding of the nonequilibrium state of the d-wave system that occurs shortly after the arrival of the pump pulse is

There is recent theoretical work aimed at understanding the dynamics of high T_C superconductors in the nonequilibrium state induced by a laser pulse. 10-13 The initial response of the system to a visible photon involves interband transitions and high-energy electron-electron intraband scattering in the strongly correlated system. In order to make some progress, people usually assume that after a sequence of fast high-energy relaxation processes, the system is left with a nonequilibrium distribution of low-energy (i.e., nodal) quasiparticles and phonons, the decay of which is governed by slower equilibration mechanisms. Of these slow relaxation rates, the conduction of heat out of the system by phonons that escape into the substrate and the recombination of quasiparticles into Cooper pairs are expected to be important. If the former rate is slowest, then heating is the only long-term effect of the pump laser (this is referred to as the T^* model and the strong bottleneck regime). 13,14 If the latter process is slowest, then the phonons and quasiparticles can achieve a common temperature while there remains an excess number of unpaired electrons. In a d-wave superconductor at a sufficiently low temperature, this corresponds to the presence of Fermi spheres of quasiparticles surrounding each node, described by Fermi distributions with a nonzero chemical potential $\mu(t)$ (this is called the μ^* model^{11,15} and the weak PACS number(s): 74.25.Gz, 74.40.+k, 74.72.-h

bottleneck regime). The final relaxation is the erosion of the Fermi spheres because of quasiparticle recombination and the return to the true equilibrium $\mu(\infty)=0$.

The two slow relaxation rates described above may be competitive in high T_C superconductors over time and temperature scales of interest. Nevertheless, it is important to characterize the dynamics expected when one or the other of these relaxation processes is dominant.

In this paper, we consider the μ^* model and study the decay of the nonequilibrium quasiparticle population due to phonon-assisted recombination. We obtain a rate equation that governs the population decrease (or, equivalently, the collapse of the nodal Fermi spheres), and estimate the time scale over which the decay occurs. The quasiparticle number is found to obey $dn/dt \propto -n^{5/2}$ in the limit that the Fermi gas at the nodes is degenerate (i.e., $\mu(t) \gg k_B T$). In the nondegenerate limit, which is expected for vanishing pump intensity, the decay is exponential with a time constant that is proportional to T^{-3} . The latter behavior has been observed in underdoped YBCO samples for very low laser intensity,⁶ and the time constant that we calculate is in reasonable agreement with the measured value. Our results suggest that phonon-assisted recombination can play an important role in the dynamic optical response over picosecond time scales for $T \leq T_C$, which contradicts earlier work¹ claiming that the recombination lifetime is of the order μ s at low measurable

We begin by obtaining an equation that governs the time evolution of the nodal Fermi sphere. The equation depends on the recombination lifetime for a single quasiparticle, which we calculate next. Finally, we determine the photoexcited quasiparticle density and compare our results to recent data before concluding.

In order to derive the rate equation for the nodal quasiparticle population, one may consider the lowest-order contribution of phonon-assisted recombination to the inverse lifetime of a quasiparticle with momentum ${\bf k}$ and a given spin, which is given by the Golden Rule as

$$\tau_{\mathbf{k}}^{-1} = 2\pi \sum_{\mathbf{k}'} g_{\mathbf{q}}^{2}(\mathbf{k}) L_{\mathbf{k},\mathbf{k}'}^{2} f_{\mathbf{k}'} (1 + n_{\mathbf{q}}) \, \delta(\omega_{\mathbf{q}} - E_{\mathbf{k}} - E_{\mathbf{k}'}), \quad (1)$$

where $\mathbf{q} = \mathbf{k} + \mathbf{k}'$, and $\omega_{\mathbf{q}}$, $E_{\mathbf{k}}$ is the phonon, quasiparticle energy, and $g_{\mathbf{q}}(\mathbf{k})$ is the electron-phonon matrix element. The Fermi and Bose functions are written as $f_{\mathbf{k}}$ and $n_{\mathbf{k}}$, respectively (note that $f_{\mathbf{k}} \equiv f(E_{\mathbf{k}})$ always refers to the Fermi function with μ included) and $L^2_{\mathbf{k},\mathbf{k}'} = (u_{\mathbf{k}}v_{\mathbf{k}'} - v_{\mathbf{k}}u_{\mathbf{k}'})^2$ is a BCS coherence factor. Equation (1) is valid only in the clean limit, that is when $k_BT \gg \gamma$, where γ is the constant impurity scattering rate of nodal quasiparticles. The total reduction in the population of quasiparticles due to such recombination is $\Sigma_{\mathbf{k},\sigma}f_{\mathbf{k}}\tau_{\mathbf{k}}^{-1}$.

An expression similar to Eq. (1), but with different occupation factors, holds for the rate of quasiparticle creation (phonon-induced pair breaking). By taking the difference of pair recombination and creation, one obtains the net recombination rate of quasiparticles as

$$\frac{dn}{dt} = -\left[1 - e^{-2\beta\mu}\right] \sum_{\mathbf{k}\sigma} f_{\mathbf{k}} \tau_{\mathbf{k}}^{-1}.$$
 (2)

The explicit μ -dependence of Eq. (2) accounts for the presence of photoinjected quasiparticles: When μ =0, the quasiparticles are in chemical equilibrium with the condensate and there is no net recombination.

If both T and μ are significantly smaller than the gap maximum Δ_0 , then Eq. (2) can be written as

$$\frac{dn}{dt} = -\frac{1}{\Delta_0^2} (1 - e^{-2\beta\mu}) \int d\epsilon \epsilon f(\epsilon) \tau^{-1}(\epsilon), \tag{3}$$

where the recombination lifetime $\tau^{-1}(\epsilon)$ is the average of $\tau_{\mathbf{k}}$ over the energy contour $E_{\mathbf{k}} = \epsilon$. Starting from Eq. (3), the number of quasiparticles n will be written in the conventional units of $4N_0\Delta_0$, where N_0 in the normal-state density of states. Also, we use $2\Delta_0 = v_2k_f$, where k_f is the length of the wave vector from the Brillouin zone center to the node and v_2 , which is the slope of the gap along the Fermi surface at the node, will always be the quantity for which experimental estimates are obtained.

The total number of quasiparticles in a CuO_2 plane n is related to the chemical potential μ by

$$n = \frac{1}{\Delta_0^2} \int_0^\infty d\epsilon \epsilon \frac{1}{e^{\beta(\epsilon - \mu)} + 1}.$$
 (4)

Taking the time derivative of this equation and comparing it to Eq. (3), we find that

$$\frac{d\mu}{dt} = -\frac{1}{k_B T} \frac{1 - e^{-2\beta\mu}}{\ln(1 + e^{\beta\mu})} \int d\epsilon \epsilon f(\epsilon) \tau^{-1}(\epsilon), \tag{5}$$

which is the desired equation of motion for the collapse of the Fermi sphere. The degenerate (nondegenerate) limit is the lowest-order term in μ/k_BT (k_BT/μ).

In obtaining Eq. (5), we assumed that the recombination rate $d\mu/dt$ is either much faster or much slower than the time variation of the temperature dT/dt. In either case, recombination tends to relax the quasiparticle distribution toward a Fermi function with μ =0 and temperature T. However, only

in the latter case will the value of T correspond to the measured temperature of the substrate T_s . The time-dependent part of the quasiparticle population is given by

$$\delta n = \frac{1}{4N_0 \Delta_0} \sum_{\mathbf{k}\sigma} \left[f_{\mathbf{k}}(\mu, T) - f_{\mathbf{k}}(0, T) \right]. \tag{6}$$

In this paper, we refer to δn as the number of photoexcited quasiparticles even though this terminology is not accurate when $T \neq T_s$.

Before proceeding, we address two possible concerns with the model. First, since phonons emitted by recombination can break pairs, one might expect that a nonequilibrium phonon distribution needs to be considered for consistency. For small μ/k_BT , the entire system is close to equilibrium so this effect is higher order in μ/k_BT . For large μ/k_BT , it can be neglected, since it is far more probable that a phonon emitted from recombination will be absorbed in quasiparticle scattering than in pair breaking. To see this, one may consider that for large μ/k_BT quasiparticles fill the states with energy less than μ and an emitted phonon has energy between 0 and 2μ . Scattering can occur for arbitrary phonon energy since quasiparticles are available at the Fermi surface. Pair breaking requires a minimum energy of 2μ in order for there to be unfilled states to accept the created quasiparticles, which leaves no phase space for single-phonon recombination creation at T=0. The rate for pair breaking is clearly higher order in k_BT/μ in the degenerate limit, so it is not unreasonable to assume that the phonons are in equilibrium (at the instantaneous temperature T). Second, we are considering phonon-assisted recombination but not quasiparticlequasiparticle recombination processes (i.e., Auger-type processes that, at low energy, are equivalent to recombination with emission of a spin fluctuation). 16,17 Several authors, e.g., Refs. 6 and 11, have pointed out that quasiparticlequasiparticle recombination cannot dissipate energy from the system and thus cannot relax it to true equilibrium. However, it could relax a μ^* -distribution toward a T^* distribution, and give a transient response due to a difference in the optical properties of these models.¹¹ Although both processes may contribute, we consider only the phonon-assisted process for simplicity. Some aspects of quasiparticle-quasiparticle recombination have been treated previously.¹²

We now use Eq. (1) to calculate $\tau(\epsilon)$ in the clean limit, and its dependence on μ , and insert it into Eq. (5). (We also study the dirty limit by calculating the electron self-energy evaluated to lowest order in the electron-phonon interaction with a constant scattering rate γ included for electrons, which is appropriate when $\mu \ll k_B T \ll \gamma$, see Ref. 18.)

The momentum integral in Eq. (1) can be simplified by considering the energy-conserving δ -function. For $\mu + k_B T \ll \omega_D$, where ω_D is the Debye frequency, only processes involving acoustic phonons and quasiparticles at opposite nodes are possible (all others are suppressed by a factor $e^{-\beta(\omega_D-\mu)}$). The condition for energy conservation in the opposite node-acoustic phonon case is illustrated in Fig. 1. The fact that $v_2, v_f \gg c_s$, where c_s is the speed of sound for any acoustic mode, implies that energy conservation can only be satisfied if the phonon wave vector has a large component in the direction normal to the CuO₂ plane. To a good approxi-

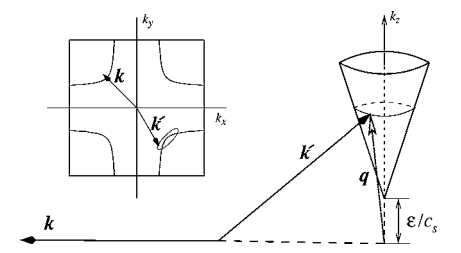


FIG. 1. Low-energy phonon-assisted recombination in *d*-wave superconductors viewed along the (001) and (110) directions. A quasiparticle, with wave vector \mathbf{k} and energy $\boldsymbol{\epsilon}$, recombines with a quasiparticle \mathbf{k}' and emits a phonon \mathbf{q} . To conserve energy and momentum, \mathbf{q} and \mathbf{k}' must lie on the surface of the cone. The cone is narrow (it has slopes v_f/c_s and v_2/c_s along and into the page), so the phonon wave vector is nearly parallel to the k_z axis. The figure is approximate.

mation, the phonon energy can be taken to be $\omega_{\bf q} = c_s |q_z|$. (The argument implies that for large $\beta\mu$ the nonequilibrium distribution of phonons emitted from recombination is unusual since phonons propagate along nearly the same line.) This simplification makes trivial the integrals along the inplane energy contours.

We calculate $\tau^{-1}(\epsilon)$ using the procedure described above and the electron-phonon matrix element from Ref. 17 and obtain

$$\tau^{-1}(\epsilon) = \frac{N_0 \alpha_c}{\Delta_0 c_s} F^2(k_f) \int_0^\infty dx x (x + \epsilon) f(x) [1 + n(\epsilon + x)], \quad (7)$$

where α_c is the *c*-axis lattice constant and $F^2(k_f)$ is a constant with the dimensions of energy:

$$F^{2}(k_{f}) = \frac{g^{2} \eta^{2}}{2MNc_{s}^{2}}.$$
 (8)

M is the mass of the unit cell, N is the total number of unit cells, and g is the electron-phonon coupling energy, (which is equal to the derivative of a hopping matrix element t, in the effective single-band Hamiltonian, with respect to bond length multiplied by the lattice constant). The dimensionless factor η^2 comes from the electron-phonon matrix element, we estimate that η^2 is of order 10^{-2} (this is discussed in a footnote in Refs. 19 and 20).

In the degenerate limit $\mu \gg k_B T$, the integral in Eq. (7) is equal to $\mu^2(\mu/3 + \epsilon/2)$. After substituting this value into Eq. (5), evaluating the integral for $\mu \gg k_B T$, and expressing the result in terms of quasiparticle number, one obtains

$$-\frac{dn}{dt} = \frac{2\Lambda}{3} n^{5/2}, \quad \mu \gg k_B T, \tag{9}$$

which has the solution

$$\delta n(t) = n(t) = \frac{n(0)}{[1 + \Lambda n^{3/2}(0)t]^{2/3}}, \quad \mu \gg k_B T.$$
 (10)

The relaxation is similar to, but distinguishable from, second-order kinetics for which $dn/dt \propto -n^2$.

The time constant Λ^{-1} is given by

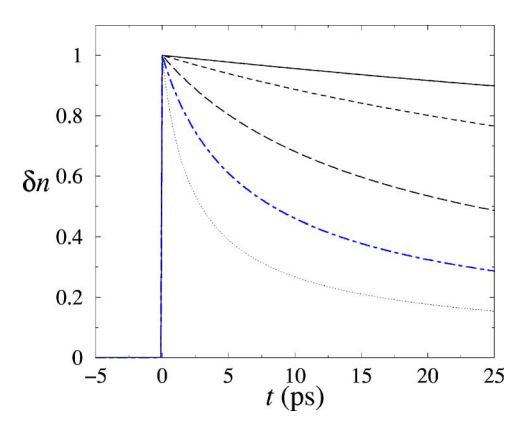


FIG. 2. (Color online) The population of photoexcited quasiparticles δn in the degenerate limit, given by Eq. (10). The normalized curves correspond to different values of the initial population $\delta n(0)$. In the top curve $\delta n(0) = n_0 \equiv 0.004$; and the rest, in descending order, are for $\delta n(0) = 2n_0$, δn_0 , δn_0 , and δn_0 . Superconductivity breaks down at roughly δn_0 (according to Ref. 10).

$$\Lambda = \frac{\sqrt{8}\Delta_0^2 \alpha_c}{c_s} \left(\frac{N_0 g^2 \eta^2}{2NMc_s^2} \right). \tag{11}$$

Using experimental values for cuprates (the main variation between different cuprate materials comes from the gap magnitude), we obtain Λ^{-1} =1-10 fs.

For sufficiently long times, the condition $\mu > k_B T$ must be violated. After this, the spread of the quasiparticles in **k** space is no longer affected by μ . During this final stage of relaxation, recombination occurs between one of the few remaining photoexcited quasiparticles and one of the much larger number of thermal quasiparticles [if $\mu(t=0) \ll k_B T$, then this is the only stage of relaxation in our model]. Repeating the calculations above for $\mu \ll k_B T$, we find that the nonequilibrium quasiparticle population follows:

$$\delta n(t) = \delta n(0)e^{-\Lambda(T)t}, \quad \mu \ll k_B T,$$
 (12)

where the time constant is given as

$$\Lambda(T) = \frac{3}{\ln(2)\sqrt{8}} \left(\frac{k_B T}{\Delta_0}\right)^3 \Lambda. \tag{13}$$

All of the preceding results are for the clean limit $\gamma \ll k_B T$, μ . In the dirty nondegenerate limit, the result is Eqs. (12) and (13) with one of the powers of $(k_B T/\Delta_0)$ replaced by $(\gamma/2\Delta_0)\ln(\Delta_0/\gamma)$.

We will briefly compare our results to recent experiments by making the tentative assumption that the differential reflectance $\Delta R/R$, measured at optical frequency, decays with time in proportion to the number of remaining quasiparticles. For high pump intensity Φ and low temperature, the degenerate limit, Eq. (10), may be achieved. In Fig. 2, we plot n in the degenerate limit, as given by Eq. (10). We have chosen values for n(0) (see caption of Fig. 2) such that the evolution occurs over the time scale probed by recent experiments, which is 10 ps, and have used η =0.1. The behavior is qualitatively similar to that seen in the optical response of underdoped cuprates, but the observed decay rate is proportional to n(0) rather than $n^{3/2}(0)$. This discrep-

ancy might point to the importance of a phonon-heat bottleneck, i.e., of the dT/dt term discussed above, for highintensity measurements.¹³

For low intensity, we expect that the nondegenerate limit, Eqs. (12) and (13), is valid. In measurements made on ortho-II YBCO, Segre *et al.*⁶ observed that the low-intensity decay rate is proportional to T^3 , in agreement with Eq. (13). If we use Δ_0 =66 meV for Ortho-II (Ref. 21) and η^2 =0.1, then our result for the decay rate matches that extracted from the data. This value of η^2 is larger by a factor of 10 than the rough estimate given above, but is not an implausible value. This is suggestive that, for low enough pump intensity, phonon-assisted recombination may determine the time evolution of the optical response on the picosecond time scale.

The fact that our low-T recombination lifetime is orders of magnitude smaller than that calculated by Feenstra¹ should be discussed. Feenstra claimed that, because the quasiparticle velocity is larger than the sound velocity, energy momentum cannot be conserved in recombination processes involving acoustic phonons and quasiparticles at opposite nodes (which results in exponentially slow recombination at low T). This conclusion is only true if the phonons are constrained to propagate along the CuO₂ plane. For *in-plane* phonons, energy momentum is conserved when the phononwave vector is zero, i.e., when both quasiparticles lie exactly at the nodes, but cannot be conserved if quasiparticles are displaced from the nodes in any direction, since the quasiparticle energy increases more quickly than the phonon en-

ergy. However, if the emitted phonon propagates along the c axis, then it can carry away energy without any change in the in-plane momentum. (The quasiparticles can have any momentum along the c axis since they are assumed to be confined in real space.) By bending the phonon wave vector away from the c axis, energy conservation involving phonons and opposite-node quasiparticles is satisfied, as in Fig. 1. Thus, in a correct treatment in which phonons propagating out of the ${\rm CuO}_2$ plane are considered, the lifetime for low-temperature quasiparticle recombination in equilibrium is found to be of the order 10-100 ps at 10 K, as above.

In summary, we have studied the effect of phonon-assisted recombination on the relaxation of a *d*-wave superconductor in a low-energy nonequilibrium state. The time evolution of the nodal Fermi sphere, which contains the photoexcited quasiparticles prior to recombination, has been calculated in both the degenerate and nondegenerate limits. There is good agreement between the result for the nondegenerate limit and observations made on underdoped YBCO with low laser intensity. The degenerate limit results may be useful toward understanding high-intensity data, although it is likely that the effects of laser heating and the associated phonon heat bottleneck are important in this case. Here, our work may complement phenomenological rate-equation approaches in which terms associated with both phonon heat conduction and recombination are included.¹³

One of the authors (P.P.) acknowledges support from the Thailand Research Fund (Grant No. RMU 4880012).

^{*}Electronic address: msmith@nsrc.or.th

¹B. J. Feenstra, J. Schutzmann, D. van der Marel, R. Perez-Pinaya, and M. Decroux, Phys. Rev. Lett. **79**, 4890 (1997).

²P. Gay, D. C. Smith, C. J. Stevens, C. Chen, G. Yang, S. J. Abell, D. Z. Wang, J. H. Wang, Z. F. Ren, and J. F. Ryan, J. Low Temp. Phys. **117**, 1025 (1999).

³D. C. Smith, P. Gay, C. J. Stevens, D. Z. Wang, J. H. Wang, Z. F. Ren, and J. F. Ryan, J. Low Temp. Phys. **117**, 1059 (1999).

⁴D. C. Smith, P. Gay, D. Z. Wang, J. H. Wang, Z. F. Ren, and J. F. Ryan, Physica C **341**, 2219 (2000).

⁵J. Demsar, R. Hudej, J. Karpinski, V. V. Kabanov, and D. Mihailovic, Phys. Rev. B **63**, 054519 (2001).

⁶G. P. Segre, N. Gedik, J. Orenstein, D. A. Bonn, R. Liang, and W. N. Hardy, Phys. Rev. Lett. 88, 137001 (2002).

⁷N. Gedik, P. Blake, R. C. Spitzer, J. Orenstein, R. Liang, D. A. Bonn, and W. N. Hardy, Phys. Rev. B **70**, 014504 (2004).

⁸N. Gedik, M. Langner, J. Orenstein, S. Ono, Y. Abe, and Y. Ando, Phys. Rev. Lett. **95**, 117005 (2005).

⁹P. Kusar, J. Demsar, D. Mihailovic, and S. Sugai, Phys. Rev. B 72, 014544 (2005).

¹⁰E. J. Nicol and J. P. Carbotte, Phys. Rev. B **67**, 214506 (2003).

¹¹J. P. Carbotte and E. Schachinger, Phys. Rev. B **70**, 014517 (2004).

¹²P. C. Howell, A. Rosch, and P. J. Hirschfeld, Phys. Rev. Lett. **92**, 037003 (2004).

¹³ V. V. Kabanov, J. Demsar, and D. Mihailovic, Phys. Rev. Lett. 95, 147002 (2005).

¹⁴W. H. Parker, Phys. Rev. B **12**, 3667 (1975).

¹⁵C. S. Owen and D. J. Scalapino, Phys. Rev. Lett. **28**, 1559 (1972).

¹⁶S. M. Quinlan, D. J. Scalapino, and N. Bulut, Phys. Rev. B 49, 1470 (1994).

¹⁷ M. B. Walker and M. F. Smith, Phys. Rev. B **61**, 11285 (2000).

¹⁸The rate equation, Eq. (5), is also valid in the dirty limit as long as the appropriate expression for the scattering rate $\tau_{\mathbf{k}}^{-1}$ is inserted. This can be shown by taking the difference of terms in the imaginary part of the self-energy that correspond to quasiparticle pairing and recombination. For brevity, only the clean-limit derivation [i.e., going from Eq. (1) to Eq. (5)] is shown above.

¹⁹An estimate of the coupling constant g for modes that stretch nearest-neighbor bonds has been obtained, from thermal conductivity data, but those associated with next-nearest neighbors, g' and out-of-plane neighbors g_{\perp} are unknown. By considering modes, we determine that $\eta \approx \max(g_{\perp}/g, [c_s/v_2]\mathbf{g}'/\mathbf{g}, [c_s/v_2]^2)$. If we roughly approximate $g'/g \approx t'/t$, then we get $\eta^2 \approx 10^{-2}$ for the second estimate. The third estimate gives $\eta^2 \approx 10^{-3}$, which sets a lower bound.

²⁰M. F. Smith, J. Paglione, M. B. Walker, and L. Taillefer, Phys. Rev. B **71**, 014506 (2005).

²¹ M. Sutherland, D. G. Hawthorn, R. W. Hill, F. Ronning, S. Wakimoto, H. Zhang, C. Proust, E. Boaknin, C. Lupien, L. Taillefer, R. Liang, D. A. Bonn, W. N. Hardy, R. Gagnon, N. E. Hussey, T. Kimura, M. Nohara, and H. Takagi, Phys. Rev. B 67, 174520 (2003).

Tunneling conductance of a two-dimensional electron gas with Rashba spin-orbit coupling

B. Srisongmuang and P. Pairor*

School of Physics, Institute of Science,

Suranaree University of Technology, Thailand

M. Berciu

Department of Physics and Astronomy,
University of British Columbia, British Columbia, Canada
(Dated: August 29, 2008)

Abstract

We theoretically studied the in-plane tunneling spectroscopy of the hybrid structure composed of a metal and a two-dimensional electron gas with Rashba spin-orbit coupling. We found that the energy spacing between two distinct features in the conductance spectrum can be used to directly measure the Rashba energy. We also considered the effect that varying the probability of spin-conserving and spin-flip scattering at the interface has on the overall conductance. Surprisingly, an increase in interface scattering probability can actually result in increased conductance under certain conditions. Particularly, in the tunneling regime, an increase in spin-flip scattering probability enhances the conductance. It is also found that the interfacial scattering greatly affects the spin polarization of the conductance in metal, but hardly affects that in the Rashba system.

PACS numbers: 73.40.Ns, 73.40.Gk, 73.23.-b, 72.25.Dc, 72.25.Mk

^{*}Electronic address: pairor@sut.ac.th

I. INTRODUCTION

Structural inversion asymmetry of the confining electrostatic potential results in an intrinsic spin-orbit coupling of electrons in a two-dimensional (2D) electron gas (EG), which can be described by the Rashba Hamiltonian: [1–3]

$$\mathcal{H} = \frac{\vec{p}^2}{2m^*} - \lambda \hat{j} \cdot (\vec{p} \times \vec{\sigma}) \tag{1}$$

where \vec{p} is 2D momentum, m^* is the electron effective mass, \hat{j} is the direction perpendicular to the plane of motion, λ is the spin-orbit coupling parameter, which can be tuned by applying an external gate voltage perpendicular to the 2D plane, and the components of $\vec{\sigma}$ are the Pauli spin matrices. The spin-orbit interaction lifts the spin degeneracy and causes the original parabolic energy spectrum to split into two branches: $E_{\vec{k},\pm} = \frac{\hbar^2 k^2}{2m^*} \pm \hbar \lambda k$, where k is the magnitude of the wave vector. The density of states of this system is the same as that of the 2D free electron gas for all energies higher than the crossing point of the two branches. However, at the bottom of the band, the density of states has $E^{-\frac{1}{2}}$ van Hove singularity because the minus branch has an annular minimum for $k = k_0 \equiv m^* \lambda / \hbar$ instead of a single-point minimum as in the free electron gas. These properties lead to interesting phenomena, like the spin hall effect (see e.g. Ref. 4 for a review), and to applications in spintronics (see e.g. Ref. 5 for a review).

The Rashba effect has been seen in many systems like semiconductors, semiconductor heterostructures, and surface alloys. Several techniques have been used to study the spin-split states in these systems, for example, electron spin resonance, the Shubnikov-de Haas oscillations, angle-resolved photoemission, and scanning tunneling spectroscopy. Electron spin resonance was one of the first techniques to confirm the existence of the Rashba spin-split states in bulk semiconductors with the absence of inversion symmetry in the crystal structure [6, 7]. From magneto-transmission of far infrared radiation, electron spin resonance signal can be detected and used to obtain the Rashba parameter.

The Shubnikov-de Haas oscillations [8, 9] is another technique used to measure the Rashba parameter in semiconductor systems. The presence of the spin splitting at the Fermi energy leads to beating in the oscillations and the Rashba energy can be deduced from the position of the beating node. However, this technique tends to provide an overestimate of the Rashba energy, because it is done in the presence of magnetic field and hence includes the effect of the Zeeman spin splitting. [10]

Angle-resolved photoemission spectroscopy and scanning tunneling microscopy are used in surface alloys. The former technique is utilized mainly to obtain the energy dispersion and the Fermi surface map, from which the effective mass, the magnitude of the band splitting, and hence the Rashba spin-orbit coupling energy, $E_{\lambda} \equiv \hbar^2 k_0^2/(2m^*)$, can be extracted.[11–15] In the latter technique, the electric current is driven through a sharp tip perpendicular to the 2D plane and the differential conductance (dI/dV) spectrum can be obtained. One can deduce the Rashba energy by fitting the dI/dV spectrum to the local density of states of the 2DEG.[16] In both cases, to obtain information about the Rashba spin-orbit coupling, extensive data fitting is needed.

In this article, we propose a way to measure the spin-splitting energy more directly from experimental data, using in-plane tunneling spectroscopy. In this technique, the Rashba energy equals the energy difference between two features in the conductance spectrum. The required condition for the measurement is that the energy resolution of the tunneling spectra is at least of the order of the Rashba energy itself. This condition can be easily achieved in modern tunneling measurements.[17]

An intriguing property of 2DEG with Rashba spin-orbit interaction is spin-dependent transport. Many theoretical investigations have shown that both electric and spin transport in hybrid structures between the Rashba system and various materials, like metals,[18–20] ferromagnets,[20–23] and superconductors,[24] are affected by the strength of the spin-orbit coupling,[18–24] the inequality of the effective masses,[18, 19, 22, 23] and the transparency of the interface.[21, 22, 24] However, in these previous studies, only spin-conserving interfacial scattering was considered.

In principle, one can introduce interfacial spin-flip scattering in these systems by embedding magnetic impurities in the insulating layer, or at the interface. The interaction between the tunneling electrons and localized spins can give rise to spin-flip tunneling [25–29]. The equations describing the spin-up and spin-down spin states in the presence of spin-flip scattering are coupled, and one expects interesting consequences of this. For instance, in the study of the tunneling conductance spectrum of a semiconductor/superconductor junction,[30] the non-spin-flip scattering, when present alone, is found to suppress the Andreev reflection process and hence the subgap conductance as expected. However, when the spin-flip potential scattering is also present at the interface, their combined effect surprisingly enhances the subgap conductance,[30]

Here, we also consider how the scattering potential barrier affects both the conductance spectrum and the spin polarization of the conductance of a junction consisting of a metal and a Rashba system. As in previous work by Zutic and Das Sarma [30], we find that the conductance spectrum, which is usually suppressed in the presence of the interfacial scattering, can be enhanced by the combined effect of both types of scattering. We also find that the spin polarizations of conductance of the metal and the Rashba system are not equal. The spin polarization in the latter depends weakly on interfacial scattering, while that in the former is greatly affected. This suggests that a spin imbalance in the Rashba system is robust against variation in the quality of the junction interface.

This article is organized as follows: in the next section, we describe the theoretical method and assumptions. In Section III, we provide the results and discussion. Our conclusions are presented in the last section.

II. METHOD OF CALCULATION AND ASSUMPTIONS

We represent our junction by an infinite 2D system which lies on xz plane, where the metal and the Rashba system occupy the x < 0 and x > 0 region respectively. The two regions are separated by a flat interface at x = 0. The interfacial scattering is modeled by a Dirac delta function potential. [31] We consider ballistic transport in our junction. In the one-band effective-mass approximation, we describe our system by the following Hamiltonian:

$$\mathcal{H} = \left(\hat{p} \frac{1}{2m(x)} \hat{p} + V(x, z)\right) \mathcal{I} + \mathcal{H}_R(x). \tag{2}$$

Each term is the 2×2 matrix acting on spinor states. $\hat{p} = -i\hbar \left(\hat{x} \frac{\partial}{\partial x} + \hat{z} \frac{\partial}{\partial z}\right)$. The effective mass m(x) is position-dependent, i. e., $[m(x)]^{-1} = m^{-1}\Theta(-x) + (m^*)^{-1}\Theta(x)$, where m and m^* are effective electron masses in the metal and the Rashba system respectively, and $\Theta(x)$ is the Heaviside step function. V(x,z) is also a position-dependent function and is modeled by the expression

$$V(x,z) = H\delta(x) + E_0\Theta(x) - E_F\Theta(-x)$$
(3)

where H represents the scattering potential at the interface, E_0 is the energy difference between the Fermi level and the bottom of the plus branch (see FIG. 1), and $E_F = \hbar^2 q_F^2/(2m)$ is the Fermi energy of the metal. We assume that E_F is much larger than E_0 . The diagonal

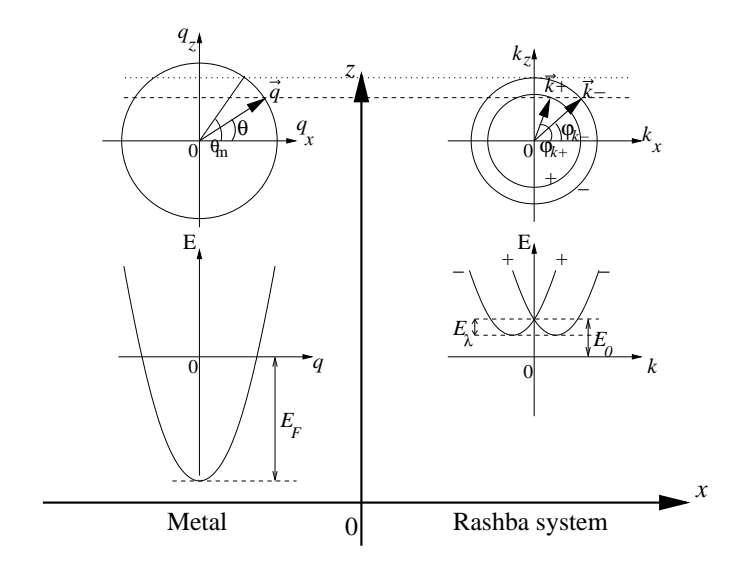


FIG. 1: The top sketches are the energy contours of the electron in the metal (left) and the Rashba system (right). The angles θ and φ are defined as those between the x axis and the momenta of electrons in the metal and the Rashba system respectively. The dashed line that crosses both sides shows the momentum states with the same k_z . The dotted line is the line of the maximum value of k_z , which defines the maximum incident angle θ_m . The lower sketches are the corresponding energy spectra (E vs the magnitude of momentum). E_F and E_0 are the metal Fermi energy and the off-set energy of the Rashba system respectively.

elements of H, $H_{\uparrow\uparrow}$ and $H_{\downarrow\downarrow}$ correspond to the non-spin-flip scattering potential characterizing the quality of the junction, while $H_{\uparrow\downarrow}=H_{\downarrow\uparrow}$ describe spin-flip scattering. [30] The Rashba Hamiltonian is written as [32]

$$\mathcal{H}_R(x) = \frac{\hat{j}}{2} \cdot [\lambda(x) (\vec{p} \times \vec{\sigma}) + (\vec{p} \times \vec{\sigma}) \lambda(x)]$$
 (4)

where $\lambda(x) = \lambda \Theta(x)$.

From the Hamiltonian, one can obtain the eigenstates and eigenenergy for the electrons in each region as follows. In the x < 0 region, the energy spectrum is

$$E(q) = \frac{\hbar^2 q^2}{2m} - E_F \tag{5}$$

where $q = \sqrt{q_x^2 + q_z^2}$ is the magnitude of the 2D momentum of the electrons. In the x > 0 region, the eigenenergy is obtained as

$$E^{\pm}(k) = \frac{\hbar^2}{2m^*} \left[(k \pm k_0)^2 - k_0^2 \right] + E_0 \tag{6}$$

where $k = \sqrt{k_x^2 + k_z^2}$ is the magnitude of the 2D momentum and $k_0 = m^* \lambda / \hbar$. FIG. 1 shows the energy spectra and energy contours of the excitations in both sides of the junction.

The wave function of the electrons with energy E in the metal is written as a linear combination of incident momentum state and a reflected state of the same energy and k_z . Because electron spins are not polarized in metal, there are two equally likely incident spin states, opposite in direction to each other, with the spin quantization axis arbitrary. Any choice of two incident states with opposite spin orientations will lead to the same result for total conductance spectrum. Here, for simplicity we choose the spins of the incident electrons be along the z-axis. The two corresponding electron wave functions in the metal are written as:

$$\Psi_{M}^{(1)}(x,z) = \left(\begin{bmatrix} 1\\0 \end{bmatrix} e^{iq_{x}x} + \begin{bmatrix} b_{1\uparrow}\\b_{1\downarrow} \end{bmatrix} e^{-iq_{x}x} \right) e^{ik_{z}z}
\Psi_{M}^{(2)}(x,z) = \left(\begin{bmatrix} 0\\1 \end{bmatrix} e^{iq_{x}x} + \begin{bmatrix} b_{2\uparrow}\\b_{2\downarrow} \end{bmatrix} e^{-iq_{x}x} \right) e^{ik_{z}z}$$
(7)

where the $b_{i\sigma}$ are the amplitudes of reflection of electrons with spin σ for incident state with spin-up (i = 1) and spin-down (i = 2). $q_x = q \cos \theta$ and $k_z = q \sin \theta$, where θ is the angle between \vec{q} and the x axis. The magnitude of the momentum, q, depends on energy as

$$q = \sqrt{\frac{2m}{\hbar^2}(E + E_F)} \tag{8}$$

Similarly, in the Rashba system, the wave function is obtained as a linear combination of two outgoing eigenstates of the same energy and k_z :

$$\Psi_{RS}^{(i)}(x,z) = \begin{pmatrix} c_{i+} \begin{bmatrix} \cos\frac{\varphi_{k+}}{2} \\ \pm\sin\frac{\varphi_{k+}}{2} \end{bmatrix} e^{\mp ik_x^+ x} \\
+ c_{i-} \begin{bmatrix} \sin\frac{\varphi_{k-}}{2} \\ \cos\frac{\varphi_{k-}}{2} \end{bmatrix} e^{ik_x^- x} \end{pmatrix} e^{ik_z z} \tag{9}$$

where i = 1, 2 refer to the wave functions of the Rashba system corresponding to the two cases of spin orientations of incident electrons, $\varphi_{k^{\pm}}$ are the angles between \vec{k}^{\pm} and the x axis. For $E > E_0$, c_{i+} and c_{i-} are the transmission amplitudes of electrons to plus and minus branch respectively. When $E < E_0$, c_{i+} and c_{i-} refer to the transmission amplitudes of electrons to states with smaller and larger k of the minus branch respectively. The upper

and lower signs in the first term of Eq. (9) are for $E \leq E_0$ and $E > E_0$ respectively. $k_x^{\pm} = k^{\pm} \cos \varphi_{k^{\pm}}$ and $k_z = k^{\pm} \sin \varphi_{k^{\pm}}$, where the magnitudes of the momenta, k^{\pm} , depend on energy as

$$k^{-} = k_0 + \sqrt{k_0^2 + \frac{2m^*}{\hbar^2}(E - E_0)}$$
 (10)

$$k^{+} = \pm \left(k_{0} - \sqrt{k_{0}^{2} + \frac{2m^{*}}{\hbar^{2}}(E - E_{0})}\right)$$
(11)

Again, in Eq. (11) the upper and lower signs are for $E \leq E_0$ and $E > E_0$ respectively. The relationship between the angles $\varphi_{k^{\pm}}$ and θ is

$$k^{\pm} \sin \varphi_{k^{\pm}} = q \sin \theta. \tag{12}$$

We can obtain the probability amplitudes $b_{i\uparrow}, b_{i\downarrow}, c_{i+}$ and c_{i-} from the following matching conditions that ensure probability conservation. [32]

$$\Psi_M^{(i)}(x=0,z) = \Psi_{RS}^{(i)}(x=0,z) \equiv \Psi_0^{(i)}, \tag{13}$$

$$\left(\frac{m}{m^*} \frac{\partial \Psi_{RS}^{(i)}}{\partial x} - \frac{\partial \Psi_M^{(i)}}{\partial x} \right) \bigg|_{x=0} = \left(2q_F \mathcal{Z} - i \frac{m}{m^*} k_0 \sigma_z \right) \Psi_0^{(i)}, \tag{14}$$

where $\mathcal{Z} = mH/(\hbar^2 q_F)$. The diagonal elements of \mathcal{Z} will henceforth be referred to as $Z_u \equiv Z_{\uparrow\uparrow}$ and $Z_d \equiv Z_{\downarrow\downarrow}$, while the off-diagonal element will be denoted by $Z_F = Z_{\uparrow\downarrow} = Z_{\downarrow\uparrow}$. In what follows the spin flip term Z_F will be responsible for the enhancement of a feature at the branch-crossing point in the conductance spectrum.

The particle current density along the x direction is obtained from

$$j_x^p = \frac{1}{2} \left[\Psi^{\dagger}(x) \hat{v}_x \Psi(x) + (\hat{v}_x \Psi(x))^{\dagger} \Psi(x) \right], \tag{15}$$

where $\Psi(x)$ is the spinor wave function, and $\hat{v}_x = d\hat{x}/dt = i \left[\mathcal{H}(x), \hat{x}\right]/\hbar$. From the current density, the reflection and transmission probabilities can be obtained:

$$R_{i\uparrow} = |b_{i\uparrow}|^2 \tag{16}$$

$$R_{i\downarrow} = |b_{i\downarrow}|^2 \tag{17}$$

$$T_{i+} = \frac{m}{m^*} |c_{i+}|^2 \left(\frac{\mp k_x^+ + k_0 \cos \varphi_{k_x^+}}{q_x} \right)$$
 (18)

$$T_{i-} = \frac{m}{m^*} |c_{i-}|^2 \left(\frac{k_x^- - k_0 \cos \varphi_{k_x^-}}{q_x} \right)$$
 (19)

where $R_{i\uparrow}$, $R_{i\downarrow}$ are the reflection probabilities to spin-up and spin-down states, and T_{i+} , T_{i-} are the corresponding transmission probabilities. Also, the upper and lower signs in T_{i+} are for $E \leq E_0$ and $E > E_0$ respectively. As mentioned earlier, the matching conditions ensure that $R_{i\uparrow} + R_{i\downarrow} + T_{i+} + T_{i-} = 1$.

Since the electric current is independent of x, we consider the electric current density in the metal for simplicity. It can be written as a function of applied voltage V as follows.

$$j_x^e(eV) = \sum_{q_x > 0, q_z} ev_x \sum_{i=1}^2 (1 - R_{i\uparrow} - R_{i\downarrow}) \times [f(E(q) - eV) - f(E(q))]$$
(20)

where e is the electron charge, v_x is the x component of the electron group velocity, and f(E) is Fermi distribution function. The sum over the spins of incident electron assumes that both are equally probable in metal.

By changing the integration variable and setting temperature to zero for simplicity, one can obtain the expression for the electric current as

$$j_x^e(eV) = \frac{e}{h} \frac{\mathcal{L}^2 q_F}{2\pi} \int_0^{eV} dE \int_{-\theta_m}^{\theta_m} d\theta \cos \theta$$
$$\times \sqrt{1 + \frac{E}{E_F}} \sum_{i=1}^2 (1 - R_{i\uparrow} - R_{i\downarrow})$$
(21)

where \mathcal{L}^2 is the area of the metal and θ_m is the maximum angle of the incident electrons from the metal (see FIG. 1): $\theta_m = \sin^{-1}(k^-(E)/q(E))$. Thus, the differential conductance $G(V) \equiv dj_x^e/dV$ at zero temperature is

$$G(V) = \frac{e^2}{h} \frac{\mathcal{L}^2 q_F}{2\pi} \int_{-\theta_m}^{\theta_m} d\theta \cos \theta \sqrt{1 + \frac{eV}{E_F}}$$

$$\times \sum_{i=1}^{2} (1 - R_{i\uparrow} - R_{i\downarrow})$$
(22)

The finite temperature will smear the features in the conductance spectrum but will not change their positions (assuming that the strength of the Rashba spin-orbit coupling does not depend on temperature).

In order to investigate the spin imbalance due to the tunneling current in both metal and Rashba system, we consider the spin polarization of conductance $\mathcal{P}(E)$ defined as the difference in the number of spin carriers crossing a plane normal to x in unit time, normalized

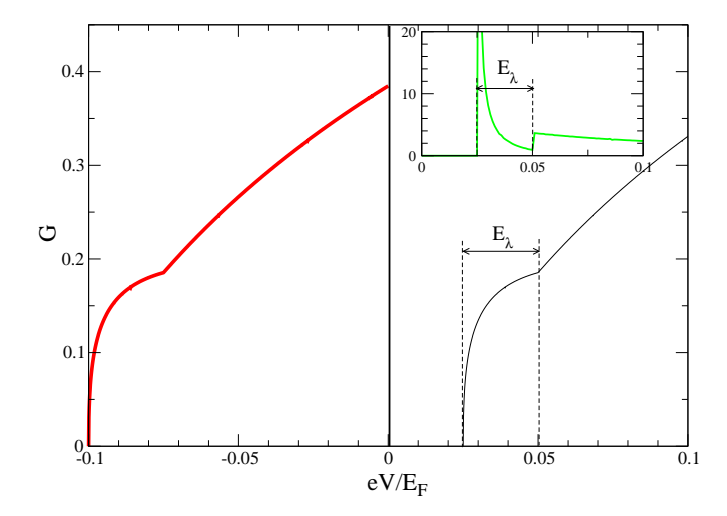


FIG. 2: (color online) The plot on the left is the conductance spectrum in the case where the energy band of the Rashba system is partly occupied $(E_0 = -0.075E_F)$ and on the right is the plot in the case where the band is unoccupied $(E_0 = 0.05E_F)$. The derivative of the conductance spectrum on the right (dG/dV) is shown in the inset. Z and Z_F are set equal to zero. $m/m^* = 10$ and $k_0 = 0.05q_F$.

to the total particle current at energy E:

$$\mathcal{P}(E) = \frac{\sum_{q_x>0,q_z}' \left(j_{x,\uparrow}^p - j_{x,\downarrow}^p\right)}{\sum_{q_x>0,q_z}' \left(j_{x,\uparrow}^p + j_{x,\downarrow}^p\right)},\tag{23}$$

where $j_{x,\sigma}^p$ is the particle current density with spin σ . The \sum' indicates that the summations are over q_x, q_z with a specific value of energy E. In metal, this spin polarization of the conductance can be written in terms of the reflection probabilities as

$$\mathcal{P}_M(E) = \frac{\int_{-\theta_m}^{\theta_m} d\theta \, \cos\theta \, \sum_{i=1}^2 \left(-R_{i\uparrow} + R_{i\downarrow} \right)}{\int_{-\theta_m}^{\theta_m} d\theta \, \cos\theta \, \sum_{i=1}^2 \left(1 - R_{i\uparrow} - R_{i\downarrow} \right)},\tag{24}$$

and in the Rashba system it can be written in terms of the transmission probabilities as

$$\mathcal{P}_{RS}(E) = \frac{\int_{-\theta_m}^{\theta_m} d\theta \, \cos\theta \, \sum_{i=1}^2 \left(T_{i+} \cos\varphi_{k^+} - T_{i-} \cos\varphi_{k^-} \right)}{\int_{-\theta_m}^{\theta_m} d\theta \, \cos\theta \, \sum_{i=1}^2 \left(T_{i+} + T_{i-} \right)}.$$
 (25)

As can be seen, $\mathcal{P}(E)$ measures the relative difference in the net number of the carriers with spin-up and spin-down.

III. RESULTS AND DISCUSSION

In this section, we discuss the effect of the interfacial scattering on the differential conductance spectra and the spin polarization of the conductance on each side of the junction. In all plots, for the purpose of illustration, we set $m/m^* = 10$ and $k_0 = 0.05q_F$, which corresponds to typical experimental values in metal/Rashba system junctions. The main results are not affected by the choice of these parameters.

Two conductance plots for two values of E_0 are shown in FIG. 2. Positives values of E_0 means the energy spectrum of the Rashba system is unoccupied and the positive eV across the junction will cause the current to flow from the metal to the Rashba system. As can be seen, when the energy spectrum of the Rashba system is partly occupied ($E_0 = -0.075E_F$), the results are identical in shape to those in the unoccupied case ($E_0 = +0.05E_F$), but the applied voltage eV across the junction has to be negative. There are two main features at the voltage corresponding to the bottom and the branch-crossing of the energy band. The distance between them depends on E_{λ} , which is the quantity of interest. The value of E_0 is not important, i. e., changing E_0 causes a rigid shift in energy, and will henceforth be set equal to zero.

We do not consider the spin filtering interface. That is, we set the non-spin-flip scattering strength $Z_u = Z_d = Z$. It is well-known that the difference in Z_u and Z_d will cause a spin-filtering effect. That is, a higher Z_u will make the transport of the spin-up electrons less favorable and vice versa. This effect cannot be seen in the conductance spectrum and will not be considered in this article.

A. Differential conductance spectra

In all conductance plots, the conductance is in units of $e^2 \mathcal{L}^2 q_F/(2\pi h)$. The conductance spectra G with different Z_F in different limits of Z are shown in FIG. 3. Junctions with metallic contacts are characterized by $Z \ll 1$, whereas those in the tunneling limit are characterized by $Z \geq 1$. In general, the conductance is zero until the applied voltage reaches $eV = -E_{\lambda}$, which is the bottom of the band of the Rashba system. The conductance increases suddenly with large initial slope that decreases steadily until a second feature: the kink occurring at eV = 0, which is the crossing point of the two branches of the band. After

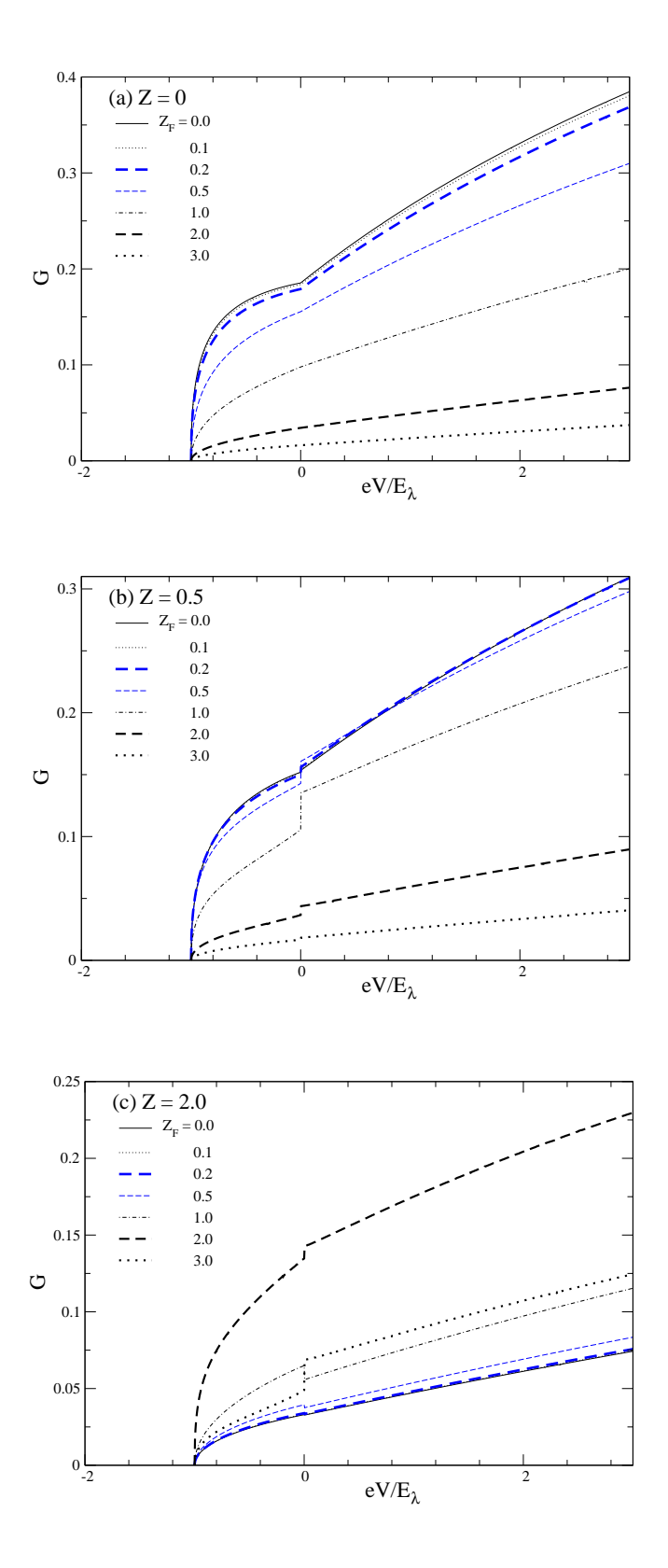


FIG. 3: (color online) Differential conductance spectra G for different Z_F in the case where (a) Z=0, (b) Z=0.5, and (c) Z=2.0.

this point, the conductance increases approximately linearly. In the presence of Z_F , there occurs a discontinuity in the conductance at eV = 0. The height of the jump depends on both Z and Z_F . This energy difference between the onset and the discontinuity in the slope of the conductance spectrum can be used to determine directly the Rashba energy E_{λ} . Note that this conclusion is not an artifact of this simple model (delta-function interface scattering, etc.). It should be generically true, because it is due to switching from transmission of electrons into only the - branch to transmission of electrons into both branches of the Rashba system.

In addition to the influence on the discontinuity at eV = 0, the interfacial scattering affects the overall conductance spectrum as well. For metallic contacts, the spin-flip scattering suppresses the conductance as expected. However, in the intermediate and the tunneling limits, the results are rather surprising. As can be seen in FIG. 3(b) when Z = 0.5, the increase in Z_F from zero to a small value (less than 0.5) does not affect the conductance much. Only when Z_F is increased beyond 0.5, does the conductance get suppressed. When Z is high, e. g. Z = 2.0 as in FIG. 3(c), the conductance spectrum can be enhanced by the increase in Z_F up to a value Z_F^* , after which the spectrum becomes suppressed. Z_F^* is found to depend strongly on Z.

One can see the effect on the conductance spectrum of spin-flip scattering more clearly by considering plots of the conductance G as a function of Z_F for energies just below and just above 0. In FIG. 4, $G^{\leq} \equiv G(-\delta)$ and $G^{\geq} \equiv G(+\delta)$, where $\delta/E_{\lambda} = 0.8$, are plotted as a function of Z_F for different values of Z. For small Z, both G^{\geq} and G^{\leq} decrease with Z_F as expected. However, this trend starts to change when Z is higher than 0.5. That is, both G^{\geq} and G^{\leq} increase with Z_F and reach a maximum value at Z_F^* (as indicated by arrows in FIG. 4), after which they decreases with Z_F . Notice that Z_F^* is a little smaller for G^{\leq} than for G^{\geq} and is approximately equal to Z. It should be noted that a similar dependence of both G^{\geq} and G^{\leq} on Z can also be seen, if one plots G^{\geq} and G^{\leq} as a function of Z instead.

B. Spin polarization of conductance

The plots of the spin polarizations of the conductance in both metal and Rashba system as a function of energy are shown in FIG. 5. The spin polarizations of the conductance of the two sides are very different. In Rashba system, it is always negative, whereas in the metal it is positive when the spin-flip scattering is not strong. This may be understood by

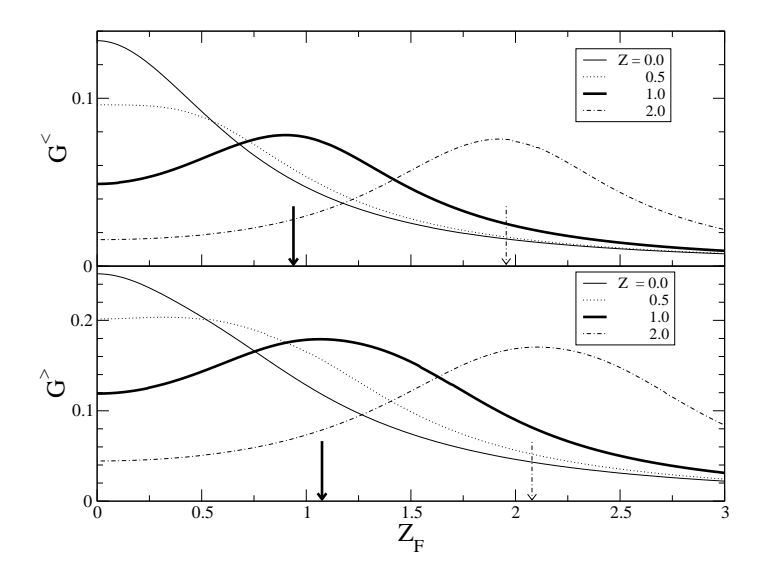
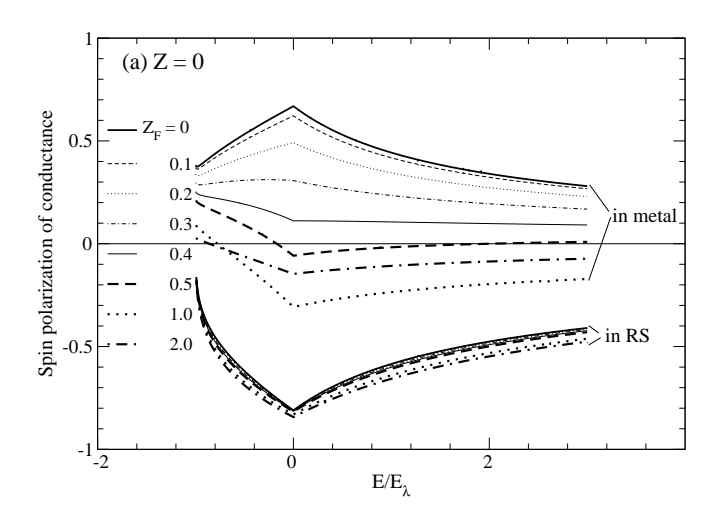


FIG. 4: Differential conductance G(eV) plotted as a function of the spin-flip barrier height Z_F at a constant energy eV slightly below [upper panel, denoted by $G^{<}(Z_F)$] and slightly above [lower panel, denoted by $G^{>}(Z_F)$)] the energy corresponding to the crossing of the Rashba-split bands. The arrows indicate the values of Z_F^* , where the maximum differential conductances $G^{>}$ and $G^{<}$ occur, for Z=1.0 (thick arrows) and 2.0 (dashed-dotted arrows).

considering the density of states of the Rashba system.

The density of states of the minus branch is larger than that of the plus branch. As we can see from FIG. 6, because the spins of the transmitted states of the minus branch are mostly pointing down, it is not surprising that the spin polarization of the conductance in the Rashba system is negative. As for the metal side, because more spin-down states are transmitted into the Rashba system, the spin polarization of the conductance is positive.

The interfacial scattering does not affect the spin polarization of the conductance in the Rashba system as much as in the metal. The increase in either Z or Z_F seems to slightly change the magnitude of the spin polarization of the conductance. However, in metal the interfacial scattering potential affects the spin polarization of the conductance a great deal. For a particular value of Z, the increase in Z_F can cause the spin polarization of the conductance in metal to change sign.



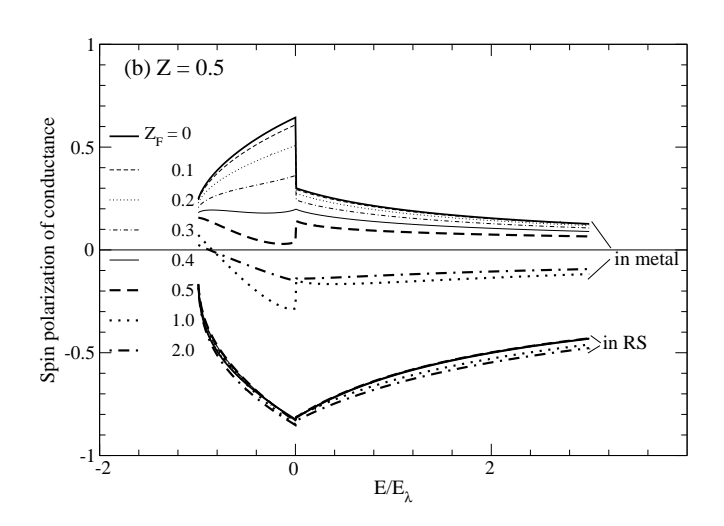


FIG. 5: The plots of the spin polarization of the conductance in metal and Rashba system (RS) as a function of energy when Z is (a) 0 and (b) 0.5.

IV. CONCLUSIONS

According to the results from our simple model, one can directly use in-plane tunneling conductance spectrum to measure the Rashba energy of a system with the Rashba spin-orbit coupling. The energy difference between the onset and the discontinuity in slope of the conductance spectrum is equal to the Rashba energy. Both features are found to be robust against variation in the quality of the junction.

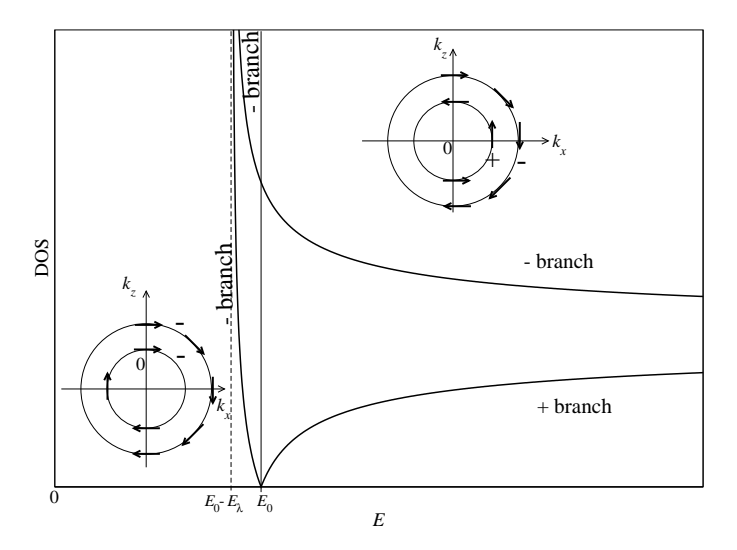


FIG. 6: Density of states of each branch of the 2DEG with the Rashba spin-orbit coupling. The contour plots on the left and on the right are those in the case where $E < E_0$ and $E > E_0$ respectively. When $E > E_0$, the outer contour is that of - branch and the inner one is that of + branch. When $E < E_0$, both energy contours belong to the - branch. The arrows represent the spin direction of the states with positive v_x .

Experimentally, to be able to measure the Rashba energy, the required energy resolution is at least of the order of the Rashba energy itself and the temperature is low enough in order that both features are visible. The Rashba energies in semiconductor-based heterostructures such as InAs, InGaAs, GaN and InSb, are of order 1 - 3 meV, [33–40] whereas those of surface alloys like Li/W(110), Pb/Ag(111), and Bi/Ag(111) can be as large as 200 meV. [16, 41–43] These conditions can be readily met in modern tunneling measurements. [17]

We also found that as the current is driven through the system, an imbalance of spin in both sides occurs. The spin polarization of the conductance in the metal is found to depend strongly on both types of the interfacial scattering and can disappear when the barrier is in the tunneling regimes. On the contrary, in the Rashba system the spin polarization of the conductance is always present and only slightly affected by interfacial scattering. This finding suggests that the spin imbalance caused by current flow in the system with the Rashba spin-orbit coupling is robust against variation in the quality of the junction as well.

Acknowledgments

We thank Dr. Michael F. Smith for critical reading of the manuscript. Also, we would like to acknowledge financial support from Cooperative Research Network (Physics). P.P. thanks Thailand Research Fund and Commission on Higher Education (grant no. RMU488012 and CHE-RES-RG "Theoretical Physics") for financial support. M.B. was supported by the Research Corporation, CIFAR and NSERC.

[1] E. I. Rashba, Sov. Phys. Solid State 2, 1109 (1960).

- [3] Y. A. Bychkov and E. I. Rashba, JETP Lett. 39, 78 (1984).
- [4] H. Engel, E. I. Rashba, and B. I. Halperin, Handbook of Magnetism and Advanced Magnetic Materials (Chichester: John Wiley and Sons Limited, 2007).
- [5] I. Zutic, J. Fabian, and S. Das Sarma, Rev. Mod. Phys. **76**, 323 (2004).
- [6] B. D. McCombe, S. G. Bishop, and R. Kaplan, Phys. Rev. Lett. 18, 748 (1967).
- [7] B.D. McCombe and R.J. Wagner, Phys. Rev. B 4, 1285 (1971).
- [8] J. Nitta, T. Akazaki, H. Takayanagi, and T. Enoki, Phys. Rev. Lett. 78, 1335 (1997).
- [9] G. Engels, J. Lange, Th. Schäpers, and H. Lüth, Phys. Rev. B 55, R1958 (1997).
- [10] G. Lommer, F. Malcher, and U. Rössler, Phys. Rev. Lett. 60, 728 (1988).
- [11] S. LaShell, B. A. McDougall, and E. Jensen, Phys. Rev. Lett. 77, 3419 (1996).
- [12] F. Reinert, J. Phys.: Condens. Matter 15, S693 (2003).
- [13] J. Henk, M. Hoesch, J. Osterwalder, A. Ernst, and P. Bruno, J. Phys.: Condens. Matter 16, 7581 (2004).
- [14] H. Cercellier, Y. Fagot-Revurat, B. Kierren, F. Reinert, D. Popović, and D. Malterre, Phys. Rev. B 70, 193412 (2004).
- [15] D. Popović, F. Reinert, S. Hüfner, V. G. Grigoryan, M. Springborg, H. Cercellier, Y. Fagot-Revurat, B. Kierren, and D. Malterre, Phys. Rev. B 72, 045419 (2005).
- [16] C. R. Ast, G. Wittich, P. Wahl, R. Vogelgesang, D. Pacilé, M. C. Falub, L. Moreschini, M. Papagno, M. Grioni, and K. Kern, Phys. Rev. B 75, 201401(R) (2007).
- [17] E. L. Wolf, Principles of tunneling spectroscopy (Oxford University Press, New York, 1989).

^[2] Y. A. Bychkov and E. I. Rashba, J. Phys. C 17, 6039 (1984).

- [18] G. Liu and G. Zhou, Chin. Phys. Lett. 22, 3159 (2005).
- [19] M. Lee and M. S. Choi, Phys. Rev. B **71**, 153306 (2005).
- [20] V. M. Ramaglia, D. Bercioux, V. Cataudella, G. De Filippis, C. A. Perroni, and F. Ventriglia, Eur. Phys. J. B 19, 365 (2003).
- [21] C. M. Hu and T. Matsuyama, Phys. Rev. Lett. 87, 066803 (2001).
- [22] T. Matsuyama, C. M. Hu, D. Grundler, G. Meier, and U. Merkt, Phys. Rev. B 65, 155322 (2002).
- [23] Y. Jiang and M. B. A. Jalil, J. Phys.: Condens. Matter 15, L31 (2003).
- [24] T. Yokoyama, Y. Tanaka, and J. Inoue, Phys. Rev. B 74, 035318 (2006).
- [25] F. Guinea, Phys. Rev. B **58**, 9212 (1998).
- [26] P. Lyu, D. Y. Xing, and J. Dong, Phys. Rev. B 58, 54 (1998).
- [27] J. Inoue and S. Maekawa, J. Magn. Magn. Mater. **198-199**, 158 (1999).
- [28] R. Jansen and J. S. Moodera, Phys. Rev. B **61**, 9047 (2000).
- [29] A. Vedyayev, D. Bagrets, A. Bagrets, and B. Dieny, Phys. Rev. B 63, 064429 (2001).
- [30] I. Zutic and S. Das Sarma, Phys. Rev. B **60**, R16322 (1999).
- [31] G. E. Blonder, M. Tinkham, and T. M. Klapwijk, Phys. Rev. B 25, 4515 (1982).
- [32] U. Zülicke and C. Schroll, Phys. Rev. Lett. 88, 029701 (2001).
- [33] S. Sasa, K. Anjiki, T. Yamaguchi, and M. Inoue, Physica B 272, 149 (1999).
- [34] D. Grundler, Phys. Rev. Lett. 84, 6074 (2000).
- [35] T. Matsuyama, R. Kürsten, C. Meissner, and U. Merkt, Phys. Rev. B 61, 15588 (2000).
- [36] T. Koga, J. Nitta, T. Akazaki, and H. Takayanagi, Phys. Rev. Lett. 89, 046801 (2002).
- [37] K. Fujii, Y. Morikami, T. Ohyama, S. Gozu, and S. Yamada, Physica E 12, 434 (2002).
- [38] I. Lo, J. K. Tsai, W. J. Yao, P. C. Ho, L. W. Tu, T. C. Chang, S. Elhamri, W. C. Mitchel, K. Y. Hsieh, J. H. Huang, H. L. Huang, and W. C. Tsai, Phys. Rev. B 65, 161306(R) (2002).
- [39] G. A. Khodaparast, R. C. Meyer, X. H. Zhang, T. Kasturiarachchi, R. E. Doezema, S. J. Chung, N. Goel, M. B. Santos and Y. J. Wang, Physica E 20, 386 (2004).
- [40] G. A. Khodaparast, R. E. Doezema, S. J. Chung, K. J. Goldammer, and M. B. Santos, Phys. Rev. B 70, 155322 (2004).
- [41] E. Rotenberg, J. W. Chung, and S. D. Kevan, Phys. Rev. Lett. 82, 4066 (1999).
- [42] D. Pacilé, C. R. Ast, M. Papagno, C. Da Silva, L. Moreschini, M. Falub, A. P. Seitsonen, and M. Grioni, Phys. Rev. B 73, 245429 (2006).

[43] C. R. Ast, J. Henk, A. Ernst, L. Moreschini, M. C. Falub, D. Pacilé, P. Bruno, K. Kern, and M Grioni, Phys. Rev. Lett. 98, 186807 (2007). Tunneling conductance in two-dimensional electron gas/s-wave superconductor junctions with Rashba spin-orbit coupling

B. Srisongmuang and P. Pairor

School of Physics, Institute of Science,

Suranaree University of Technology, Thailand

M. Berciu

Department of Physics and Astronomy,

University of British Columbia, British Columbia, Canada

Abstract

We theoretically studied spin-dependent charge transport in two-dimensional electron gas/s-

wave superconductor (2DEG/S) junctions. It was found that the tunneling conductance depends

strongly on 1) the strength of RSOC, 2) the potential barrier and 3) the mismatch of electron

effective masses. The influence of the RSOC, potential barrier and mismatch of electron effective

mass are associated and also depends on the Fermi levels of the 2DEG. We found that Andreev

reflection amplitude at the superconducting gap energy is always increased with the RSOC strength,

but is unaffected by the change in the potential barrier. One can use the Andreev reflection at the

superconducting gap to measure the strength of RSOC. In the other hand, can use gate voltage

controlling Andreev reflection at the gap. The effect of the mismatch effective mass and the

potential barrier are not always equivalent as it was believed.

PACS numbers: 73.40.Ns, 73.40.Gk, 73.23.-b, 72.25.Dc, 72.25.Mk

1

I. INTRODUCTION

In the past decade, spintronics has received much attention because of its potential benefit electric devices[1]. For example, interesting in spin-dependent transport were studied in a ferromagnet/normal metal (F/N) junction[2-6] and in ferromagnet/superconductor (F/S) junction[7, 8]. Two-dimensional electron gas (2DEG) with Rashba spin-orbit coupling (RSOC) is among the systems of interest. RSOC is known to lift the spin degeneracy of 2DEG. This system can be potentially used as a part of the spin-polarized field-effect transistor (Spin-FET)[9], spin interference device[10] and spin filters[11, 12]. In general, RSOC is present in the system with structure breaks inversion symmetry [13, 14] as in III-V semiconductor heterostructure. For example, InGaAs/InAlAs, GaSb/InAs/GaSb, GaAs/AlGaAs, InAs/AlSb, InAl/ AlSb [15–20]. The electron-spin splitting in Rashba system has been studied through the measurement of Shubnikov-de Haas (SdH) oscillations [15, 16, 18] and weak antilocalization [20][20]. The former the spin splitting is deduced from SdH oscillations frequency and the beating node position. The latter, the magnitude of RSOC is extracted from applied gate voltage which inducing a crossover between weak localization and antilocalization. In both techniques, the experimental results need extensive data fitting to obtain the information about RSOC. One of the most advantage of Rashba system to realizing spin devices is the control of RSOC strength by applying a gate voltage perpendicular to the 2D plane [21–23]. RSOC is also expected to affect the charge transport in 2DEG/S junctions as in the case of the exchange field in F/S junction. However, only a few works have been done on these junctions. It is desirable to extend the study for incorporating the effect of RSOC in these junctions for better understanding of Rashba system. Recently, Yokoyama et al. were interesting in the effect of RSOC on the subgap conductance spectra in comparison to that of exchange field in ferromagnet. They found that the effect of RSOC on the conductance depends on the potential barrier and the results are essentially different from the previously predicted in F/S junction[24]. In their work, the Fermi level of 2DEG is usually considered to be much higher than the Rashba energy. They did not show explicitly the effect of the different in the electron effective mass of both side of junction. Since 2DEG with RSOC is usually found in a semiconductor, in which the Fermi level can be varied by adjusting the density of carrier. In present work, in addition to study the effect of RSOC, mismatch effective mass and the insulating potential barrier at the interface, the level of the Fermi FIG. 1: (a) The sketch of energy dispersion of the 2DEG with RSOC (b) The energy contours of the plus and minus branches. \vec{k}^+ and \vec{k}^- are the wave vectors of the same k_z . The thick arrows show the direction of the spins for each \vec{k} -state along the energy contours.

energy of the 2DEG are also considered.

This article is organized as follows. In the next section, we describe the theoretical method and assumptions. We then provide the results and discussion in Section 3. The conclusion is given in the last section.

II. METHOD OF CALCULATION AND ASSUMPTIONS

The spin degeneracy splitting of 2DEG can be described by the Rashba Hamiltonian [14]:

$$\hat{H} = \frac{\hat{p}^2}{2m^*} - \lambda \vec{\sigma}.(\vec{y} \times \vec{p}) \tag{1}$$

where λ represents the strength of RSOC, or known as Rashba parameter, m^* is effective mass of the electron in 2DEG, \vec{p} is momentum, $\vec{\sigma}$ is the Pauli matrices and \vec{y} is the direction perpendicular to the 2D plane. The Rashba spin-orbit coupling cause the usual parabolic energy spectrum to split into two branches: $E^{\pm} = \frac{\hbar^2 k^2}{2m^*} \pm \hbar \lambda k$ where (see Fig. 1). In this work, we defined our system as an infinite 2D system, which lies on xz plane(electrons confined in the y direction), where the 2DEG and superconductor occupy the x < 0 and x > 0 region respectively. The 2DEG and superconductor are separated by a flat interface at , which is modeled by a Dirac delta function potential[25]. We consider a ballistic transport in our junction.

The Schrödinger equations describing the system is written as

$$\begin{bmatrix} \hat{H}_{0} + \hat{H}_{R\uparrow} + H_{S}\delta(x) & 0 & \Delta\Theta(x) & 0\\ 0 & \hat{H}_{0} + \hat{H}_{R\downarrow} + H_{S}\delta(x) & 0 & \Delta\Theta(x)\\ \Delta\Theta(x) & 0 & -\hat{H}_{0} + \hat{H}_{R\uparrow} - H_{S}\delta(x) & 0\\ 0 & \Delta\Theta(x) & 0 & -\hat{H}_{0} + \hat{H}_{R\downarrow} - H_{S}\delta(x) \end{bmatrix} \Psi(x, z) = E\Psi(x, z) \quad (2)$$

where \hat{H}_0 is free electron Hamiltonian and $\hat{H}_{R\uparrow\downarrow}$ is Rashba Hamiltonian (term with spatially varying coefficients that contain the momentum operator have to be symmetrized to ensure that hybrid Hamiltonian is Hermitian)[26]. That is,

$$\hat{H}_{0} = \hat{p} \frac{1}{2m(x)} \hat{p} - E_{F,S} \Theta(x) - E_{F,2DEG} \Theta(-x)$$

$$\hat{H}_{R\uparrow} = \frac{\lambda}{2} \left(\Theta(-x) (\sigma_{z(11)} \hat{p}_{x} - \sigma_{x(12)} \hat{p}_{z}) + (\sigma_{z(11)} \hat{p}_{x} - \sigma_{x(12)} \hat{p}_{z}) \Theta(-x) \right)$$

$$\hat{H}_{R\downarrow} = \frac{\lambda}{2} \left(\Theta(-x) (\sigma_{z(22)} \hat{p}_{x} - \sigma_{x(12)} \hat{p}_{z}) + (\sigma_{z(22)} \hat{p}_{x} - \sigma_{x(12)} \hat{p}_{z}) \Theta(-x) \right),$$

where \hat{p} is a momentum operator in $2D, \frac{1}{m(x)} = \frac{1}{m^*}\Theta(-x) + \frac{1}{m}\Theta(x)$ is the effective mass of the system $(m^*$ in 2DEG and m in the superconductor). $\Psi(x,z)$ is a four-component wave

function
$$\Psi(x,z)=\begin{pmatrix} \Psi_{e\uparrow} \\ \Psi_{e\downarrow} \\ \Psi_{h\uparrow} \\ \Psi_{h\downarrow} \end{pmatrix}$$
. From the Hamiltonian, one can obtain the eigenenergy and

eigenstates for electron and hole in each region as follows. In the x<0 region, the energy spectrum is $E=\sqrt{\xi_k^2+\Delta^2}$, where $\xi_k=\frac{\hbar^2k^2}{2m}-E_{F,S}$ and Δ is the superconducting gap energy. In x<0 region, the energy spectrum are: $E^\pm=\frac{\hbar^2}{2m^*}(q\pm q_0)^2-\frac{\hbar^2q_0^2}{2m^*}-E_{F,2DEG}$ for electrons and $E^\pm=E_{F,2DEG}-\frac{\hbar^2}{2m^*}(q\pm q_0)^2+\frac{\hbar^2q_0^2}{2m^*}$ for holes, where $q_0=\frac{m^*\lambda}{\hbar}$ also represent the strength of Rashba spin-orbit coupling in unit of momentum.

The wave function of quasiparticle in superconductor can be written as a combination of the four outgoing eigenstates of the same energy and k_z :

$$\Psi_{S}(x>0,z) = \begin{bmatrix} c_{1}e^{ik_{x}^{+}x} & u_{k+}^{+} & 0 \\ 0 & 0 \\ -v_{k+} & 0 \end{bmatrix} + c_{2}e^{ik_{x}^{+}x} \begin{bmatrix} 0 \\ u_{k+} \\ v_{k+} \\ 0 \end{bmatrix} + d_{2}e^{-ik_{x}^{-}x} \begin{bmatrix} 0 \\ u_{-k-} \\ v_{-k-} \\ 0 \end{bmatrix} e^{ik_{z}z} \tag{3}$$

where c_1 , c_2 , d_1 and d_2 are the amplitudes of the four transmissions. $k^+ = \sqrt{\frac{2m}{\hbar^2}(E_F + \sqrt{E^2 - \Delta^2})}$, $k^- = \sqrt{\frac{2m}{\hbar^2}(E_F - \sqrt{E^2 - \Delta^2})}$, u_k and v_k are the electron-like and hole-like quasiparticle amplitudes and are defined as

$$u_k = \frac{E + \xi_k}{\sqrt{|E + \xi^2|^2 + |\Delta_k|^2}} \tag{4}$$

$$v_k = \frac{\Delta_k}{\sqrt{|E + \xi^2|^2 + |\Delta_k|^2}} \tag{5}$$

so that $|u_k|^2 + |v_k|^2 = 1$.

In 2DEG, we consider the two cases of difference Fermi level. The first one is when Fermi level lies above the crossing point of 2DEG (E_0) and the second one is when Fermi level lies below E_0 . The sketch of excitation energy of 2DEG/S junction depict in Fig. 2. Similarly, in 2DEG, the wave function is obtained as a linear combination of an incoming eigenstate, two normal reflected states and two Andreev reflected states of the same energy and k_z , which different for different Fermi level. The wave function of the first case ($E_F > E_0$) is as follows:

$$\Psi_{2DEG}(x < 0, z) = \begin{bmatrix}
e^{iq_1^+ x} & \cos \varphi_1^+ \\
-\sin \varphi_1^+ \\
0 \\
0
\end{bmatrix} + a_1 e^{iq_1^- x} \begin{pmatrix} 0 \\
0 \\
-\sin \varphi_1^- \\
-\cos \varphi_1^- \end{pmatrix} + a_2 e^{iq_2^- x} \begin{pmatrix} 0 \\
0 \\
\cos \varphi_2^- \\
-\sin \varphi_2^- \end{pmatrix}$$

$$+b_1 e^{-iq_1^+ x} \begin{pmatrix} \sin \varphi_1^+ \\
-\cos \varphi_1^+ \\
0 \\
0
\end{pmatrix} + b_2 e^{-iq_2^+ x} \begin{pmatrix} \cos \varphi_2^+ \\
\sin \varphi_1^+ \\
0 \\
0
\end{pmatrix} = e^{ik_z z} \qquad (6)$$

for an incident electron from plus branch of 2DEG. In case of electron is injected from minus

branch only the first term of the wave function is modified to be $e^{iq_1^+x} \begin{pmatrix} sin\varphi_1^+ \\ cos\varphi_2^+ \\ 0 \\ 0 \end{pmatrix}$. $\varphi = \frac{\phi}{2} \ (\phi - \phi)$

is an incident angle see Fig. 2(b)), a_1 and a_2 are the Andreev reflection amplitudes, b_1 and b_2 are the normal reflection amplitudes. The x-components of the momenta $q_1^{+,-}$ and $q_2^{+,-}$ are defined as follows.

$$q_1^+ = \sqrt{(-q_0 + \sqrt{q_0^2 + \frac{2m^*}{\hbar}(E + E_F)})^2 - k_z^2}, \quad q_2^+ = \sqrt{(q_0 + \sqrt{q_0^2 + \frac{2m^*}{\hbar}(E + E_F)})^2 - k_z^2},$$

$$q_1^- = \sqrt{(-q_0 + \sqrt{q_0^2 + \frac{2m^*}{\hbar}(-E + E_F)})^2 - k_z^2}, \quad q_2^- = \sqrt{(q_0 + \sqrt{q_0^2 + \frac{2m^*}{\hbar}(-E + E_F)})^2 - k_z^2}$$
The wave function for of the second case $(E_F < E_0)$ is

$$\Psi_{2DEG}(x < 0, z) = \begin{bmatrix}
e^{-iq_1^+ x} \begin{pmatrix} \cos \varphi_1^+ \\ \sin \varphi_1^+ \\ 0 \\ 0 \end{pmatrix} + a_1 e^{-iq_1^- x} \begin{pmatrix} 0 \\ 0 \\ -\cos \varphi_1^- \\ -\sin \varphi_1^- \end{pmatrix} + a_2 e^{iq_2^- x} \begin{pmatrix} 0 \\ 0 \\ \cos \varphi_2^- \\ -\sin \varphi_2^- \end{pmatrix} + b_1 e^{iq_1^+ x} \begin{pmatrix} \sin \varphi_1^+ \\ \cos \varphi_1^+ \\ 0 \\ 0 \end{pmatrix} + b_2 e^{-iq_2^+ x} \begin{pmatrix} \cos \varphi_2^+ \\ \sin \varphi_1^+ \\ 0 \\ 0 \end{pmatrix} e^{ik_z z}, \tag{7}$$

for an incident electron with wave vector q_1^+ . When incoming electron comes from state

with
$$q_2^+$$
 the first term of the wave function is modified to be $e^{iq_2^+x}\begin{pmatrix} \cos\varphi_2\\ \sin\varphi_2^+\\ 0\\ 0\end{pmatrix}$. Note

that the wave function of this case is satisfied the energy higher than the crossing, below the crossing, the AR term with momentum \vec{q}_1 in equation (7) is modified to be

$$a_1e^{iq_1^-x}\begin{pmatrix}0\\0\\\cos\varphi_1^-\\--\sin\varphi_1^-\end{pmatrix}.$$
 The x-components of the momenta and in this case are as follows. $q_1^+=\sqrt{(q_0-\sqrt{q_0^2+\frac{2m^*}{\hbar}(E-E_0)})^2-k_z^2}$ for all E's,

lows.
$$q_1^+ = \sqrt{(q_0 - \sqrt{q_0^2 + \frac{2m^*}{\hbar}(E - E_0)})^2 - k_z^2}$$
 for all E's,
 $q_2^+ = \sqrt{(q_0 + \sqrt{q_0^2 + \frac{2m^*}{\hbar}(E - E_0)})^2 - k_z^2}$ for all E's,
 $q_1^- = \sqrt{(-q_0 + \sqrt{q_0^2 - \frac{2m^*}{\hbar}(E + E_0)})^2 - k_z^2}$ for all $E > E_0$,
 $q_1^- = \sqrt{(q_0 - \sqrt{q_0^2 - \frac{2m^*}{\hbar}(E + E_0)})^2 - k_z^2}$ for all $E < E_0$,
 $q_2^- = \sqrt{(q_0 + \sqrt{q_0^2 - \frac{2m^*}{\hbar}(E + E_0)})^2 - k_z^2}$ for all E's.

We obtain the Andreev reflection, normal reflection and transmission amplitudes a_1 , a_2 , b_1 , b_2 , c_1 , c_2 , d_1 and d_2 from the following matching conditions that ensure probability conservation[27].

$$\Psi_S(x=0) = \Psi_{2DEG}(0) = \Psi(0), \tag{8}$$

$$\frac{\partial \Psi_S}{\partial x} \mid_{x=0^+} -\frac{m}{m^*} \frac{\partial \Psi_{2DEG}}{\partial x} \mid_{x=0^-} = (2k_F z + i\sigma_0 \frac{m}{m^*} q_0) \Psi(0), \tag{9}$$

where $z = \frac{mH_s}{\hbar^2 k_{F,S}}$ is the unitless parameter that characterizes the strength of the potential

barrier,
$$k_F$$
 is the Fermi wave vector of the superconductor, $\sigma_0 = \begin{pmatrix} 1 & 0 & 0 & 0 \\ 0 & -1 & 0 & 0 \\ 0 & -1 & 0 & 0 \\ 0 & 0 & 0 & 1 \end{pmatrix}$.

We find the current across the junction as a function of an applied voltage is

$$I_{2DEG\to S} = \frac{L^2 e}{4\pi^2 \hbar} \int \int dk_z dE v_x (1 + A_1 + A_2 - B_1 - B_2) [f(E - eV) - f(E)], \tag{10}$$

where A_1, A_2, B_1 and B_2 are the Andreev reflection and normal reflection probabilities. v_x is the x component of group velocity of the incoming electron and f(E) is the Fermi-Dirac distribution function.

The Andreev reflection, normal reflection and transmission probabilities of each cases are defined as

Case 1 : $E_F > E_0$

$$A_{1(2)} = \frac{|a_{1(2)}|^2 [-q_{1(2)}^- \mp q_0 (\cos^2 \varphi_{1(2)}^- - \sin^2 \varphi_{1(2)}^+))]}{q_1^+ + q_0 (\cos^2 \varphi_1^+ - \sin^2 \varphi_1^+)}$$

$$B_1 = |b_1|^2, B_2 = \frac{|b_2|^2[-q_2^+ + q_0(\cos^2\varphi_2^+ - \sin^2\varphi_2^+))]}{q_1^+ + q_0(\cos^2\varphi_1^+ - \sin^2\varphi_1^+)}$$

$$C_{1(2)} = \frac{|c_{1(2)}|^2 |\xi_k k^+|^2}{r_m \times E(q_1^+ + q_0(\cos^2 \varphi_1^+ - \sin^2 \varphi_1^+)}$$

$$D_{1(2)} = \frac{|d_{1(2)}|^2 |-\xi_k k^-|^2}{r_m \times E(q_1^+ + q_0(\cos^2 \varphi_1^+ - \sin^2 \varphi_1^+)},$$

for electron from plus branch. When incoming electron from minus branch the divisor term corresponding to the group velocity of injection electron $q_1^+ + q_0(\cos^2\varphi_1^+ - \sin^2\varphi_1^+)$ is modified to be $q_2^+ - q_0(\cos^2\varphi_2^+ - \sin^2\varphi_2^+)$. Therefore, $B_1 = \frac{|b_1|^2[-q_1^+ - q_0(\cos^2\varphi_1^+ - \sin^2\varphi_2^+)]}{q_2^+ - q_0(\cos^2\varphi_2^+ - \sin^2\varphi_2^+)}$ and $B_2 = |b_2|^2$. The subscript 1(2) indicates the state corresponding to plus and minus branches respectively.

Case 2: $E_F < E_0$

$$A_{1(2)} = \frac{|a_{1(2)}|^2 \left[\pm q_{1(2)}^- \mp q_0 \left(\cos^2 \varphi_{1(2)}^- - \sin^2 \varphi_{1(2)}^+\right)\right)\right]}{-q_1^+ + q_0 \left(\cos^2 \varphi_1^+ - \sin^2 \varphi_1^+\right)}$$

$$B_1=\mid b_1\mid^2,\ B_2=\frac{|b_2|^2[-q_2^++q_0(\cos^2\varphi_2^+-\sin^2\varphi_2^+))]}{-q_1^++q_0(\cos^2\varphi_1^+-\sin^2\varphi_1^+)}$$

$$C_{1(2)} = \frac{|c_{1(2)}|^2 |\xi_k k^+|^2}{r_m \times E(-q_1^+ + q_0(\cos^2 \varphi_1^+ - \sin^2 \varphi_1^+)}$$

$$D_{1(2)} = \frac{|d_{1(2)}|^2 |-\xi_k k^-|^2}{r_m \times E(-q_1^+ + q_0(\cos^2 \varphi_1^+ - \sin^2 \varphi_1^+)},$$

for incident electron with \vec{q}_1 . When incoming electron from the state with \vec{q}_2 the divisor term corresponding to the group velocity of injection electron, $-q_1^+ + q_0(\cos^2\varphi_1^+ - \sin^2\varphi_1^+)$ is modified to be $q_2^+ - q_0(\cos^2\varphi_2^+ - \sin^2\varphi_2^+)$. Therefore, $B_1 = \frac{|b_1|^2[q_1^+ - q_0(\cos^2\varphi_1^+ - \sin^2\varphi_2^+))]}{q_2^+ - q_0(\cos^2\varphi_2^+ - \sin^2\varphi_2^+)}$ and $B_2 = |b_2|^2$. The subscript 1(2) indicates the state with wave vector $\vec{q}_1(\vec{q}_2)$ respectively.

The conductance at zero temperature is, thus

$$G(eV) = \frac{dI_{2DEG \to S}}{dV} = \frac{L^2 e^2}{4\pi\hbar} \int dk_z (1 + A_1 + A_2 - B_1 - B_2)$$
 (11)

III. RESULTS

In this section, we discuss the effect of the RSOC strength (q_0) , the potential barrier (z) and the different in electron effective masses $(r_m = \frac{m}{m^*})$ on differential conductance spectra in two cases of Fermi level, i.e. $E_F > E_0$ and $E_F < E_0$, E_0 is energy at the crossing branches of 2DEG. We concentrate the conductance spectra of the energy range between zero to the superconducting gap energy ($\Delta = 0.01E_F$). In all conductance plots, the conductance is in the units of $\frac{e^2L^2k}{\pi h}$. First we consider the differential conductance as a function of bias voltage V for different value of q_0 in Fig. 3. In the range of interested q_0 , we found the

FIG. 2: The sketch of excitation energy of 2DEG/S junction.

difference in the effect of q_0 on the conductance below the gap between the two cases of Fermi level. In the first case, the tunneling conductance is suppressed by q_0 in Andreev limit (z = 0), while in tunneling limit (z = 1), q_0 turn to slightly enhance the conductance. For $E_F < E_0$, the conductance is increased with increasing q_0 . In addition to the peak at the gap, there is a feature at the voltage corresponding to the position of E_0 (the arrows in the right column).

In order to more careful study the effect of q_0 below the energy gap, we plot the conductance as a function of q_0 for different value of z at eV=0 in Fig. 4 and 5. It is shown that the effect of q_0 associated with z, r_m as well as the Fermi level. As shown in Fig. 4, when $E_F > E_0$ and $r_m = 1$ (the left column) RSOC suppress the conductance for z = 0, and the conductance is increased up to a critical value and then decreased for z=0.7. For z=1, RSOC turn to enhance the conductance. The effect of RSOC on the conductance at zero voltage for rm = 10 shown in the right column. When z=0, q_0 suppress zero conductance similar to z (Fig. 7(b)). For finite z, q_0 almost not affect the conductance for the range of small q_0 . The dimension of the range is increased as z increase. Beyond the range, q_0 enhance the conductance up to critical value then the conductance is decreased. For $E_F < E_0$ (Fig. 5), it is found that in both cases of r_m , the conductance at zero voltage is enhanced with RSOC up to a critical value of each z. When q0 is higher than that value, the conductance is decreased. For $r_m=1$ this critical value of q_0 is very different for different value of z.

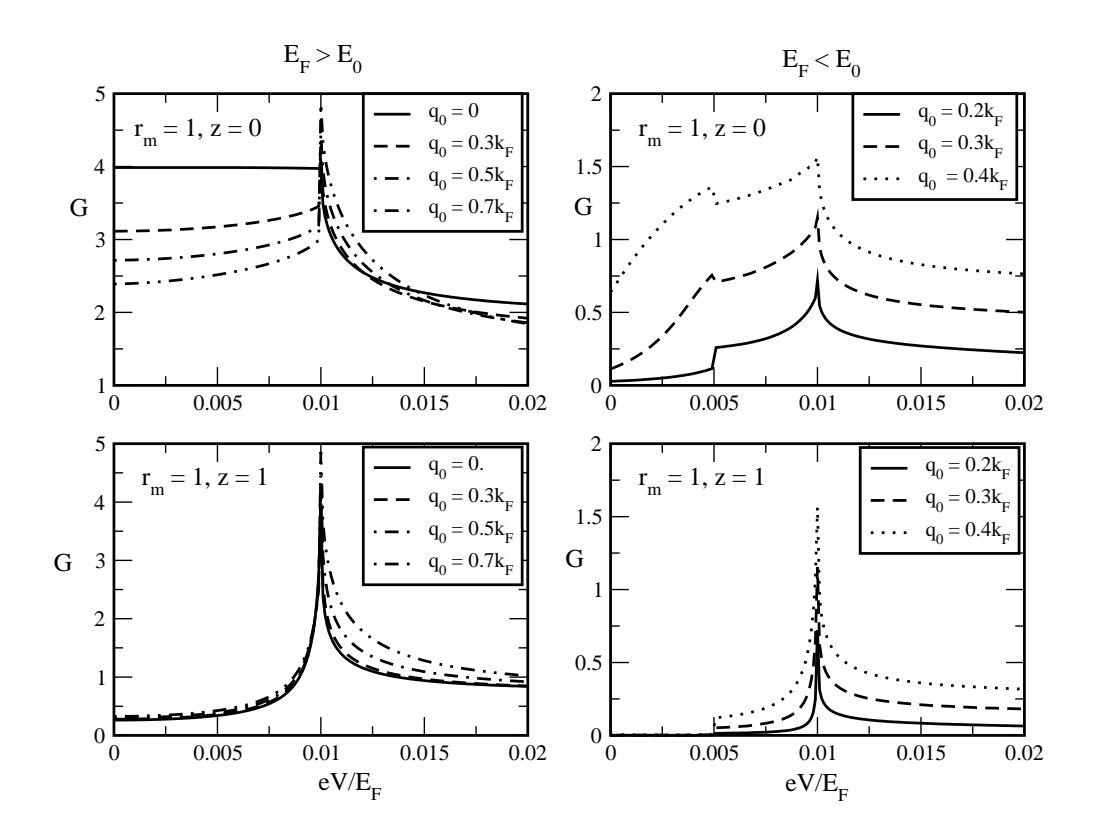


FIG. 3: The conductance spectra as a function of bias voltage V for different value of q0. The left column is for $E_F > E_0$ and the right column for $E_F < E_0$. The upper row is for z = 0 and the lower row for z = 1. The arrows in the right column indicate the position of E_0 .

While $r_m = 10$, this critical value is slowly forward shifted.

Fig. 6 shows the plots of differential conductance as a function of q0 for $eV = \Delta$. We found that q0 always increased the conductance in both cases of Fermi level and r_m especially when $E_F < E_0$, the conductance more linearly dependence on q0 and almost not depends on r_m . The conductance at the energy gap does not change by changing z as shown in Fig. 7. The independence of conductance on z at the superconducting gap was also found in ferromagnet/S (F/S) junction, previous work by Igor Zutic[28]. In their work, they suggested to use the conductance at the energy gap measure the spin polarization. However, the spin polarization does not linear depend on RSOC strength as it does on the exchange energy of F. In order to measure the spin polarization of 2DEG/S junction, we suggest to include the spin polarization P by decomposing the current in equation (10)(section 2) into two part $I = (1 - P)I_u + PI_p$, where $(1 - P)I_u$ is the fully unpolarized part and PI_p is the fully polarized part [29]. However, in 2DEG/S junction, even when z = 0 the conductance at

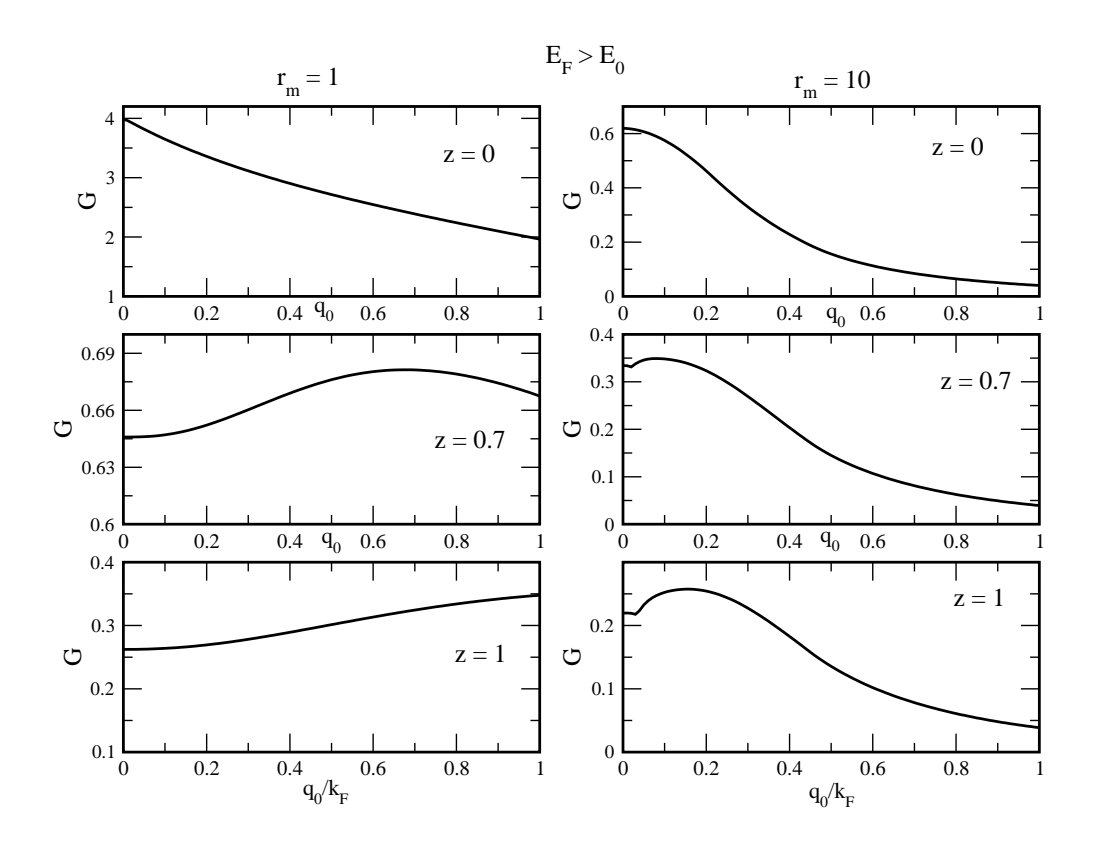


FIG. 4: The conductance spectra as a function of q_0 at eV = 0 for different value of z when $E_F > E_0, r_m = 1$ in the left column and $r_m = 10$ in the right column.

zero bias voltage can not measure directly the spin polarization as in metal-ferromagnet/S junction[29] due to Andreev reflection in 2DEG/S junction depends on q0 and r_m as well. To extract the spin polarization, fitting the experimental data with four parameter $(P, z, q_0$ and r_m) in the above extend model is needed.

Fig. 7 (b) shows the plots of differential conductance for fixed q_0 ($q_0 = 0.2k_F$) at eV = 0 and as a function of z for $E_F > E_0$. A similar dependence of conductance on z when $E_F < E_0$ also be seen. Fig. 8 is the plots of conductance as a function of r_m . It is found that the effect of z and r_m are not always equivalence as in most work believed. When $E_F > E_0$, r_m suppress the conductance both at eV = 0 and Δ , while z can not suppress the conductance at $eV = \Delta$ (Fig. 7). Moreover, when $E_F < E_0$, the effect of r_m at eV = 0 similar to that of q0 but at $eV = \Delta$ the influence of r_m on the conductance similar to that of z.

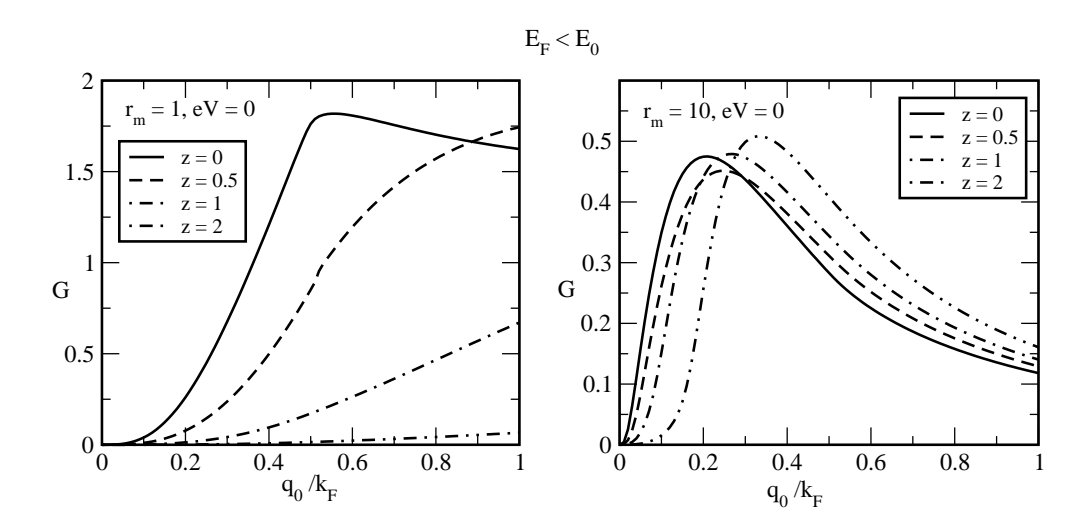


FIG. 5: The conductance spectra as a function of q_0 at eV=0 for different value of z when $E_F < E_0$. (a) $r_m = 1$ (b) $r_m = 10$.

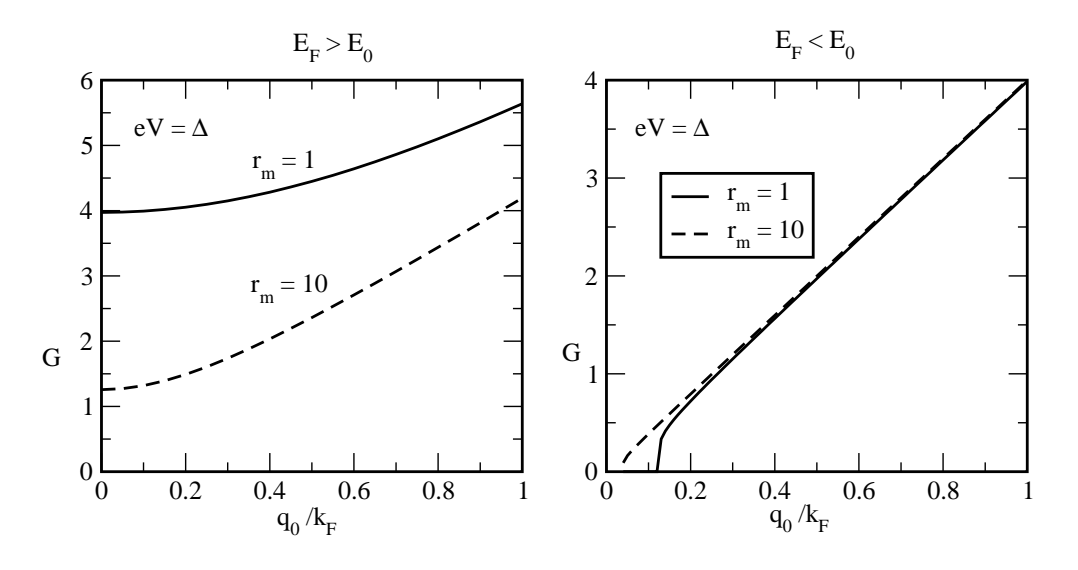


FIG. 6: The conductance spectra as a function of q0 at $eV = \Delta$ for $r_m = 1$ and 10. (a) $E_F > E_0$ (b) $E_F < E_0$

IV. CONCLUSION

We have examined the effect of the strength of RSOC, the potential barrier, and the mismatch of electron effective masses on the tunneling conductance of 2DEG/S junction. The influence of RSOC, potential barrier and mismatch of electron effective mass on the conductance are mostly associated and depends on the Fermi levels of the 2DEG as well. We found that the tunneling conductance at the superconducting gap which reflected to AR

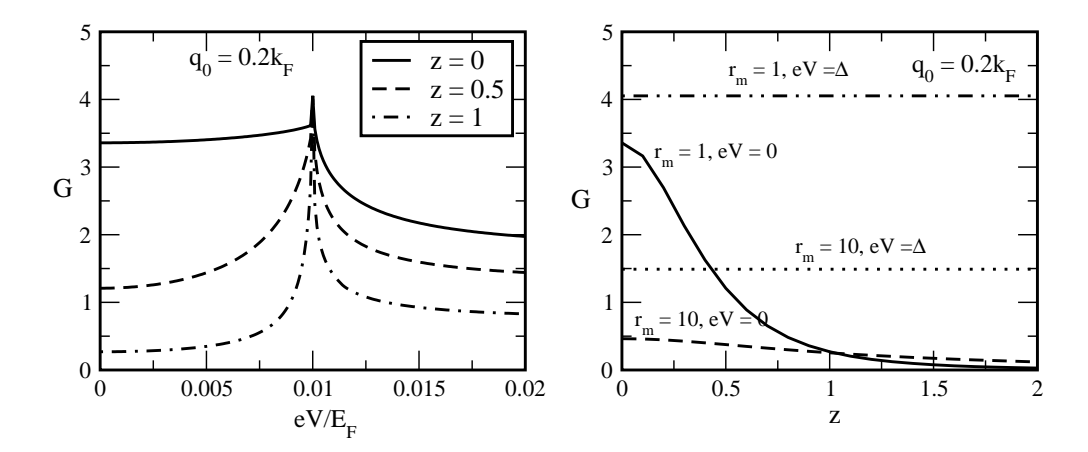


FIG. 7: (a) The conductance spectra as a function of bias voltage V for different value of z. (b) The conductance spectra as a function of z at eV=0 and Δ .

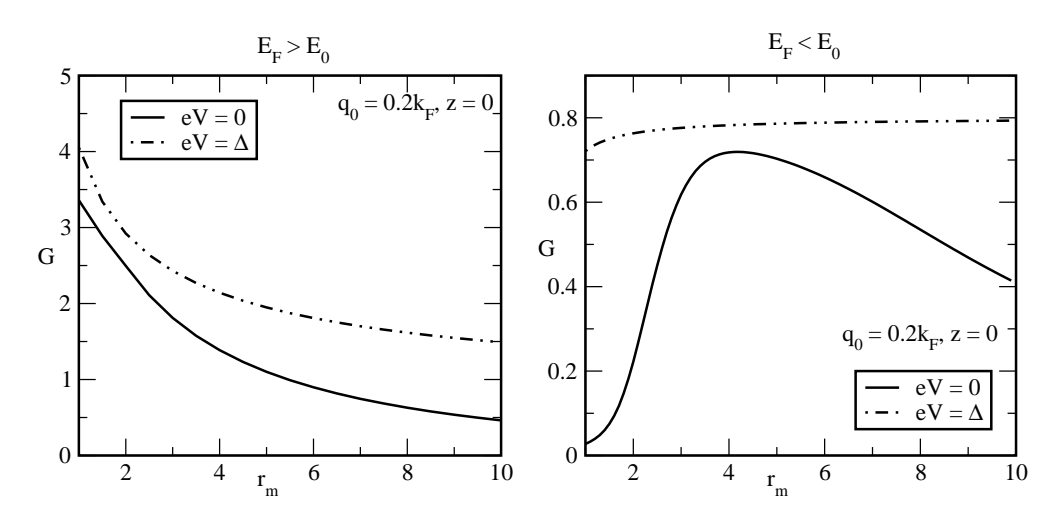


FIG. 8: The conductance spectra as a function of r_m at eV = 0 and Δ (a) $E_F > E_0$ (b) $E_F < E_0$.

is enhanced by the RSOC strength, but is unaffected by the change in the potential barrier. These results give possibility to controlling AR at the superconducting gap by gate voltage and to measure the RSOC strength by AR amplitude at the gap. The effect of the mismatch effective mass and the potential barrier are not always equivalent. When $E_F < E_0$, the effect of the different in electron effective masses is similar to that of RSOC strength.

Acknowledgments

We would like to acknowledge financial support from Cooperative Research Network (Physics). P.P. thanks Thailand Research Fund and Commission on Higher Education (grant

no. RMU488012 and CHE-RES-RG "Theoretical Physics") for financial support. M.B. was supported by the Research Corporation, CIFAR and NSERC.

[1] I. Zutic, J. Fabian and S. Das Sarma, Rev. Mod. Phys. 72, 323-410(2004).

- [1] 1. Zutic, 5. Pabian and 5. Das barma, Itev. Wod. 1 mys. 72, 525-410(20
- [2] M. Johnson and R. H. Silsbee, Phys. Rev. B **37**, 5326 (1988).
- [3] G. E. Bauer, Phys. Rev. Lett. **69**, 1676 (1992).
- [4] M. A. M. Gijs and G. E. Bauer, Adv. Phys. 46, 285 (1997).
- [5] C.-M. Hu and T. Matsuyama, Phys. Rev. Lett. 87 066803 (2001).
- [6] A. Saffarzadeh, J. Mag. Mat. **269**, 327 (2004).
- [7] P. M. Tedrow and R. Meservey, Phys. Rev. Lett. 26, 192 (1971).
- [8] K. Shashi Upadhyay, Akilan Palanisami, Richard N. Louie, and R. A. Buhrman, Phys. Rev. Lett. 81, 3247 (1998).
- [9] S. Datta, and B. Das, Appl. Phys. Lett., **56**, 665 (1990).
- [10] A. G. Aronov and Y. B. Lyanda-Geller, Phys. Rev. Lett., 70, 343 (1993).
- [11] T. Koga, J. Nitta, H. Takayanagi, anf S. Datta, Phys. Rev. Lett. 88, 126601 (2002).
- [12] IA. W. Cummings, R. Akis and D. K. Ferry, Appl. Phys. Lett. 89, 172115 (2006).
- [13] E. I. Rashba, Sov. Phys. Solid State 2, 1109 (1960).
- [14] Yu. A. Bychkov and E. I. Rashba, J. Phys. C 17, 6039 (1984).
- [15] J. Luo, H. Munekata, F. F. Fang and P. J. Stiles, Phys. Rev. B 38, 10142 (1988).
- [16] B. Das, D. C. Miller, S. Datta, R. Reifenberger, W. P. Hong, P. K. Bhattacharya, J. Singh and M. Jaffe, Phys. Rev. B 39, 1411 (1989).
- [17] S. Datta, and B. Das, Appl. Phys. Lett. **56**, 665 (1990).
- [18] J. Luo, H. Munekata, F. F. Fang and P. J. Stiles, Phys. Rev. B 41, 7685 (1990).
- [19] J. Nitta, T. Akazaki, H. Takayanagi and T. Enoki, Phys. Rev. Lett. 78, 1335 (1997).
- [20] J. B. Miller, D. M. Zumb?hl, C. M. Marcus, Y. B. Lyanda-Geller, D. Goldhaber- Gordon, K. Campman and A. C. Gossard, Phys. Rev. Lett. 90, 076807(2003).
- [21] G. L. Chen, J. Han, T. T. Huang, S. Datta and D. B. Janes, Phys. Rev. B 47, 4084 (1993).
- [22] W. Knap, C. Skierbiszewski,, A. Zduniak,, E. Litwin-Staszewska, D. Bertho, F. Kobbi and J. L. Robert, Phys. Rev. B 53, 3912 (1996).
- [23] J. Nitta, T. Akazaki, H. Takayanagi and T. Enoki, Phys. Rev. Lett. 78, 1335 (1997).

- [24] T. Yokoyama, Y. Tanaka and J. Inoue, Phys. Rev. B 74, 035318 (2006)
- [25] G. E. Blonder, M. Tinkham and T. M. Klapwijk, Phys. Rev. B 25, 4515 (1982).
- [26] U. Zulicke and C. Schroll, Phys. Lev. Lett. 88, 029701(2002).
- [27] Ch. Schniittler and M. Kirilov, Phys. Stat. Sol.(b) **176**, 143 (1993).
- [28] I. Zutic and S. Das Sarma, Phys. Rev. B 60, 16322 (1999).
- [29] G. J. Strijkers, Y. Ji., F. Y. Yang, C. L. Chien and J. M. Byers, Phys. Rev. B 63, 104510 (2001).

Tunneling conductance in two-dimensional electron gas/d-wave

superconductor junctions with Rashba spin-orbit coupling

B. Srisongmuang and P. Pairor

Institute of Science, Suranaree University of Technology, Thailand

M. Berciu

Department of Physics and Astronomy, University of British Columbia, Canada

Abstract

The tunneling conductance spectrum of a junction of two-dimensional electron

gas (2DEG) with Rashba spin-orbit coupling (RSOC) and a d-wave superconductor is theoretically studied. The spectrum shows strong dependence on junction orientation.

The effects of RSOC strength and potential barrier on the tunneling conductance are

different for different Fermi levels of the 2DEG.

PACS number: 73.40.Ns, 73.40.Gk, 73.23.-b, 72.25.Dc, 72.25.Mk

1

I. INTRODUCTION

In the past decade, spintronics has received much attention because of its potential benefit electric devices [1]. Two-dimensional electron gas (2DEG) with Rashba spin-orbit coupling (RSOC) is among the systems of interest. RSOC is known to lift the spin degeneracy of 2DEG. This system can be potentially used as a part of the spin-polarized field-effect transistor [2], spin interference device [3] and spin filters [4, 5]. In general, RSOC is present in the system with structure breaks inversion symmetry [6, 7]. Recently, 2DEG-superconductor junction was studied by T. Yokoyama and co-workers. [8] They considered s-wave superconductor. They found the tunneling conductance of the junction is suppressed by RSOC for low insulating barriers while for high insulating barriers the RSOC is almost not effect the conductance.

In this paper, we are interested in the charge transport of a junction consisting of 2DEG and a cuprate superconductor. The gap symmetry of cuprate superconductors is d-wave.[9] The sign change in the gap function leads to a zero-bias conductance peak in the conductance spectrum. [10, 11] It is therefore interesting to see how the characteristics of 2DEG with RSOC will affect this feature. In particular, the effect of RSOC, potential barrier, different Fermi levels of the 2DEG, and the junction orientation will be examined.

II. ASSUMPTIONS AND METHOD OF CALCULATION

The 2DEG/d-wave superconductor (2DEG/D) junction is modeled as an infinite 2D system. The geometry of the junction is depicted in Fig. 4.1. The potential barrier of 2DEG/D junction is represented by a delta-function potential of strength H_s . The superconducting gap is assumed to be zero in the 2DEG and to be spatially constant with a $d_{a^2-b^2}$ -wave symmetry in the superconductor.

That is, the superconducting gap depends on wave vector \vec{k} as follows:

$$\Delta(\theta_{\bar{\nu}}) = \Delta_0 \cos[2(\theta_{\bar{\nu}} - \alpha)], \tag{1}$$

where θ_k is the angle between wave vector \vec{k} and the interface normal vector, and α is the angle

between the a-axis of the $d_{a^2-b^2}$ -wave superconductor and the interface normal vector. This angle specifies the orientation of the junction, for example, $\{100\}$ junction is equivalent to $\alpha = 0$.

The Hamiltonian of our 2DEG/D junction is

$$\begin{pmatrix}
\hat{H}_{0} + \hat{H}_{R\uparrow} + H\delta(x) & 0 & \Delta\Theta(x) & 0 \\
0 & \hat{H}_{0} + \hat{H}_{R\downarrow} + H\delta(x) & 0 & \Delta\Theta(x) \\
\Delta\Theta(x) & 0 & -\hat{H}_{0} + \hat{H}_{R\uparrow} - H\delta(x) & 0 \\
0 & \Delta\Theta(x) & 0 & -\hat{H}_{0} + \hat{H}_{R\downarrow} - H\delta(x)
\end{pmatrix} \psi(x, z) = E\psi(x, z),$$
(2)

where \hat{H}_0 and $\hat{H}_{R\uparrow,\downarrow}$ are the Hamiltonian of the free electron and Rashba Hamiltonian of electron and/or hole with spin up and spin down respectively. That is,

$$\begin{split} \hat{H}_0 &= \hat{p} \frac{1}{2m(x)} \, \hat{p} - E_{F,S} \Theta(x) - E_{F,2DEG} \Theta(-x) \\ \hat{H}_{R\uparrow} &= \frac{\lambda}{2} (\Theta(-x) (\sigma_{z(11)} \hat{p}_x - \sigma_{x(12)} \hat{p}_z) + (\sigma_{z(11)} \hat{p}_x - \sigma_{x(12)} \hat{p}_z) \Theta(-x)) \\ \hat{H}_{R\downarrow} &= \frac{\lambda}{2} (\Theta(-x) (\sigma_{z(22)} \hat{p}_x - \sigma_{x(12)} \hat{p}_z) + (\sigma_{z(22)} \hat{p}_x - \sigma_{x(12)} \hat{p}_z) \Theta(-x)) \,, \end{split}$$

where \hat{p} is a momentum operator in 2D, $\frac{1}{m(x)} = \frac{1}{m^*} \Theta(-x) + \frac{1}{m} \Theta(x)$ is the effective mass of the system (m* in 2DEG and m in the superconductor). $\psi(x, z)$ is a four-component wave function

$$\psi(x,z) = \begin{pmatrix} \psi_{e\uparrow} \\ \psi_{e\downarrow} \\ \psi_{h\uparrow} \\ \psi_{h\downarrow} \end{pmatrix}.$$

The wave function of the superconducting side is the combination of the four transmitted excitations. That is,

$$\psi_{s}(x>0,z) = \begin{bmatrix} c_{1}e^{ik_{x}^{+}x} & \begin{pmatrix} u_{k^{+}} \\ 0 \\ 0 \\ -v_{k^{+}} \end{pmatrix} + c_{2}e^{ik_{x}^{+}x} & \begin{pmatrix} 0 \\ u_{k^{+}} \\ v_{k^{+}} \\ 0 \end{pmatrix} + d_{1}e^{-ik_{x}^{-}x} & \begin{pmatrix} u_{-k^{-}} \\ 0 \\ 0 \\ -v_{-k^{-}} \end{pmatrix} + d_{2}e^{-ik_{x}^{-}x} & \begin{pmatrix} 0 \\ u_{-k^{-}} \\ v_{-k^{-}} \\ 0 \end{pmatrix} \end{bmatrix} e^{ik_{z}z},$$

where c_1 , c_2 , d_1 and d_2 are the amplitudes of the four transmissions. u_k and v_k are the electron-like and hole-like quasiparticle amplitudes and are defined as $u_k = \frac{E + \xi_k}{\sqrt{\left|E + \xi_k\right|^2 + \left|\Delta_k\right|^2}}$

and $v_k = \frac{\Delta_k}{\sqrt{\left|E + \xi_k\right|^2 + \left|\Delta_k\right|^2}}$. E is the quasiparticle energy and ξ_k is the electron energy of state

 \vec{k} in normal state. The relation between E, ξ_k and $\Delta_k(\theta)$ is

$$E_k = \sqrt{\xi_k^2 + \Delta_k^2(\theta)} \tag{4}$$

Since the energy range of interest is in order of meV, which is the order of the maximum superconducting gap and is usually smaller than the Fermi energy of the superconductor, so the approximation $k^+ = k^- = k_F \cos\theta$ is used. Also, $\theta_{-k^-} = \pi - \theta_{k^+}$.

In article, 2 cases of different Fermi levels of the 2DEG are considered: (1) above the crossing of the two branches and (2) at the crossing. Also, the effect of the ratio of the effective mass on the conductance spectrum will not be considered. The ratio will be set to 10 throughout the article.

III. RESULTS AND DISSCUSSION

The conductance spectrum of 2DEG/D junction is dependent on the orientation of the junction as that of metal/D junction [11]. In all the following plots the conductance spectra is normalized by the conductance at $eV = 0.02E_F$. In the case where the Fermi level is located above the crossing, Fig. 1 shows the tunneling conductance spectra of $\{100\}$ junction ($\alpha = 0$). Unlike metal/D junction, there occurs a feature at the voltage less than the maximum gap of the d-wave superconductor. The position of this feature depends on the magnitude of the RSOC. In fact, it moves towards the peak at the maximum gap as the strength of RSOC is increased. This feature is not robust against the potential barrier, i.e., it gets smeared out as the potential barrier is larger. This feature also exists in the conductance spectrum of the junction small with non-zero α (see Figs. 2(b) and 3). Its position moves toward zero energy as α is increased (see Fig. 3). The shape of this feature is different from that of 2DEG/S junction due to the dependence on wave vector of the d-wave superconducting gap which different from that of s-wave superconductor.

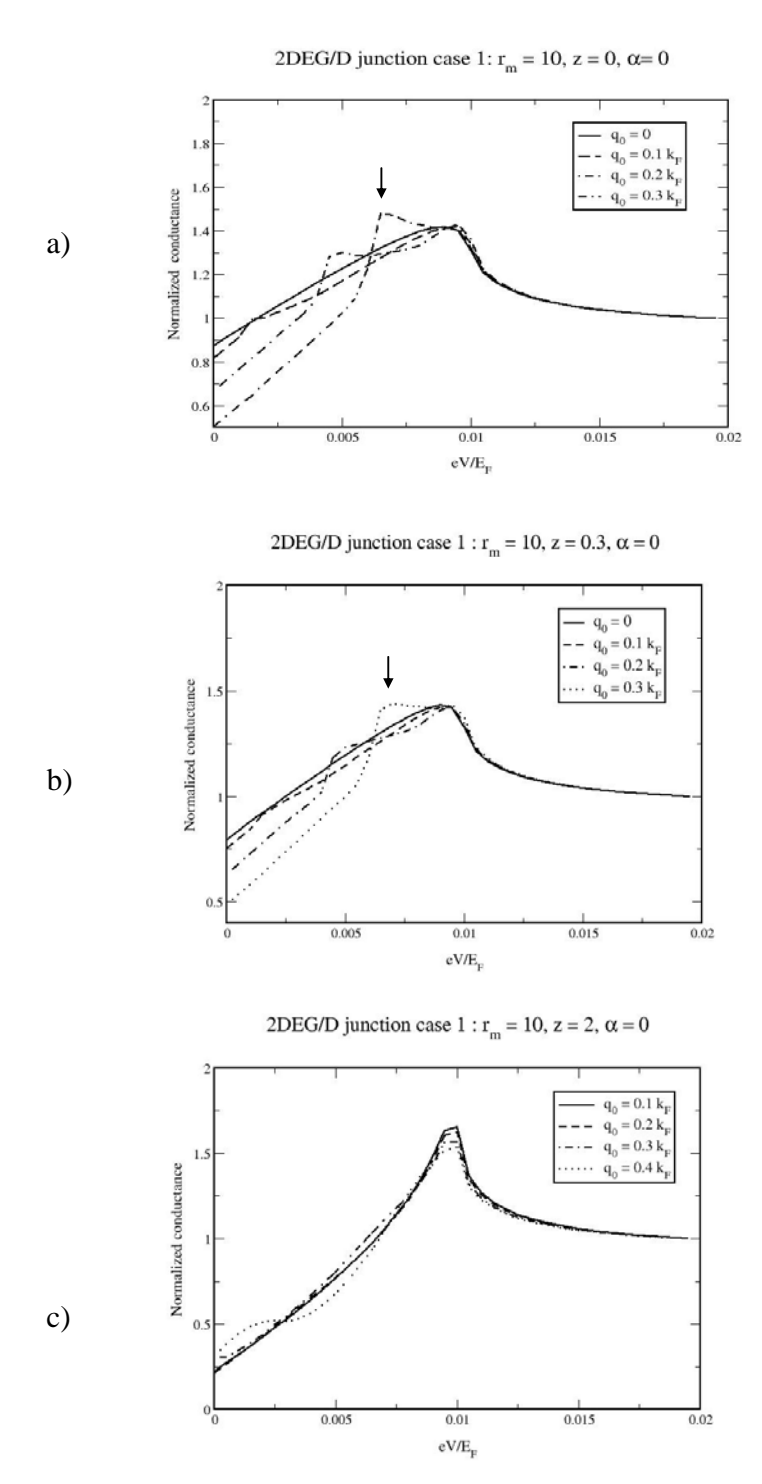
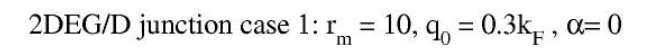
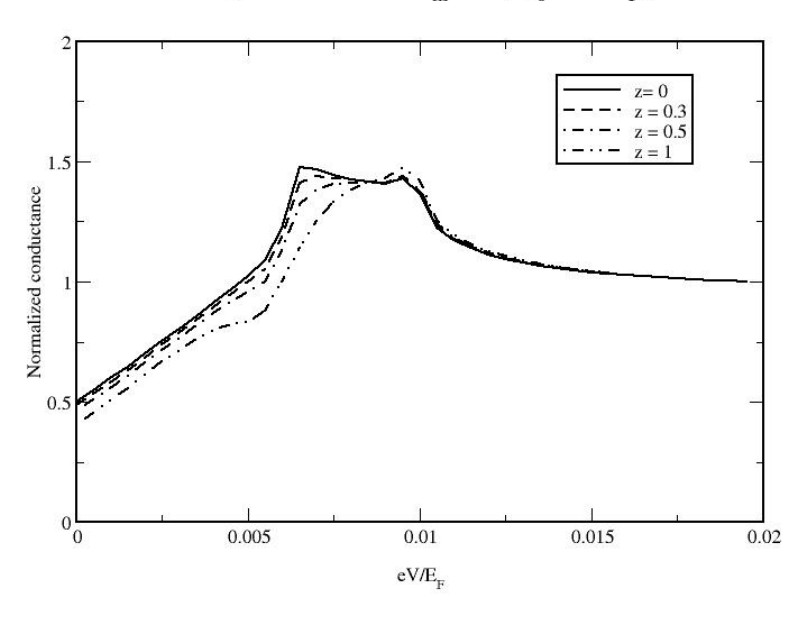


Fig. 1 The conductance spectra of 2DEG/D junction with various q_0 where $\alpha = 0$, $r_m = 10$ (a).z = 0, (b) z = 0.3 (c) z = 2. The arrows indicate the feature at $eV < \Delta$





2DEG/D junction case1: r_{m} = 10, q_{0} = 0.3 $k_{F}^{},\,\alpha$ = $\pi/16$

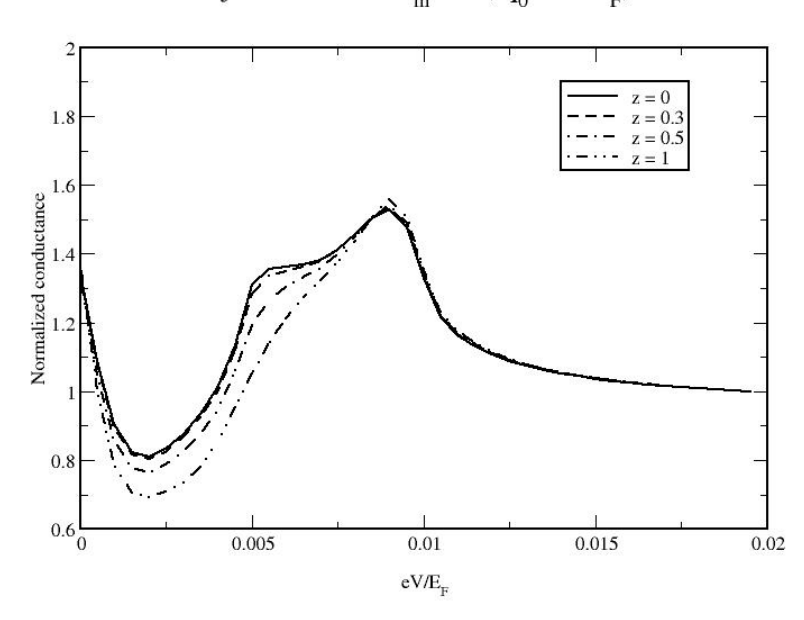


Fig. 2 The conductance spectra of 2DEG/D junction with various z , $r_m = 10$ (a). $\alpha = 0$

(b)
$$\alpha = \frac{\pi}{16}$$
.

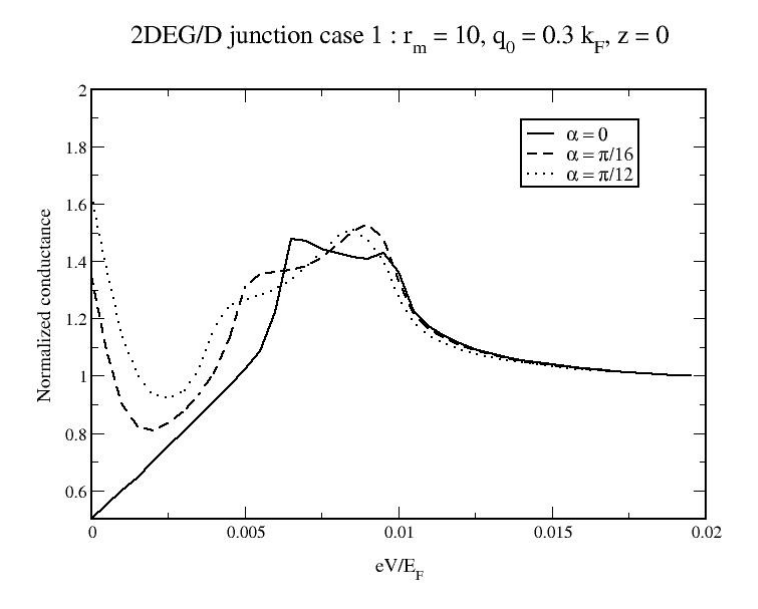


Fig. 3 The conductance spectra of 2DEG/D junction with various α , z = 0, $\rm \,r_m$ = 10 and $\rm \,q_0$ = 0.3 $k_{\rm F}$

As shown in Fig. 4, the potential barrier decreases the normalized conductance at the bias voltage below the maximum gap similar to that in the spectrum of M/D junction.

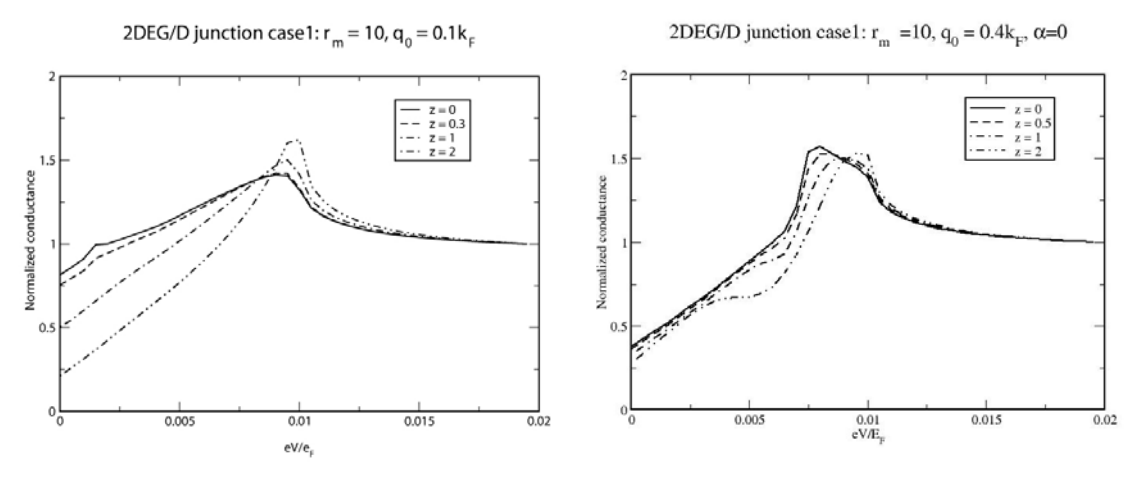
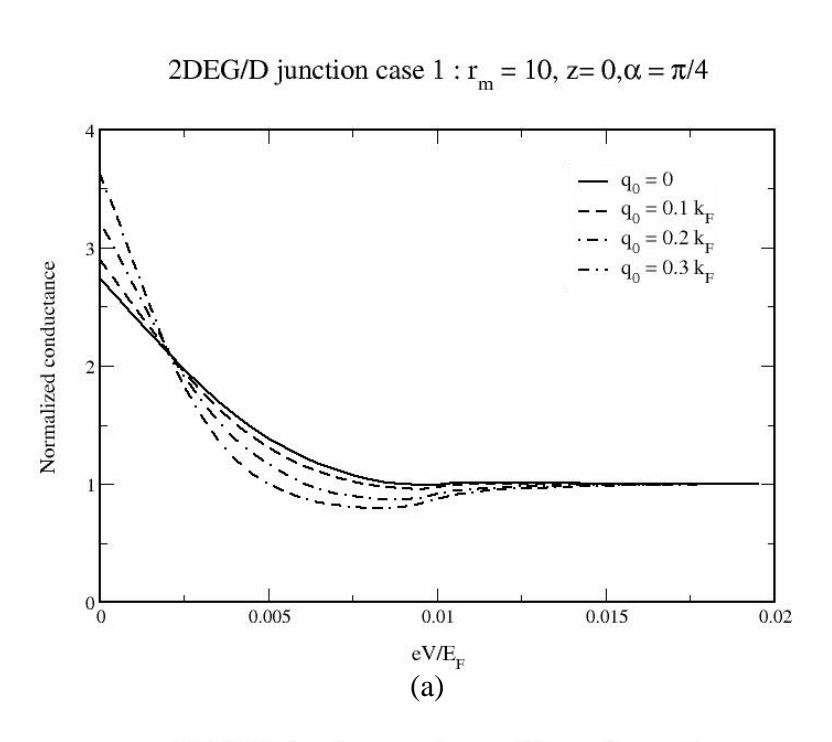


Fig. 4 The conductance spectra of 2DEG/D junction with various z=0, 0.3, 1 and 2, $\alpha=0, r_m=10$ (a) $q_0=0.1k_F$. (b) $q_0=0.4k_F$.

In the spectrum of junctions with α away from zero, there occurs a zero-bias conductance peak (ZBCP), which is the signature of the surface bound states of the d-wave superconductor. Fig. 5 shows the plots of normalized conductance vs bias voltage of the {110} ($\alpha = \frac{\pi}{4}$) junction with various values of RSOC strength (q₀). It is found that in the Andreev limit q₀ enhances the height but decreases the width of ZBCP (Fig. 5(a)). In the tunneling limit, q₀ reduces the height of the peak but does not affect its width (Fig. 5(b)). Fig. 6 contains the plot of normalized conductance for different value of potential barrier. It is found that the height of ZBCP is increased with z, whereas its width is decreased for small q₀. When q₀ is big, the potential barrier does not affect the width of ZBCP.

The effect of the RSOC and the potential barrier on ZBCP in the conductance spectrum of junction with $\alpha=\frac{\pi}{8}$ is the same as in that of {110} junction (see Figs. 7 and 8). There is a peak occurring at $eV=\Delta_0\cos2\alpha$, where $\alpha=\frac{\pi}{8}$ as also seen in M/D junction [12].



2DEG/D junction case1: r_m =10, z = 2, α = π /4

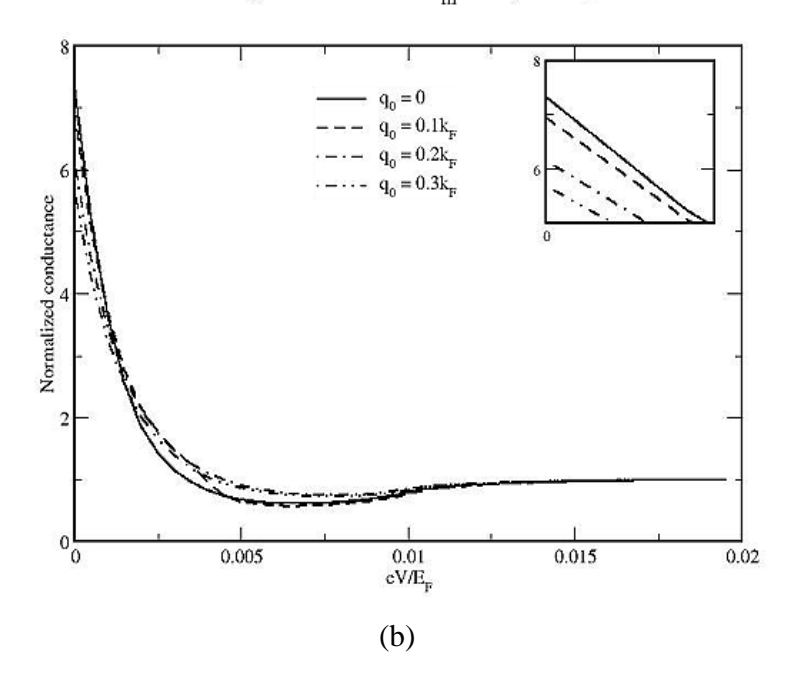
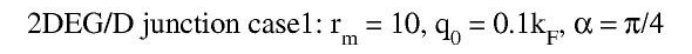
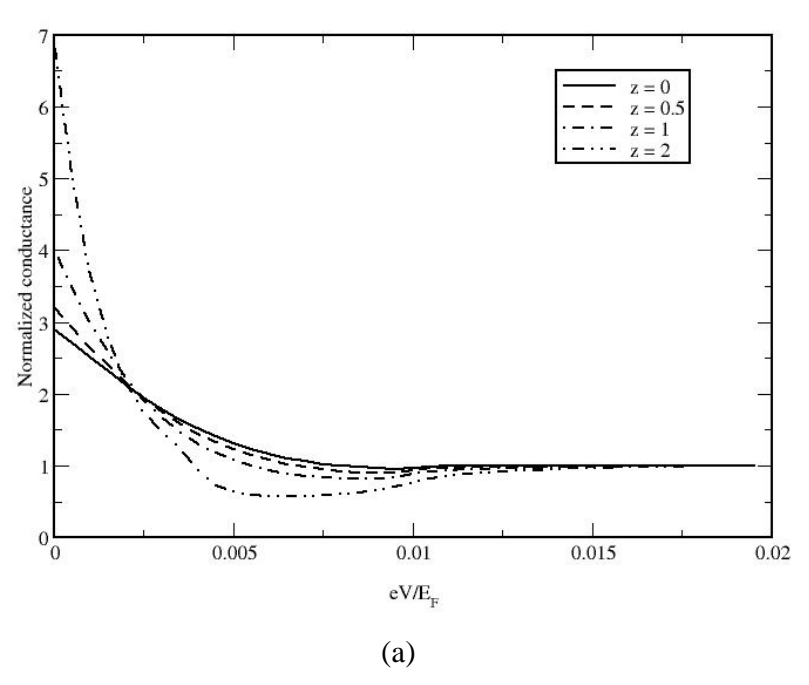


Fig. 5 The conductance spectra with various RSOC, $\alpha = \frac{\pi}{4}$, (a) z = 0 (b). z = 2. The inset is the close up plot of the conductance spectra near eV = 0





2DEG/D junction case1: $r_{\rm m}$ = 10, q_0 = 0.4k $_{\rm F},\,\alpha$ = $\pi/4$

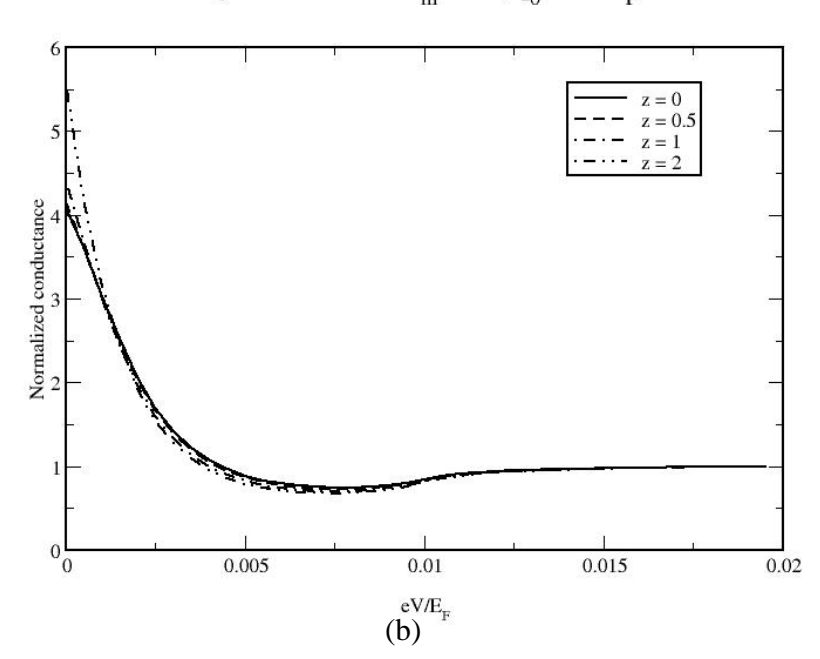
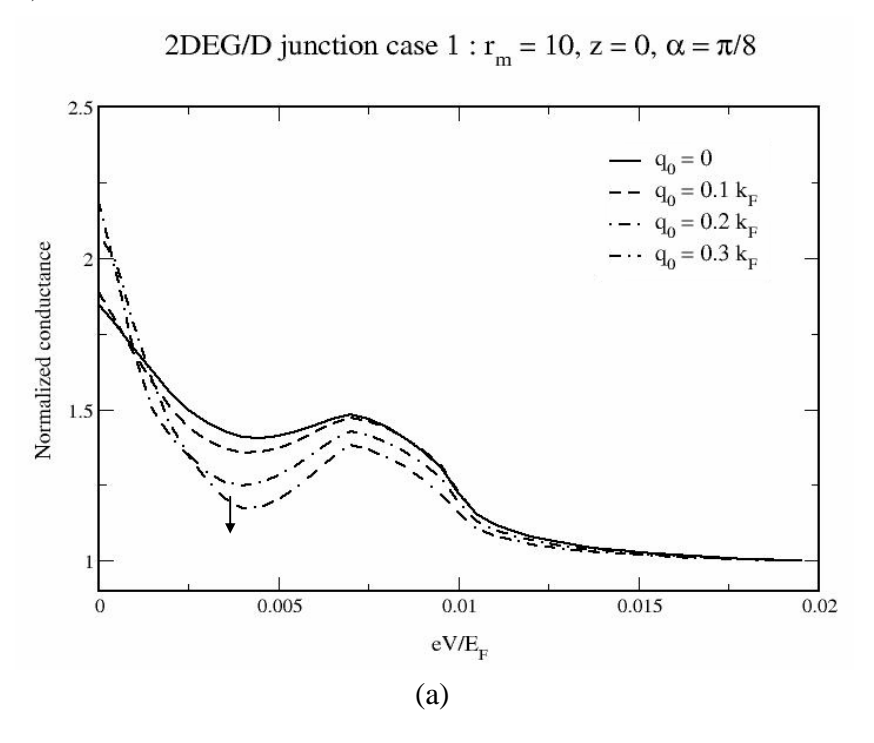


Fig. 6 The conductance spectra of 2DEG/D junction with various $z=0,\,0.5,\,1$ and 2,

$$\alpha = \frac{\pi}{4}$$
, $r_{\rm m} = 10$ (a) $q_0 = 0.1k_F$. (b) $q_0 = 0.4k_F$.



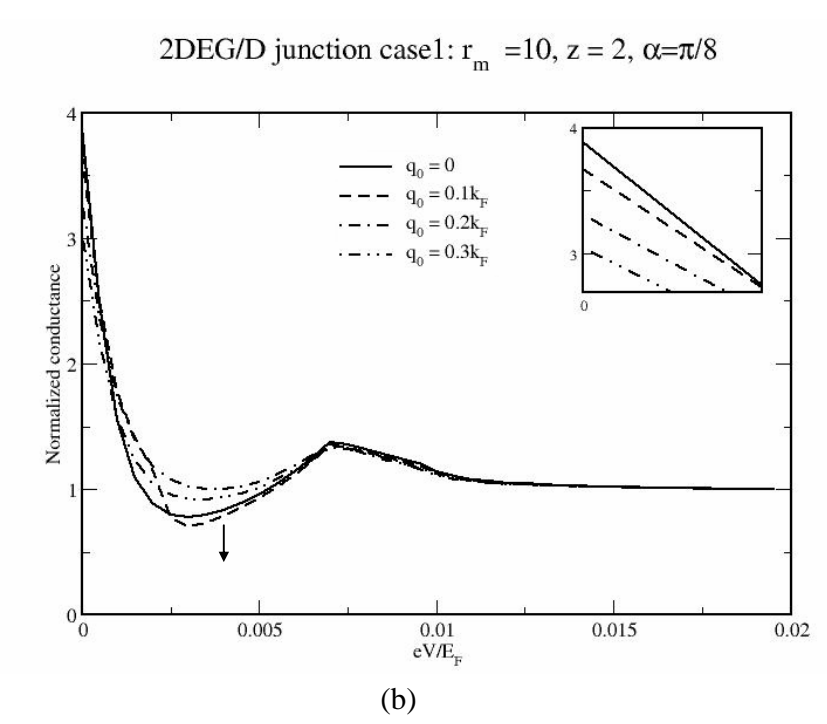
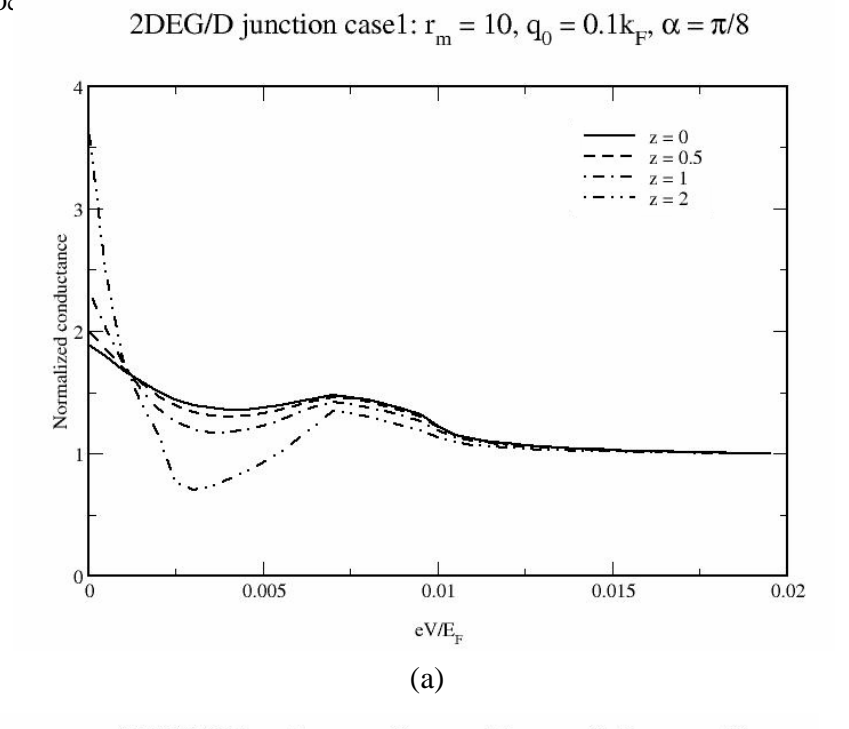


Fig. 7 The conductance spectra with various RSOC, $\alpha=\frac{\pi}{8}$, (a) z=0 (b). z=2. The arrows indicate the feature at $eV=\Delta_0\cos2\alpha$. The inset is the close up plot of the conductance spectra near eV=0

Oc · ^^ ^^ draft



2DEG/D junction case1: $r_m = 10$, $q_0 = 0.4k_F$, $\alpha = \pi/8$

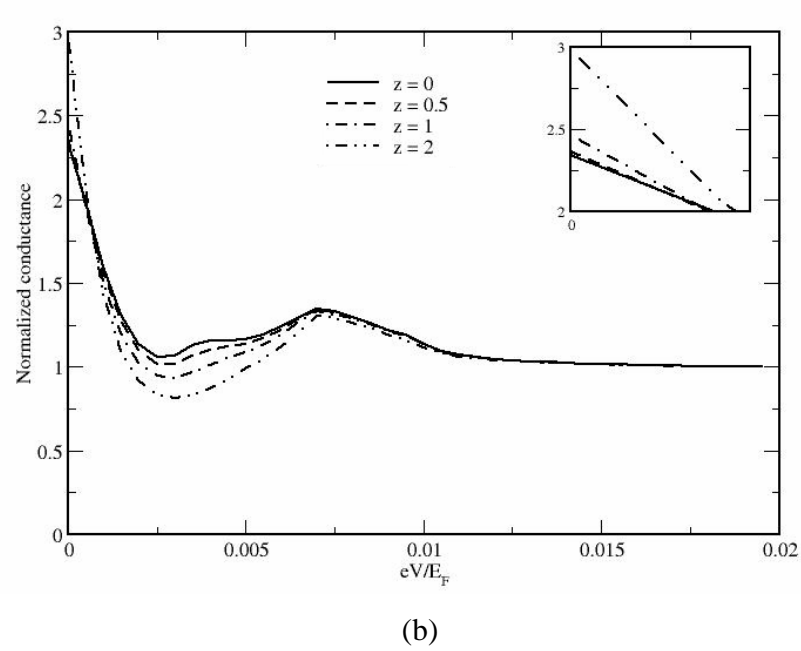


Fig. 8 The conductance spectra of 2DEG/D junction with various z=0, 0.5, 1 and 2, $\alpha=\frac{\pi}{8}, \ r_m=10 \ (a) \ q_0=0.1k_F. \ (b) \ q_0=0.4k_F.$ The inset is the close up plot of the conductance spectra near eV=0

In the case where the Fermi level lies at the crossing, for the $\{100\}$ junction, in the Andreev limit the normalized conductance at zero bias voltage is decreased with q_0 (see Fig. 9(a)). In the tunneling limit, the conductance at zero voltage is increased with q_0 and then later is decreased with q_0 (see Fig. 9(b)). Fig. 10 contains the plots of normalized conductance for different values of potential barrier for a fixed q_0 . It is found that for small q_0 , potential barrier suppresses the conductance at zero voltage, while for big q_0 , the potential barrier can enhance it.

The conductance spectra for different values of q_0 of junctions with $\alpha = \frac{\pi}{4}$ and $\alpha = \frac{\pi}{8}$ are shown in Figs. 11 and 12. In the Andreev limit, the effect of q_0 on ZBCP is the same as in the previous case where E_F is located above the crossing, that is, it enhances the height of ZBCP. However, in the tunneling limit, the increase in q_0 can cause the height of ZBCP to decrease and after a critical value of q_0 the height start to increase.

Figs. 13 and 14 contain the plots of conductance spectra of the junction with $\alpha = \frac{\pi}{4}$ and $\alpha = \frac{\pi}{8}$ for different values of z. It is found in junction with both orientations that as the potential barrier is increased, the height of ZBCP is increased for small q_0 , while for big q_0 the height of ZBCP is almost unchanged.

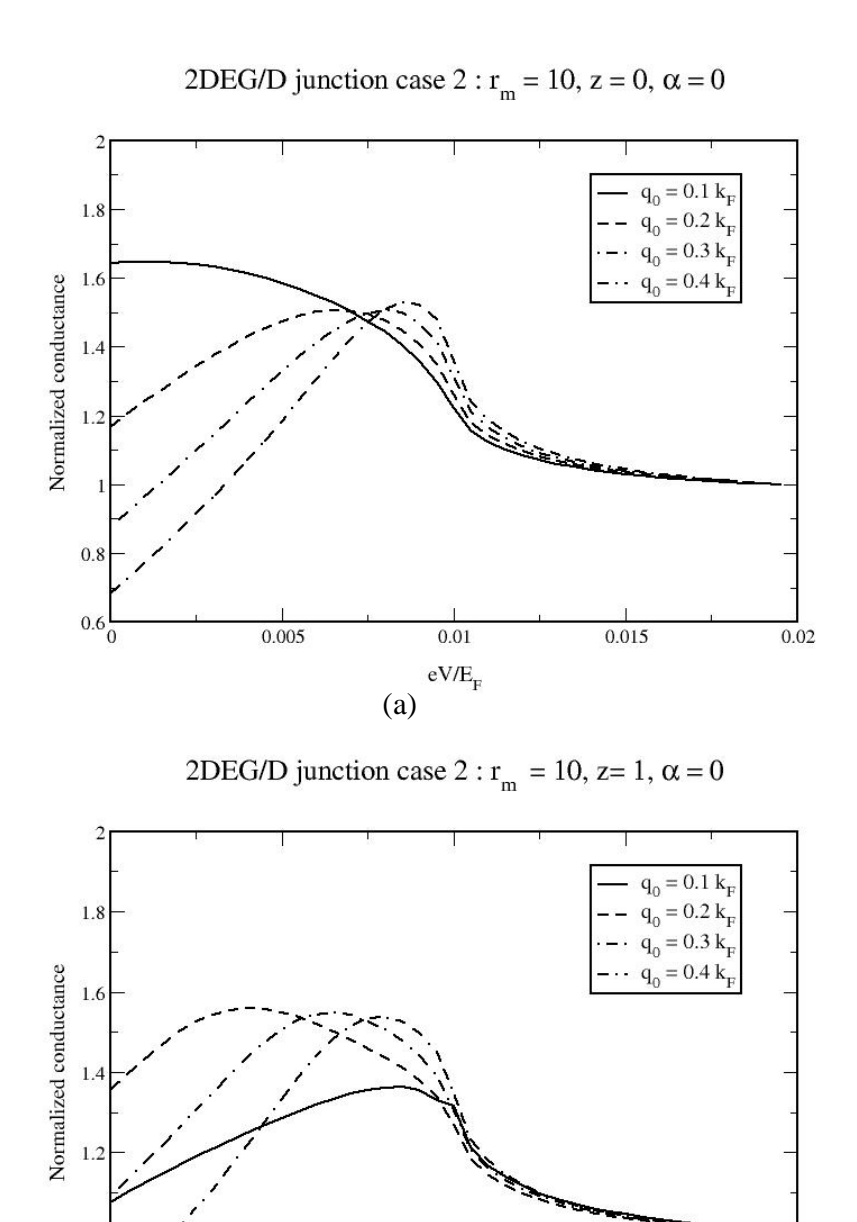


Fig. 9 The conductance spectra with various RSOC, $\alpha = 0$, (a) z = 0 (b). z = 1

0.01

eV/E_F

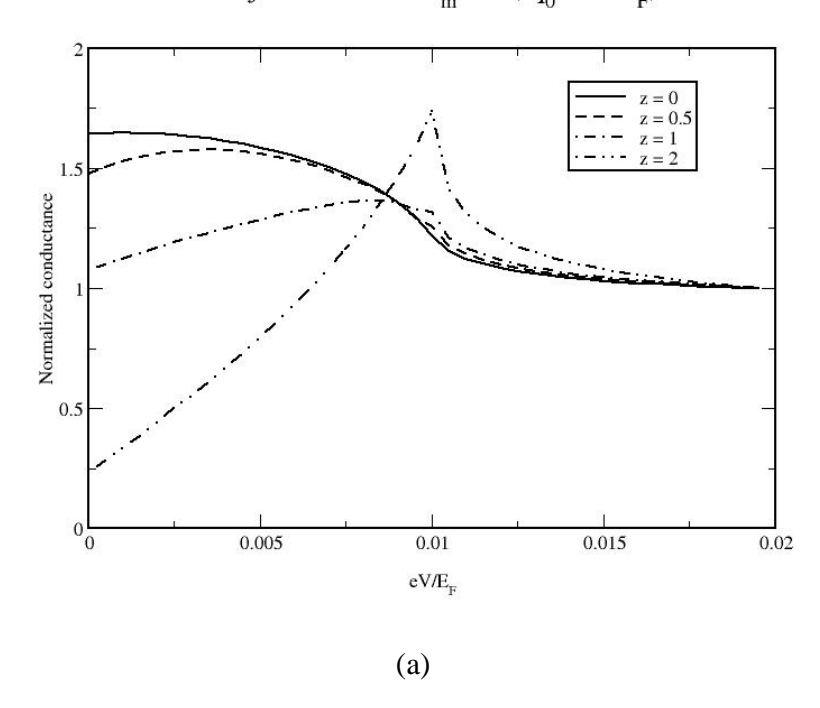
(b)

0.015

0.02

0.005

2DEG/D junction case2: r_{m} = 10, q_{0} = 0.1 $k_{F}^{},\,\alpha$ = 0



2DEG/D junction case2: r_{m} = 10, q_{0} = 0.4 k_{F} , α = 0

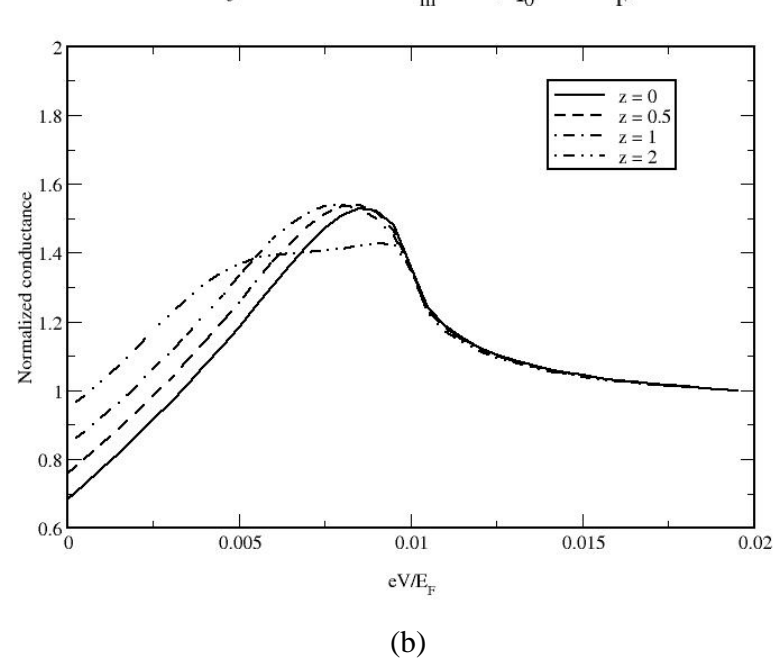


Fig. 10 The conductance spectra of 2DEG/D junction with various $z=0,\,0.5,\,1$ and 2,

$$\alpha = 0$$
, $\mathbf{r}_{\mathrm{m}} = 10$ (a) $q_{\mathrm{0}} = 0.1 k_{F}$. (b) $q_{\mathrm{0}} = 0.4 k_{F}$

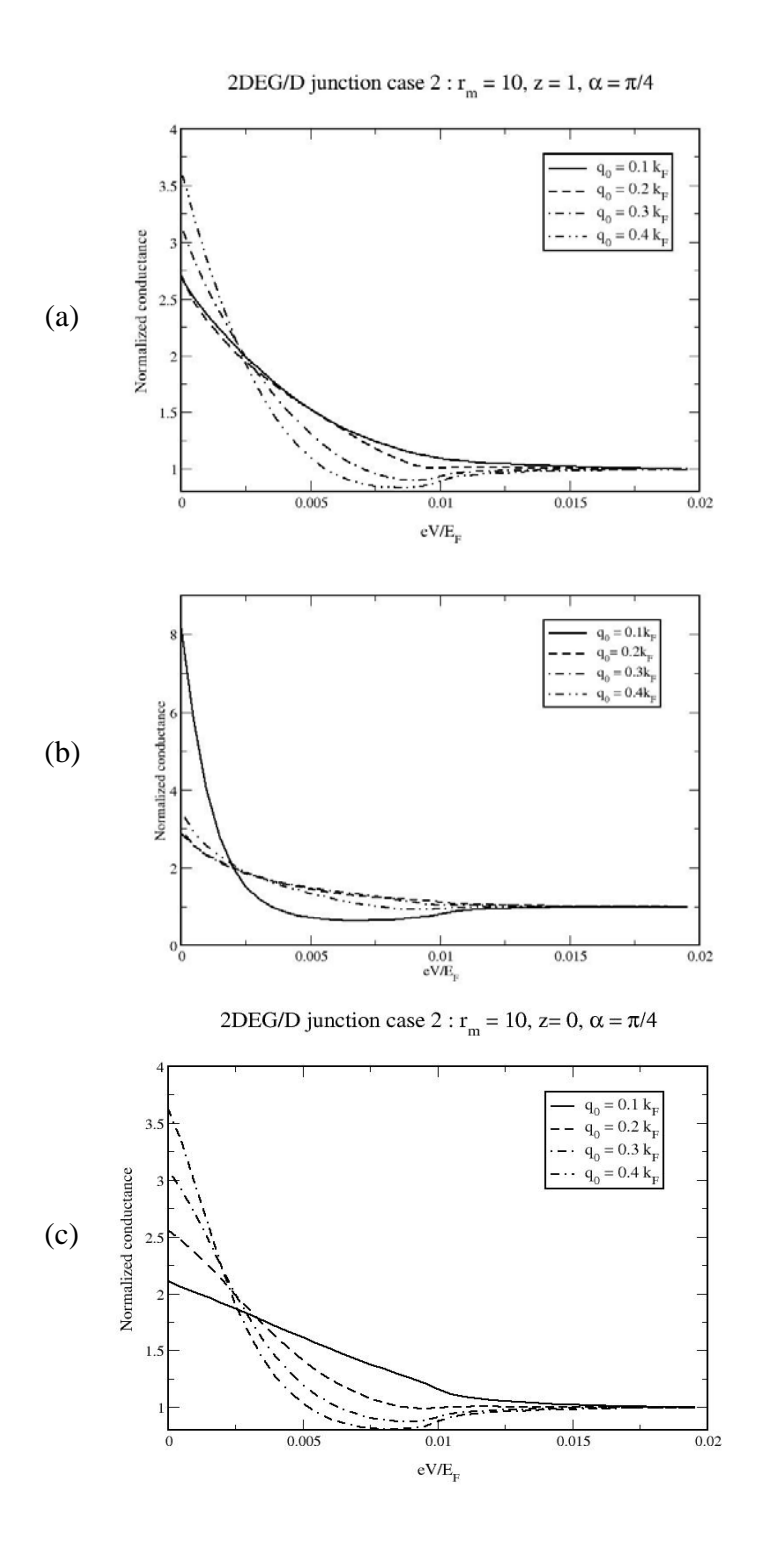


Fig. 11 The conductance spectra with various RSOC, $\alpha = \frac{\pi}{4}$, (a) z = 0 (b) z = 1 (c) z = 2

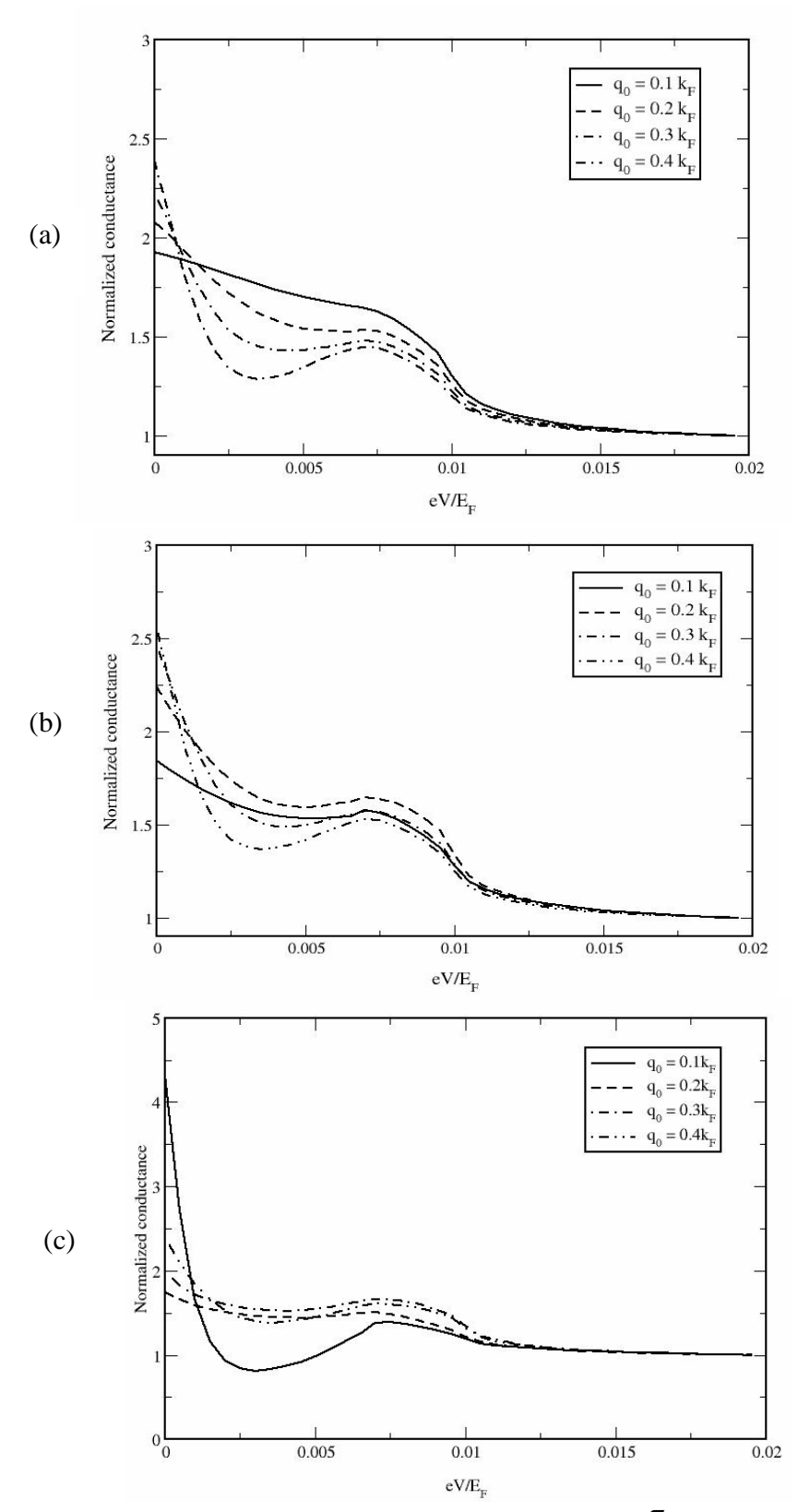
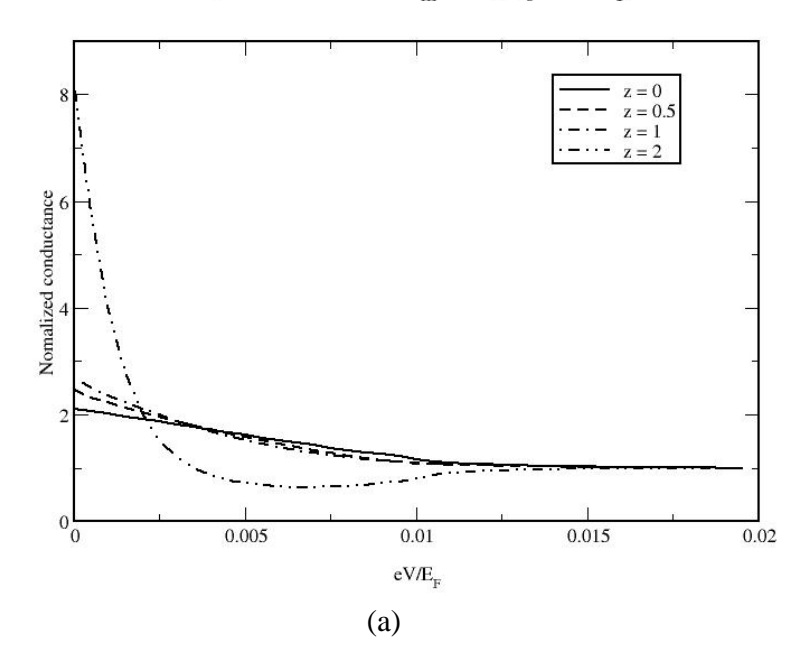


Fig. 12 The conductance spectra with various RSOC, $\alpha = \frac{\pi}{8}$, (a) z = 0 (b) z = 1 (c) z = 2

2DEG/D junction case 2 : r_{m} = 10, q_{0} = 0.1 $k_{F}^{},\,\alpha$ = $\pi/4$



2DEG/D junction case2 : $r_m = 10$, $q_0 = 0.4k_F$, $\alpha = \pi/4$

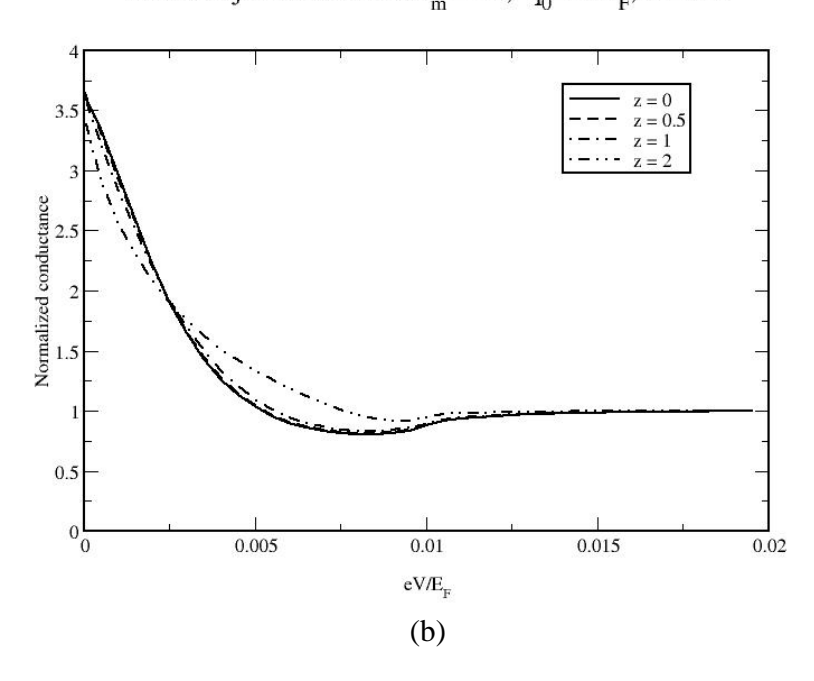
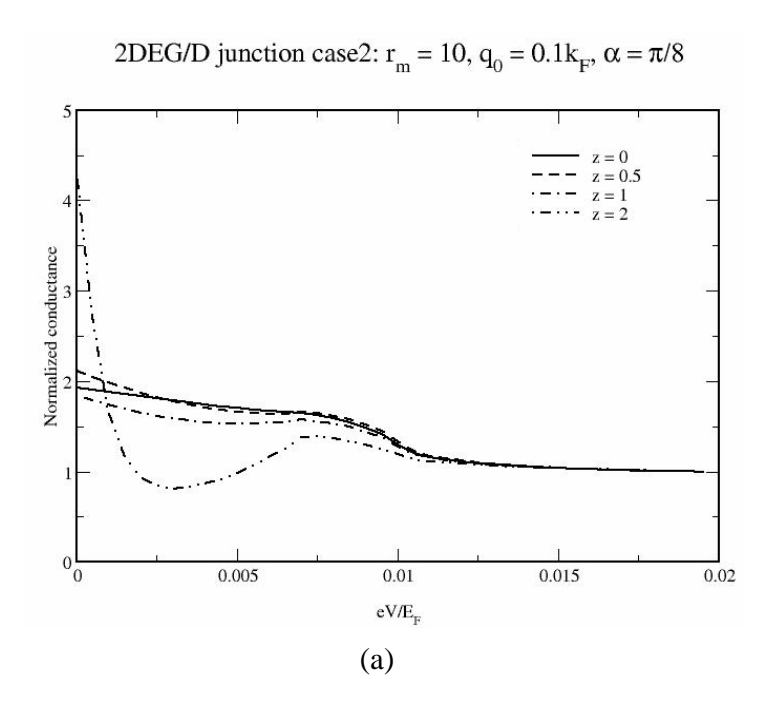


Fig. 13 The conductance spectra of 2DEG/D junction with various z = 0, 0.5, 1 and 2,

$$\alpha = \frac{\pi}{4} = 0$$
, $r_m = 10$ (a) $q_0 = 0.1k_F$ (b) $q_0 = 0.4k_F$



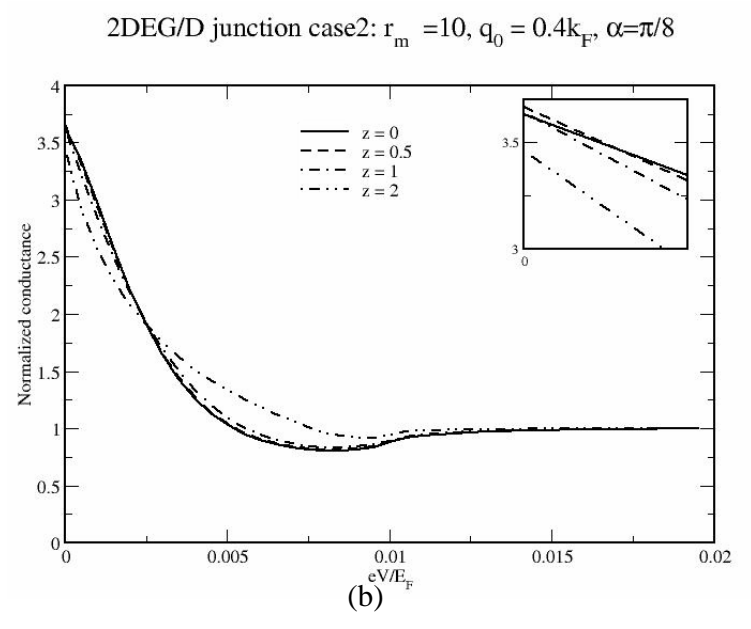


Fig. 14 The conductance spectra of 2DEG/D junction with various z=0, 0.5, 1 and 2, $\alpha=\frac{\pi}{8}=0, r_m=10$ (a) $q_0=0.1k_F$. (b) $q_0=0.4k_F$ The inset is the close up plot of the conductance spectra near eV=0

IV CONCLUSIONS

The tunneling conductance spectra of 2DEG/D junction show strong dependence on junction orientation. In junction with {100} orientation, a peak near the maximum gap of the d-wave superconductor is present in the conductance spectra. In junction away from {100}, there occurs a ZBCP, which is the signature of the surface bound states of d-wave superconductor [10, 11]. It is found that the effects of RSOC strength and potential barrier on the tunneling conductance are different for different Fermi levels of the 2DEG.

When the Fermi level lies above the crossing of the two branches, there occurs a peak at finite bias voltage but less than the maximum gap in {100} junction. The position of this feature depends on the magnitude of the RSOC. However, this feature is not robust against the barrier potential, i. e. it disappear when the barrier potential is in the tunneling limit. The normalized conductance at the bias voltage below the maximum gap is decreased by the potential barrier. In the junction with $\alpha = \frac{\pi}{4}$ and $\alpha = \frac{\pi}{8}$, RSOC enhance the height but decrease the width of ZBCP in Andreev limit. In the tunneling limit, RSOC reduce the height of the peak but does not affect its width. It is found that the height of ZBCP is increased with the barrier potential, whereas its width is decreased for small RSOC. When RSOC is big, the barrier potential does not affect the width of ZBCP.

In the case where the Fermi level of the 2DEG lies at the crossing, for the {100} junction, the normalized conductance at zero bias voltage is decreased with RSOC in the Andreev limit. In the tunneling limit, the conductance at zero bias voltage is increased with RSOC and then later is decreased with RSOC. It is found that for small RSOC, potential barrier suppress the conductance at zero bias voltage, while for big RSOC, the potential barrier can enhance it. In the junction with $\alpha = \frac{\pi}{4}$ and $\alpha = \frac{\pi}{8}$, the effect of RSOC on ZBCP in Andreev limit is the same as in the case where Fermi level lies above the crossing, that is, it enhances the height of ZBCP. However, in the tunneling limit, the increase in RSOC strength can cause the height of ZBCP to decrease and after a critical value of RSOC the height start to increase. It is found in the junction with both $\alpha = \frac{\pi}{4}$ and $\alpha = \frac{\pi}{8}$ orientations that the barrier potential increases

the height of ZBCP for small RSOC, while for RSOC is big the height of ZBCP is almost not affected.

Acknowledgements

We would like to acknowledge financial support from Cooperative Research Network (Physics). P.P. thanks Thailand Research Fund and Commission on Higher Education (grant no. RMU488012 and CHE-RES-RG "Theoretical Physics") for financial support. M.B. was supported by the Research Corporation, CIFAR and NSERC.

- [1] I. Zutic, J. Fabian and S. Das Sarma, Rev. Mod. Phys. 72, 323-410(2004).
- [2] S. Datta, and B. Das, Appl. Phys. Lett. **56**, 665 (1990).
- [3] A. G. Aronov and Y. B. Lyanda-Geller, Phys. Rev. Lett. **70**, 343 (1993).
- [4] T. Koga, J. Nitta, H. Takayanagi, anf S. Datta, Phys. Rev. Lett. 88, 126601 (2002).
- [5] A. W. Cummings, R. Akis and D. K. Ferry, Appl. Phys. Lett. 89, 172115 (2006).
- [6] E. I. Rashba, Sov. Phys. Solid State 2, 1109 (1960).
- [7] Yu. A. Bychkov and E. I. Rashba, J. Phys. C 17, 6039 (1984).
- [8] T. Yokoyama, Y. Tanaka and J. Inoue, Phys. Rev. B 74, 035318 (2006).
- [9] C. C. Tsuei and J. R. Kirtley, Rev. Mod. Phys. **72**, 969 (2000).
- [10] C.-R. Hu, Phys. Rev. Lett. 72, 1526 (1994).
- [11] Y. Tanaka and S. Kashiwaya, Phys. Rev. Lett. 74, 3451 (1995).
- [12] P. Pairor and M. B. Walter, Phys. Rev. B 65, 64507 (2002).

Josephson Effect in two YBCO twinned Crystals

P. Pairor*

School of Physics, Institute of Science,
Suranaree University of Technology, Thailand
(Dated: September 3, 2008)

Abstract

The free energies of a tetragonal system and both untwinned and twinned systems of orthorhombic symmetry are studied in order to derive the Josephson tunneling between two YBCO grains. A model based on the Ginzburg-Landau theory and the idea of twinning is introduced to describe the anomalous dependence of the critical current on an external magnetic field in a YBCO asymmetric 45° grain boundary.

PACS numbers: 03.75.Lm, 74.50.+r

^{*}Electronic address: pairor@sut.ac.th

I. INTRODUCTION

YBCO(YBa₂Cu₃O_{7- δ}) is one of the high-T_c cuprate materials which have startled condensed matter physicists for years[1]. There has been a question of what mechanisms make these materials have very high transition temperatures to the superconducting states and are responsible for their superconducting properties. It is well-known that in conventional superconductors isotropic s-wave pairing of electrons gives rise to superconductivity. However, in high-T_c materials because of their complicated crystal structures, the situation is more subtle. There are a number of experimental results suggesting that d-wave pairing occurs in high-T_c superconductors. It has been challenging to investigate the symmetry of the superconducting state both theoretically and experimentally.

The Josephson effect, one of the distinctive phenomena occurring in superconductors, can help study the symmetry of the order parameter. Without the aid of microscopic theories, the Josephson effect can be understood by the Ginzburg-Landau theory[2]. According to this theory, see for example in Ref. [3–5], the order parameter symmetry of a superconducting system determines the Josephson tunneling. From a study of Josephson tunneling experiments, it has been concluded that the order parameter of YBCO can be thought of as a combination of $d_{x^2-y^2}$ and s— wave components[5, 6]. To reach this conclusion, it is necessary to investigate the free energy of the system.

As will be discussed in Section II, the crystal symmetry of YBCO plays an important role in identifying the Ginzburg-Landau free energy[7]. The crystal structure of superconducting YBCO is orthorhombic, but since the two basis vectors \vec{a} and \vec{b} defining the basal plane are orthogonal and have almost the same magnitude, the symmetry of the order parameter is often described in terms of the symmetry of a tetragonal system. Furthermore, YBCO crystals are often twinned. Hence, this report will discuss the free energy of tetragonal and orthorhombic systems, and of orthorhombic systems with twins.

After the discussion of the free energy, in Section III the expression for the Josephson current density across the junction between two YBCO crystals will be examined, followed by the Josephson tunneling through an asymmetric 45^{0} grain boundary in a YBCO film. In several experiments, an anomalous dependence on an applied magnetic field of the critical current across the grain boundary has been observed[8, 9]. This anomalous dependence can be described by a model based on the idea of an s- and d- wave combination of the order

parameter and the idea of twinning. This model will be presented in Section III B. Finally, the conclusion will be summarized in Section IV.

II. GINZBURG-LANDAU FREE ENERGY AND ORDER PARAMETER SYMMETRY

The Ginzburg-Landau theory, although phenomenological, is very successful in describing superconductivity, at least on macroscopic scales. This theory is based on the Landau theory of second-order phase transitions. The transition from the normal to the superconducting state is a phase transition of this kind. According to the Landau theory, a symmetry of a system is spontaneously broken on the way across its transition point. The system can be characterized by an order parameter, ψ_i , which is zero in the normal state and nonzero in the superconducting state. In a conventional superconductor, it is gauge symmetry which is broken below the transition point. In an unconventional system, in addition to gauge symmetry, some other symmetries such as point group operations, lattice group operations, and spin rotation symmetries may be broken[7].

The main starting point of the Ginzburg-Landau theory of superconductivity is the socalled Ginzburg-Landau free energy. When dealing with the free energy of a superconducting system, there are three symmetry groups which are necessarily considered. The first one is U(1), the group of global gauge transformations which transform $\psi_i \to e^{i\phi}\psi_i$. The second one is T, the group of time-reversal transformations $\psi_i \to \psi_i^*$. The last one is G_0 , the group of the crystal symmetry of the system. If the superconducting state does not break the lattice translation symmetry, the group G_0 becomes the point group of the crystal alone[7], and the order parameter will then transform as one of the irreducible representations (or symmetry types) of that point group. Each irreducible representation of the point group corresponds to a basis function in real space with the same transformation properties. In addition, the number of complex components of the order parameter is given by the dimensionality of the irreducible representation to which the order parameter belongs. However, under the group G, $G = G_0 \times U(1) \times T$, no matter how the order parameter transforms, the free energy must be invariant.

From the microscopic theory of the condensation of Cooper pairs, there are two possible spin pairing states, namely singlet and triplet. Owing to strong spin-orbit coupling, for singlet states only the even parity irreducible representations whereas for triplet states only the odd parity irreducible representations occur[7].

A. Orthorhombic and Tetragonal Systems

YBCO is an orthorhombic but nearly tetragonal crystal, believed to have a singlet superconducting state[11]. Therefore, in this section the order parameters and the free energies of orthorhombic and tetragonal systems with singlet pairing will be discussed.

From the character table for an orthorhombic system in Table 1(a), the orthorhombic group has only one-dimensional irreducible representations. Thus, the order parameter of this system has only one complex component. Since only even parity irreducible representations can occur in a strong spin-orbit coupling system with singlet pairing states, the order parameter should belong to one of the following representations: A_{1g} , B_{1g} , B_{2g} , or B_{3g} .

TABLE 1 Character tables for (a) the D_{2h} point group and (b) the D_{4h} point group.

	D_{2h} basis	Representation	E	C_2^z	C_2^y	C_2^x	i	iC_2^z	iC_2^y	iC_2^x
	$ux^2 + vy^2$	A_{1g}	1	1	1	1	1	1	1	1
(a)	xy	B_{1g}	1	1	-1	-1	1	1	-1	-1
	xz	B_{2g}	1	-1	1	-1	1	-1	1	-1
	yz	B_{3g}	1	-1	-1	1	1	-1	-1	1
(α)										
	xyz	A_{1u}	1	1	1	1	-1	-1	-1	-1
	z	B_{1u}	1	1	-1	-1	-1	-1	1	1
	y	B_{2u}	1	-1	1	-1	-1	1	-1	1
	x	B_{3u}	1	-1	-1	1	-1	1	1	-1

	D_{4h} basis	Representation	E	C_2	$2C_4$	$2C_2'$	$2C_2''$	i	iC_2	$2iC_4$	$2iC_2'$	$2iC_2''$
(b)	$x^2 + y^2$	A_{1g}	1	1	1	1	1	1	1	1	1	1
	$xy(x^2 - y^2)$	A_{2g}	1	1	1	-1	-1	1	1	1	-1	-1
	$x^2 - y^2$	B_{1g}	1	1	-1	1	-1	1	1	-1	1	-1
	xy	B_{2g}	1	1	-1	-1	1	1	1	-1	-1	1
	(xz, yz)	E_g	2	-2	0	0	0	2	-2	0	0	0
	$xyz(x^2 - y^2)$	A_{1u}	1	1	1	1	1	-1	-1	-1	-1	-1
	z	A_{2u}	1	1	1	-1	-1	-1	-1	-1	1	1
	xyz	B_{1u}	1	1	-1	1	-1	-1	-1	1	-1	1
	$z(x^2 - y^2)$	B_{2u}	1	1	-1	-1	1	-1	-1	1	1	-1
	(x,y)	E_u	2	-2	0	0	0	-2	2	0	0	0

Let ψ denote the order parameter. According to Table 1(a), if, for example, ψ belongs to A_{1g} , ψ will transform under the D_{2h} point group operations like the basis $ux^2 + vy^2$, where x, y are the coordinate axes in the basal plane and u, v are arbitrary constants.

Because the free energy must be invariant under overall gauge transformations, time reversal, and the D_{2h} point group operations, the free energy density can be expanded in terms of ψ (to fourth order) and its derivatives as

$$f(\psi) = \alpha |\psi|^2 + \beta |\psi|^4 + K_x |D_x \psi|^2 + K_y |D_y \psi|^2 + K_z |D_z \psi|^2 + \frac{h^2}{8\pi}$$
 (1)

where $D_q = -i\hbar \frac{\partial}{\partial q} + \frac{|e^*|}{c} A_q$, (q = x, y, or z) and \vec{h} is a magnetic field $(\vec{h} = \vec{\nabla} \times \vec{A})$.

Table 1(b) shows the character table for the tetragonal point group D_{4h} . In this case, there are two possibilities for the number of complex components of the order parameter: one and two. Again, only even parity irreducible representations are of interest. If the order parameter transforms like $ux^2 + vy^2$, $xy(x^2 - y^2)$, $x^2 - y^2$, or xy under the D_{4h} point group, the free energy density has the form:

$$f(\psi) = \alpha |\psi|^2 + \beta |\psi|^4 + K_{xy}[|D_x\psi|^2 + |D_y\psi|^2] + K_z |D_z\psi|^2 + \frac{h^2}{8\pi}$$
 (2)

according to its invariance under overall gauge transformations, time reversal, and the D_{4h} point group operations.

The free energy is different, when the order parameter transforms like the E_g representation basis under the D_{4h} point group operations. Let (ψ_1, ψ_2) represent the order parameter transforming like (xz, yz). Then, the free energy density of the system becomes

$$f(\psi_{1}, \psi_{2}) = \alpha[|\psi_{1}|^{2} + |\psi_{2}|^{2}] + \beta_{1}[(\psi_{1}^{*}\psi_{2})^{2} + c.c.] + \beta_{2}|\psi_{1}|^{2}|\psi_{2}|^{2} + \beta_{3}[|\psi_{1}|^{4} + |\psi_{2}|^{4}]$$

$$+K_{xy}[|D_{x}\psi_{1}|^{2} + |D_{y}\psi_{2}|^{2}] + K_{yx}[|D_{y}\psi_{1}|^{2} + |D_{x}\psi_{2}|^{2}]$$

$$+K_{z}[|D_{z}\psi_{1}|^{2} + |D_{z}\psi_{2}|^{2}] + K'_{xy}[(D_{x}\psi_{1})^{*}(D_{y}\psi_{2}) + c.c.]$$

$$+K'_{yx}[(D_{y}\psi_{1})^{*}(D_{x}\psi_{2}) + c.c.] + \frac{h^{2}}{8\pi}$$

$$(3)$$

according to its invariance under overall gauge transformations, time reversal, and the D_{4h} point group operations.

B. Symmetry Type of YBCO Order Parameter

The YBCO crystal structure has orthorhombic symmetry. As discussed in the previous section, under the orthorhombic point group operations, the order parameter of an orthorhombic singlet state transforms as one of the following basis functions representing the first four irreducible representations of the group: $ux^2 + vy^2$, xy, xz, yz.

When the Josephson effect between YBCO and a conventional superconductor, such as Pb, is considered, it can be determined to which irreducible representation the YBCO order parameter belongs[5]. In experiments on the Josephson junction between YBCO and a conventional superconductor[12–14], nonzero Josephson currents along all three principal axes of YBCO were observed. Assuming the Josephson current is determined by the bilinear terms of the interface free energy, it can be concluded[5] that the YBCO order parameter transforms like the function $ux^2 + vy^2$. In other words, the YBCO order parameter belongs to the A_{1g} representation. Since $ux^2 + vy^2$ can be written as $s(x^2 + y^2) + d(x^2 - y^2)$, where $s = \frac{u+v}{2}$ and $d = \frac{u-v}{2}$, the YBCO order parameter can be considered a sum of s— and $d_{x^2-y^2}$ —wave components. Note that in this way the orthorhombic symmetry type of the order parameter is expressed in terms of representations of the tetragonal point group.

Let ψ_s and ψ_d be the s- and d-wave components, respectively and $\psi_s = |\psi_s|e^{i(\phi_d+\phi_{sd})}, \psi_d = |\psi_d|e^{i\phi_d}$, where ϕ_d is the phase of ψ_d ; and ϕ_{sd} is the relative phase between ψ_s and ψ_d . From Ref.[15], the YBCO free energy has the form:

$$f(\psi_{s}, \psi_{d}) = \alpha_{s} |\psi_{s}|^{2} + \alpha_{d} |\psi_{d}|^{2} + \alpha(\psi_{s} \psi_{d}^{*} + c.c.) + \frac{1}{2} \beta_{s} |\psi_{s}|^{4} + \frac{1}{2} \beta_{d} |\psi_{d}|^{4}$$

$$+ \beta_{4} |\psi_{s}|^{2} |\psi_{d}|^{2} + (\beta_{1} |\psi_{s}|^{2} + \beta_{2} |\psi_{d}|^{2}) (\psi_{s} \psi_{d}^{*} + c.c.)$$

$$+ \beta_{0} (\psi_{s}^{2} \psi_{d}^{2*} + c.c.) + \frac{1}{2} \sum_{\alpha} \sum_{\lambda,\mu} \frac{1}{m_{\lambda,\mu}^{\alpha}} (D_{\alpha} \psi_{\lambda})^{*} (D_{\alpha} \psi_{\mu}) + \frac{h^{2}}{8\pi},$$

$$(4)$$

where $\alpha \in x,y,z$ and $\lambda,\mu \in d,s$.

C. Free Energy Density of Twinned Crystal

Twinning is a defect which often occurs in YBCO and other orthorhombic crystals. The sizes of twin domains are in the range of 50 - 300 nm[16]. A twin boundary between any two twins is a plane of reflection symmetry of the underlying crystal as depicted in Fig. 1. In a YBCO crystal, there are two possible twin orientations, normal to the [110] and [$\bar{1}$ 10] directions.

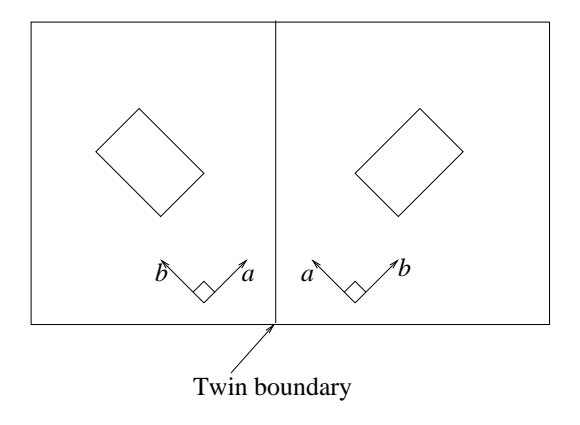


FIG. 1: A twin boundary acts as a reflection plane.

From Eq.(4), for a spatially uniform order parameter, the Ginzburg-Landau free energy for each twin orientation in the absence of a magnetic field is given by [6]

$$f(\psi_{s}, \psi_{d}) = \alpha_{s} |\psi_{s}|^{2} + \alpha_{d} |\psi_{d}|^{2} + (-1)^{\epsilon} \alpha(\psi_{s} \psi_{d}^{*} + c.c.) + \frac{1}{2} \beta_{s} |\psi_{s}|^{4} + \frac{1}{2} \beta_{d} |\psi_{d}|^{4}$$

$$+ \beta_{4} |\psi_{s}|^{2} |\psi_{d}|^{2} + (-1)^{\epsilon} (\beta_{1} |\psi_{s}|^{2} + \beta_{2} |\psi_{d}|^{2}) (\psi_{s} \psi_{d}^{*} + c.c.)$$

$$+ \beta_{0} (\psi_{s}^{2} \psi_{d}^{2*} + c.c.)$$

$$(5)$$

where $\epsilon \in 1,2$ represents one of the two twin orientations. By minimizing, the free energy with respect to ψ_s^* , it is found that ψ_s can be written in terms of ψ_d : $\psi_s = (-1)^{\epsilon+1} \frac{\alpha}{\alpha_s} \psi_d[6]$. Therefore, the interaction energy between twin 1 and 2 can be written as

$$f_{1,2} = B(\psi_{d1}^* \psi_{d2} + c.c.). \tag{6}$$

If B > 0, then $\psi_{d1} = \psi_{d2}$, $\psi_{s1} = -\psi_{s2}$, and the twin boundary is called odd. If B < 0, then $\psi_{d1} = -\psi_{d2}$, $\psi_{s1} = \psi_{s2}$, and the twin boundary is called even[6]. However, from the interpretation of Josephson tunneling experiments on twinned crystals, the superconducting state is seen to have odd symmetry[5, 6].

III. JOSEPHSON TUNNELING BETWEEN TWO YBCO CRYSTALS

The Ginzburg-Landau free energy density of an orthorhombic superconducting system presented in the previous section is now used to derive the Josephson effect between two YBCO crystals, as depicted in Fig. 2.

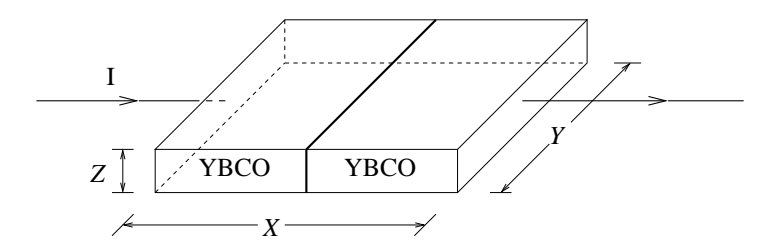


FIG. 2: The geometry of the Josephson junction between two YBCO crystals.

A. Josephson Current Density Between Two Orthorhombic Systems

From Eq.(4), it is seen that in an orthorhombic system like YBCO the free energy density, f, can be separated into three parts: the bulk terms $f_b = \alpha_s |\psi_s|^2 + \alpha_d |\psi_d|^2 + \alpha(\psi_s \psi_d^* + c.c.) + \frac{1}{2}\beta_s |\psi_s|^4 + \frac{1}{2}\beta_d |\psi_d|^4 \beta_4 |\psi_s|^2 |\psi_d|^2 + (\beta_1 |\psi_s|^2 + \beta_2 |\psi_d|^2)(\psi_s \psi_d^* + c.c.) + \beta_0(\psi_s^2 \psi_d^{2*} + c.c.)$, the gradient terms $f_{grad} = \frac{1}{2} \sum_{\alpha} \sum_{\lambda,\mu} \frac{1}{m_{\lambda,\mu}^{\alpha}} (D_{\alpha}\psi_{\lambda})^* (D_{\alpha}\psi_{\mu})$, and the field term $f_h = \frac{h^2}{8\pi}$. By minimizing the free energy density with respect to A_{α} and letting 1 and 2 denote the left and the right sides of the junction, respectively, the expression for the current in the α -direction is obtained as

$$j_{\alpha} = -c \frac{\partial f_{grad1}}{\partial A_{\alpha}}. (7)$$

For

$$f_{grad1} = \frac{1}{2} \sum_{\alpha} \sum_{\lambda_1, \mu_1} \frac{1}{m_{\lambda_1, \mu_1}^{\alpha}} (D_{\alpha} \psi_{\lambda_1})^* (D_{\alpha} \psi_{\mu_1}), \tag{8}$$

the current on the left side becomes

$$j_{\alpha} = -\frac{1}{2} \sum_{\lambda_{1},\mu_{1}} \frac{|e^{*}|}{m_{\lambda_{1},\mu_{1}}^{\alpha}} [\psi_{\lambda_{1}}^{*}(D_{\alpha}\psi_{\mu_{1}}) + c.c.]. \tag{9}$$

When considering the Josephson tunneling, the interface free energy per unit area, f_I , must be taken into account. In general, the interface free energy per unit area is

$$f_I = \sum_{\lambda_1, \lambda_2} G_{\lambda_1, \lambda_2}(\hat{n})(\psi_{\lambda_1}^* \psi_{\lambda_2} + c.c.), \tag{10}$$

where $G_{\lambda 1,\lambda 2}(\hat{n})$ is real and depends on the unit vector normal to the junction, \hat{n} . Therefore, minimizing $f_{grad1} + f_I$ with respect to $\psi_{\lambda 1}^*$ yields the boundary condition

$$\sum_{\alpha} \sum_{\lambda_1} \frac{i\hbar}{2m_{\lambda_1,\lambda_1}^{\alpha}} n_{\alpha}(D_{\alpha}\psi_{\lambda_1}) + \sum_{\lambda_2} G_{\lambda_1,\lambda_2}(\hat{n})\psi_{\lambda_2} = 0.$$
 (11)

From Eqs.(9) and(11), the expression for the current in the direction of \hat{n} is

$$\hat{n} \cdot \vec{j} = -\frac{|e^*|}{\hbar} \sum_{\lambda_1, \lambda_2} G_{\lambda_1, \lambda_2}(\hat{n}) (i\psi_{\lambda_1}^* \psi_{\lambda_2} + c.c.). \tag{12}$$

Let $\psi_{\lambda j} = |\psi_{\lambda j}| e^{(\phi_{d_j} + \phi_{\lambda_j d_j})}$, where $\phi_{d_j d_j} = 0$, $\phi_{s_j d_j} = \phi_{sd}$ which is the relative phase between s- and $d_{x^2-y^2}-$ components, and $j \in 1,2$. Substituting $\psi_{\lambda j}$ from the definition into Eqs.(10) and (12), the relation between the current and the interface free energy is obtained as

$$\frac{\Phi_0}{2\pi c}\hat{n}\cdot\vec{j} = \frac{\partial f_I}{\partial \phi},\tag{13}$$

where $\Phi_0 = \frac{hc}{|e^*|} = 2.07 \times 10^{-7} \text{ G} \text{ and } \phi = \phi_{d_1} - \phi_{d_2}$.

B. Josephson Current Across Asymmetric 45⁰ Grain Boundary

Generally, Eq.(13) can be applied to any Josephson junction where ϕ is the phase difference between the order parameters of both sides of the junction[2, 5]. In the case that both superconductors are conventional (s-wave like), f_I has the form

$$f_I = -\frac{\Phi_0}{2\pi c} j_c \cos \phi, \tag{14}$$

where j_c is the maximum current density flowing through the junction. In an external magnetic field, the result for the maximum (or critical) current across the junction, I_c , as a function of the external flux, Φ , is[11]

$$I_c = j_c Y Z \left| \frac{\sin(\pi \Phi/\Phi_0)}{\pi \Phi/\Phi_0} \right|, \tag{15}$$

where Y and Z are the length and thickness of the junction. This gives the usual Fraunhofer diffraction pattern as illustrated in Fig. 4(a). (See more details of the calculation of I_c in section III B 2.)

In the case that both superconductors are not conventional, the result for the critical current could be different. This report focuses only on the result for an asymmetric 45° grain boundary in a YBCO film where the grain boundary acts as a barrier. Figs. 3(a) and (b) depict the 45° grain boundary.

As mentioned earlier, the measured patterns of the critical current across the 45^o grain boundary as a function of a magnetic field are different from those of conventional systems, see for example in Fig. 4(b). They have quite distinctive characteristics[8–10]:

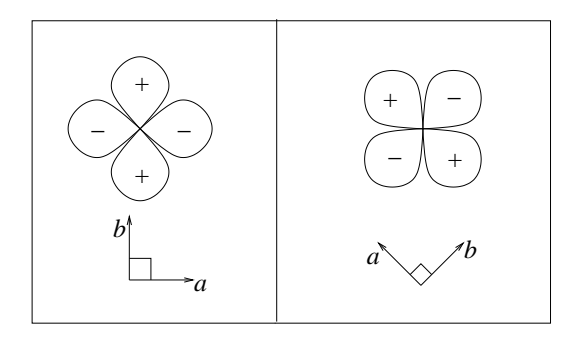


FIG. 3: An asymmetric 45^0 grain boundary. The diagram shows the two principal axes and d—wave components on both sides of the junction.

- 1. they are, though anomalous, fairly symmetric,
- 2. they show oscillatory behaviors up to fluxes $> 10\Phi_0$,
- 3. the maximum I_c can be obtained for $h_a \neq 0$,
- 4. at $h_a = 0$ the critical current may have any value between maximum and zero, and
- 5. the magnetic field rarely suppresses I_c to zero.

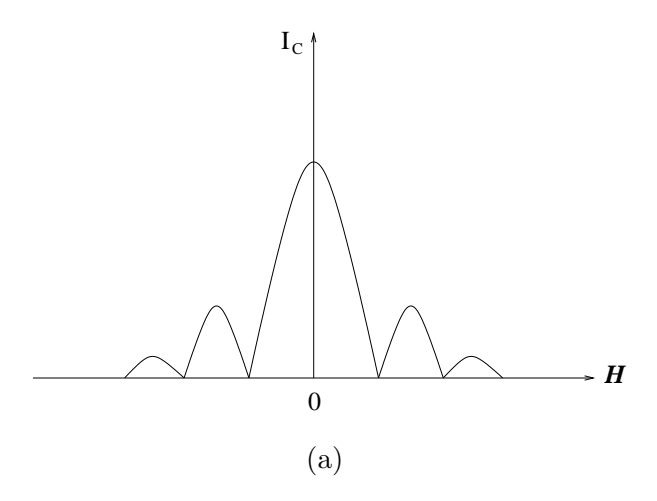
A pattern of this sort implies that the pure s—wave model fails to explain the behaviour in YBCO crystals, and so does the pure d—wave model as will be shown next. If the order parameter was pure d—wave, the interface free energy per unit area of the grain boundary would be

$$f_I = A(\psi_{d1}^* \psi_{d2} + c.c.) \tag{16}$$

where A is constant. Under a rotation of π about the x-axis (see Fig. 3(b)), $\psi_{d1}^{new} = -\psi_{d1}$ and $\psi_{d2}^{new} = \psi_{d2}$, but f_I is expected to be invariant; hence, A is zero. This result means that the currents across the junction would be also zero.

1. Josephson Current Density

As mentioned previously, the 45^{0} grain boundary is a very special case, because the Josephson critical current across the boundary is expected to vanish according to the pure d—wave model. Now it will be shown that the nonzero critical current and its dependence on an external field can be explained, using the idea of mixed s— and d— wave superconductivity and the twinning effect.



(b)

FIG. 4: The critical current across a junction of two conventional superconductors as a function of magnetic flux is shown in (a), while in (b) an example of a measured pattern of I_c across the 45^0 grain boundary in a YBCO film vs an applied magnetic field H from Ref. 8 is shown.

Let ψ be the order parameter of YBCO, which is mixed s- and d- wave. Owing to the odd symmetry of the twin boundaries, ψ changes sign at each twin boundary[17]. In other words, the phase of the order parameter changes by π at each twin boundary. Suppose there is a system as in Fig. 5. To obtain the Josephson current density across the grain boundary of the system, it is important to identify the interface free energy, which is not zero in this case. The interface free energy per unit area of the system is

$$f_I = \begin{cases} -\frac{\Phi_0}{2\pi c} j_c \cos \phi & , 0 < y < rY \\ -\frac{\Phi_0}{2\pi c} j_c \cos(\phi - \pi) & , rY < y < Y \end{cases}$$
 (17)

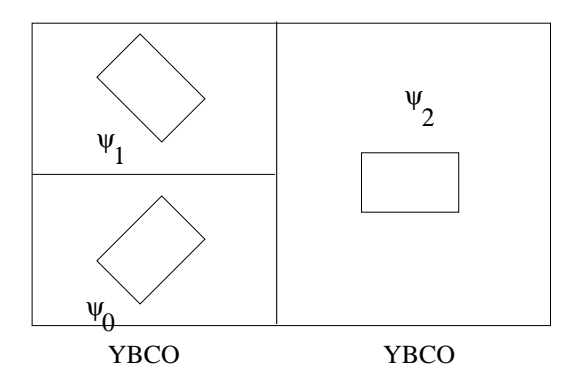


FIG. 5: shows a system which has two twins on one side and one twin on the other side.

where ϕ is the phase difference between ψ_1 and ψ_0 , and 0 < r < 1 (the definitions of ψ_0, ψ_1 , and ψ_2 are shown in Fig. 5). Therefore, according to Eq.(13) the Josephson current density is given by

$$j_x = \begin{cases} j_c \sin \phi &, 0 < y < rY \\ -j_c \sin \phi &, rY < y < Y. \end{cases}$$
 (18)

Generally, it is possible for both sides of the grain boundary to contain twins as shown in Fig. 6(a). However, in the calculation of the interface free energy per unit area, the system which has twins on both sides can be replaced by another with only one side having twins. Fig. 6(b) illustrates the idea. Both systems in Fig. 6(b) have the same interface free energy per unit area. Therefore, if a real system of an asymmetric 45° grain boundary containing m total twins on both sides is replaced with an assumed system of n twins on one side and one twin on the other, the interface free energies for both systems are the same and so is the Josephson current density, which is given by

$$j_{x} = \begin{cases} j_{c} \sin \phi &, 0 < y < r_{1}Y \\ -j_{c} \sin \phi &, r_{1}Y < y < r_{2}Y \\ j_{c} \sin \phi &, r_{2}Y < y < r_{3}Y \\ \dots & \dots \\ -j_{c} \sin \phi &, r_{n-1}Y < y < Y \end{cases}$$
(19)

where $0 < r_i < 1$ and $r_i < r_{i+1}$.

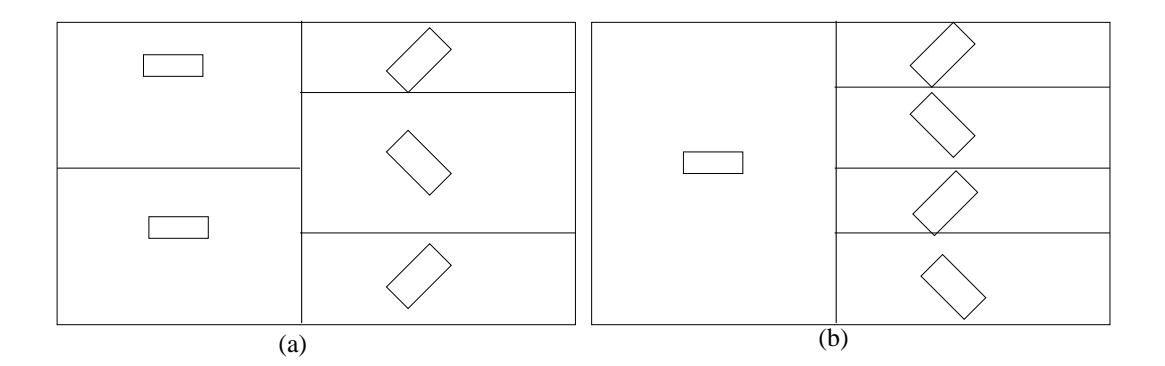


FIG. 6: (a) A 45^o grain boundary system with both sides contains twins. (b) Two different systems of 45^o grain boundary with twins. Both of them have the same interface free energy.

2. Critical Current as a Function of Applied Magnetic Flux

In an applied magnetic field, in the London approximation ϕ becomes [11]

$$\phi = \gamma_0 + \kappa y,\tag{20}$$

where γ_0 is the phase difference between ψ_1 and ψ_0 , $\kappa = \frac{2\pi}{\Phi_0}(d+2\lambda)h_a$ where d is the width of the Josephson junction, λ is the YBCO penetration depth, and h_a is an applied field. Therefore, the total current through the junction is equal to

$$I = \int \int j_x dy dz. \tag{21}$$

Substituting j_x from Eq.(19), the current yields

$$I = \frac{j_c Z}{\kappa} [\cos \gamma_0 + (-1)^n \cos(\gamma_0 + \kappa Y) + 2 \sum_{i=1}^{n-1} (-1)^i \cos(\gamma_0 + r_i \kappa Y)].$$
 (22)

To find the critical current, maximize I with respect to γ_0 . Using $\frac{\kappa Y}{2} = \frac{\pi \Phi}{\Phi_0}$, the expression for I_c is obtained

$$I_c = \left| \frac{j_c ZY}{2\pi \Phi/\Phi_0} \left[(1 + (-1)^n \cos(2\pi \Phi/\Phi_0) + 2\sum_{i=1}^{n-1} (-1)^i \cos(r_i \pi \Phi/\Phi_0))^2 + ((-1)^n \sin(2\pi \Phi/\Phi_0) + 2\sum_{i=1}^{n-1} (-1)^i \sin(r_i \pi \Phi/\Phi_0))^2 \right]^{\frac{1}{2}} \right|.$$
(23)

For each value of n with random sets of r_i , several results from Eq.(23) are depicted in Fig. 7.

From the model, the same number of twins n, for different sets of r_i , can lead to different results as shown in the figure. It can be seen that the higher the number of twins, the less the curve tends to fall as the external field is increased.

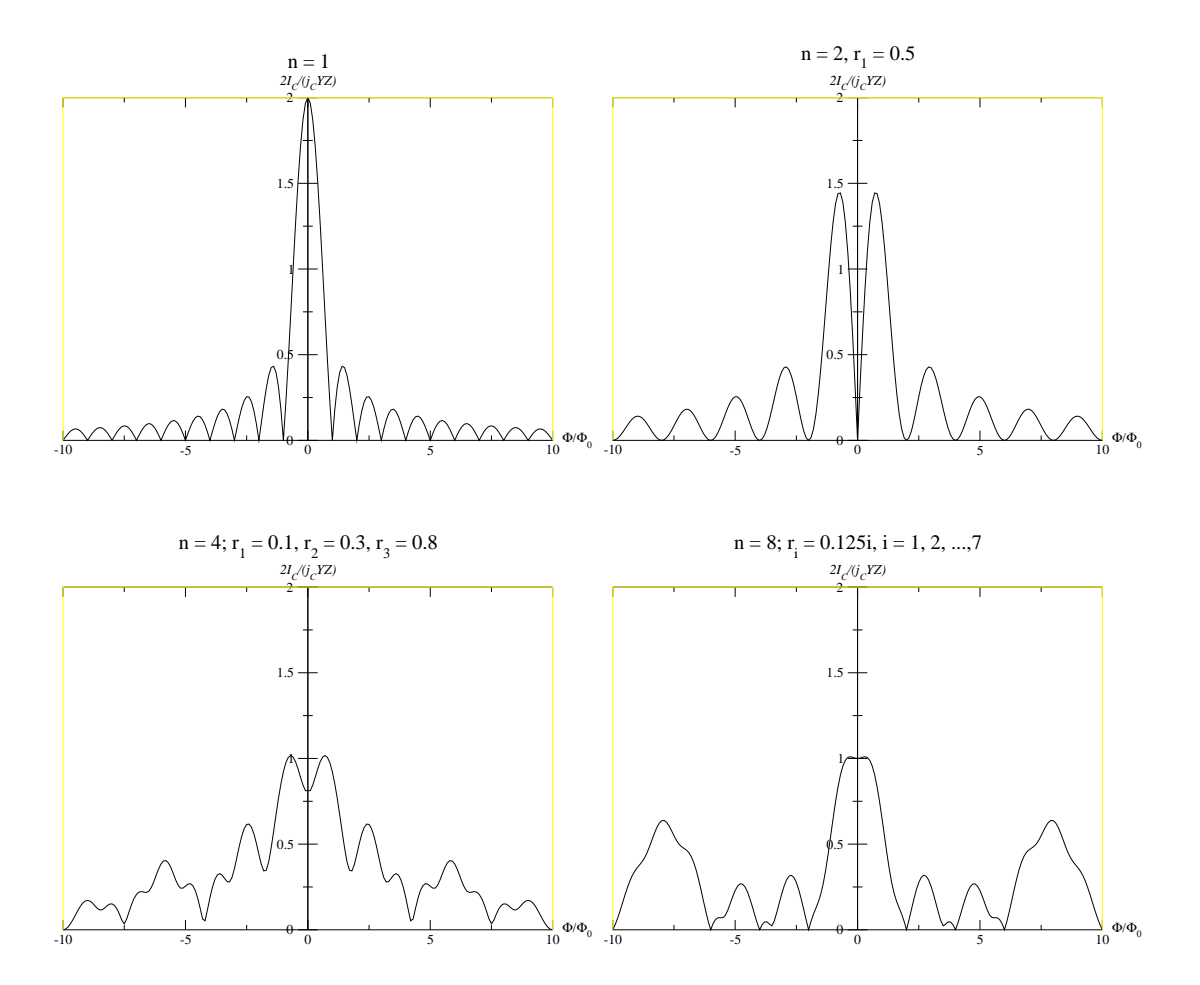


FIG. 7: shows some results of $n=1,\,2,\,4,$ and 8. Except n=1, the results for a couple sets of r_i for each n are shown. For each graph, the units of x-axis and y-axis are $\frac{\Phi}{\Phi_0}$ and $\frac{2I_c}{j_cYZ}$, respectively.

IV. CONCLUSION

The anomalous dependence on an applied magnetic field of the Josephson critical current across an asymmetric 45° grain boundary in YBCO film can be described by a model based on the Ginzburg-Landau theory of superconductivity and the twinning effect. The fact that the order parameter symmetry of YBCO is orthorhombic and belongs to the A_{1g} irreducible representation leads to the conclusion that the YBCO superconducting state can be thought of as a combination of s- and $d_{x^2-y^2}-$ wave components. Based on this conclusion, the free energy density of a twinned system can be derived. Because of the odd symmetry of the superconducting state under reflection in a twin boundary, the order parameter of a twinned system changes sign at each twin boundary. From the interface free energy of the junction between two twinned YBCO grains at 45° , the Josephson current density can be derived, and from there the expression for the critical current across the junction as a function of an applied magnetic flux can be obtained. It turns out that the pattern of the critical current depends on the density and the size distribution of twins. The results show a quite good qualitative agreement with experimental data.

Acknowledgments

I would like to thank Dr. M. B. Walker, Dr. J. Luettmer-Strathmann, and Dr. D. Agterberg for all their helpful suggestions and discussions. Also, I would like to acknowledge financial support from Thailand Research Fund and Commission on Higher Education (grant no. RMU488012)

^[1] D.M. Ginsberg, *Physical Properties of High Temperature Superconductors* vol. 1 (World Scientific, London, 1989), pp.1-38.

^[2] B.D. Josephson, Adv. Phys. **14**, 419(1965).

^[3] D.J. Van Harlingen, Rev. Mod. Phys. **67**, 515(1995).

^[4] M. Sigrist and T.M. Rice, Rev. Mod. Phys. **67**, 503(1995).

^[5] M.B.Walker and J. Luettmer-Strathmann, Phys. Rev. B 54, 588(1996).

^[6] M.B. Walker, Phys. Rev. B **53**, 5835(1996).

- [7] J.F. Annett, Adv. Phys. **39**, 83(1990).
- [8] C.A. Copetti, F. Rüders, B. Oelze, Ch. Buchal, B. Kabius, and J.W. Seo, Physica C 253, 63(1995).
- [9] J. Manhart, B. Mayer, and H. Hilgenkamp, preprint submitted to Z. Phys. B.
- [10] Y. Eltsev, K. Nakao, Y. Yamada, I. Hirabayashi, Y. Ishimaru, K. Tanabe, Y. Enomoto, J. G. Wen, N. Koshizuka, Physica C 357-360, 1572 (2001).
- [11] M. Tinkham, Introduction to Superconductivity 2nd ed. (McGraw-Hill, New York, 1996), pp.196-383.
- [12] D.A. Wollman, D.J. Van Harlingen, W.C. Lee, D.M. Ginsberg, and A.J. Leggett, Phys. Rev. Lett. 71, 2134(1993).
- [13] R.C. Dynes, Physica C **235**, 225(1994).
- [14] A.G.Sun, D.A. Gajewski, M.B. Maple, and R.C. Dynes, Phys. Rev. Lett. 72, 2267(1994).
- [15] Q.P. Li, B.E.C. Koltenbah, and R. Joynt, Phys. Rev. B 48, 437(1993).
- [16] L.S. Subhash and A.R. David, Interfaces in High- T_c Superconducting Systems (Springer-Verlag, New York, 1994), pp.140-175.
- [17] M.B. Walker, preprint.